EU Programme SAME

A survey of computational models for snow avalanche motion

581220-1 11 December 1998

Deliverable No. 4 of the EU Programme SAME
(Snow Avalanche Modelling, Mapping and Warning in Europe)

For the Norwegian Geotechnical Institute

Project Manager:

Karstein Lied

Report edited by:

Carl B. Harbitz

Carl B. Harbitz (NGI)

Reviewed by:

Karstein Lied

Postal address: P.O. Box 3930 Ullevaal Stadion, N-0806 OSLO, NORWAY
Street address: Sognsveien 72, OSLO
Internet: http://www.ngi.no
Telephone: (+47) 22 02 30 00
Telefax: (+47) 22 23 04 48
e -mail: ngi@ngi.no
Postal account: 0814 51 60643
Bank account: 5096 05 01281
Business No. 958 254 318 MVA

Fourth European Framework Programme

Environment and Climate

Contract ENV4-CT96-0258

SAME

SNOW AVALANCHE MODELLING, MAPPING, AND WARNING IN EUROPE

Deliverable n°4*: A survey of computational models for snow avalanche motion*
Also in: *Norwegian Geotechnical Institute* report no. **581220-1**

Editor: Carl B. Harbitz

Foreword

The present report is a contribution to the EU-program “Snow Avalanche Mapping and Warning in Europe (SAME)”, partly funded by the European Union under the EU contract no. ENV4-CT96-0258 and by Switzerland under the contract BBW 95.0644.

D. Issler (Swiss Federal Institute for Snow and Avalanche Research) has provided the section on powder snow avalanche dynamics models, and P. Sampl (AVL-List GmbH, Graz, Austria) has written on coupled dynamics models. C.J. Keylock (Dept. of Geography, Univ. of Cambridge; work performed as the contribution of his previous employer Icelandic Meteorological Office) has contributed with certain sections on empirical procedures and dense snow avalanche dynamics models, as well as technical and linguistic corrections. J. Fannin (University of British Columbia, Vancouver, Canada, previously Norwegian Geotechnical Institute) and B. Schieldrop (Industrial Hydro- and Aerodynamics, Norway) helped out in the early stages of the manuscript. C.B. Harbitz (Norwegian Geotechnical Institute) described many of the empirical procedures and dense snow avalanche dynamics models, and performed the editorial work.

In addition, thanks are due to the following persons for their highly acknowledged contributions or information that made it possible to write the present report:

M. Barbolini and L. Nettuno (University of Pavia, Italy)
V.P. Blagoveshchenskiy (ASDC, Kazakhstan)
A. Bozhinskiy and M.E. Eglit (Moscow State University, Russia)
U. Gruber, and P. Bartelt (Swiss Fed. Inst. for Snow and Aval. Research, Switzerland)
F. Irgens (Norwegian University of Science and Technology, Norway)
T. Jóhannesson (Icelandic Meteorological Office, Iceland)
M. Naaim and F. Rapin (CEMAGREF, France)
K. Nishimura (Hokkaido University, Inst. of Low Temp. Science, Japan)
R. Perla (National Hydrology Research Institute, Canada)

Summary

Various models for computation of avalanche motion are presented, both empirical procedures including statistical and comparative models for runout distance computations as well as dynamics models describing the physics of dense and powder snow avalanches, the coupled combination of these, and slush flows.

An examination of the existing models shows that: (1) there is not - and probably never will be - a single model that adequately describes all avalanche types; (2) in order to account for the extraordinary variability of avalanche motion in response to initial and boundary conditions, flow-regime transitions and the snow mass balance should be properly described in future models; (3) calibration and validation of these models will require a comprehensive measurement programme; (4) determination of realistic initial conditions is a serious problem. We suggest that using simple models to scan the relevant parameter space with more advanced models for detailed simulations of selected scenarios could improve this situation.

The needs for, and benefits of, co-ordinated programmes of extensive full-scale experiments and future model development in avalanche research is discussed. The authors suggest that international collaboration could produce high-quality models covering all the essential practical needs that are listed. Increased interdisciplinary collaboration would be advantageous for model development and would facilitate incorporation of other scientific disciplines.

Dynamics models describe either the internal dynamics of the material at certain stages of the motion, the dynamics of the moving mass as a whole from initiation to rest, or combinations of these. The dynamics models are presented with regard to a physical description of the moving material and the mathematical and numerical modelling of the flow. Most of the dense snow avalanche dynamics models are rooted in hydraulic theory where the moving masses are described as a fluid, but also granular flow models that have inherited geotechnical concepts from soil mechanics are included. Simple (quasi) three-dimensional models exist, but most of the models are still of one and two dimensions. The powder snow avalanche models are either density current models or binary (two-phase solid/fluid) mixture models. A few combinations of these, i.e. coupled models including both the dense and the powder snow part of the avalanche also exist.

In addition to expansion of existing avalanche dynamics models into three dimensions, the authors suggest to improve the one- and two-dimensional dynamics models further in the directions of flow-regime transitions and snow mass balance. Snow entrainment, density variations, heterogeneous particle concentration, particle size distribution, cohesion, particle rotation as well as temperature changes and energy dissipation are not adequately described in any of the dynamics dense snow avalanche models. Furthermore, there is a conspicuous lack of any description of stability and accuracy of the applied numerical methods.

Contents

Review and reference document

1 INTRODUCTION

(C.B. Harbitz)

The scope of the present report is to give a survey of the various kinds of computational models for snow avalanche motion and runout, and to conclude with recommendations for future model development.

Most avalanches consist of at least two parts. One is referred to as a dense snow avalanche (or flowing avalanche, in this report simply referred to as avalanche), which is a gravity flow. The other is a turbidity part referred to as an (airborne) powder avalanche, which is driven by the extra weight of small snow particles (< 1 mm) suspended in the air. A fully developed avalanche can be divided into four flow layers (Norem 1995a). The majority of the mass of the avalanche is represented by the basal and liquefied *dense flow layer*, where the particles are in close contact, and the volumetric density is high. The density is assumed to be almost constant. Above the dense flow layer is the transitional *saltation layer,* where the particles are transported in jumps similar to saltating particles in drifting snow. The volumetric density is reduced to the power of three with height in the saltating layer. Then follows the *suspension layer* that constitutes the snow cloud of the avalanche. Here the density and the velocity are both reduced almost linearly with height. Above and around the avalanche is a backflow of air named the *recirculation layer*, with a height one to three times that of the suspension layer.

Since the material properties differ, the distinction between wet snow (generally cohesive with possible snowball formation) and dry snow (no free water content) avalanches is useful. Dense snow avalanches can occur under both wet and dry snow conditions. A turbidity part is normally generated in both circumstances, especially in steep slopes. Pure powder avalanches require dry snow conditions.

The type of rupture of the snow cover depends on the state of intergranular cohesion. In loose snow a point fracture occurs (a loose snow avalanche), whereas sufficient intergranular cohesion favours line fracture and the resulting avalanche moves initially as a slab before it begins to break up.

The first attempt to formulate a general theory of avalanche motion was made by Voellmy (1955), and this theory is still widely used. Increased human activity in mountain regions, deforestation from pollution, forestry and ski resorts as well as a reduced acceptance of living in regions exposed to snow avalanches have caused a growing need for protection against avalanches. Both empirical procedures including statistical and comparative models for runout distance computations as well as dynamics models for avalanche motion simulations are now in existence. However, no universal model has so far been developed. The dynamics of avalanches are complex, involving properties similar to those employed in fluid, particle and soil mechanics. The limited amount of data available from real events makes it hard to evaluate or calibrate existing models. Often several models with different physical descriptions of the avalanche movement can all be used to replicate the information contained in the available, deficient, recorded observations.

An overview of all the models is presented in Fig. 1.1. The dynamics models included in the present report are discussed in terms of the physical description of the dynamics, and the material properties of the flowing snow. Assumptions and simplifications inherent in the

mathematical equations of each model are outlined, as well as possible numerical methods and results. The limitations and practical applications of each model are discussed. All models in common use are one- or (quasi) two-dimensional. The term “dimension” is discussed further in Sec. 3.

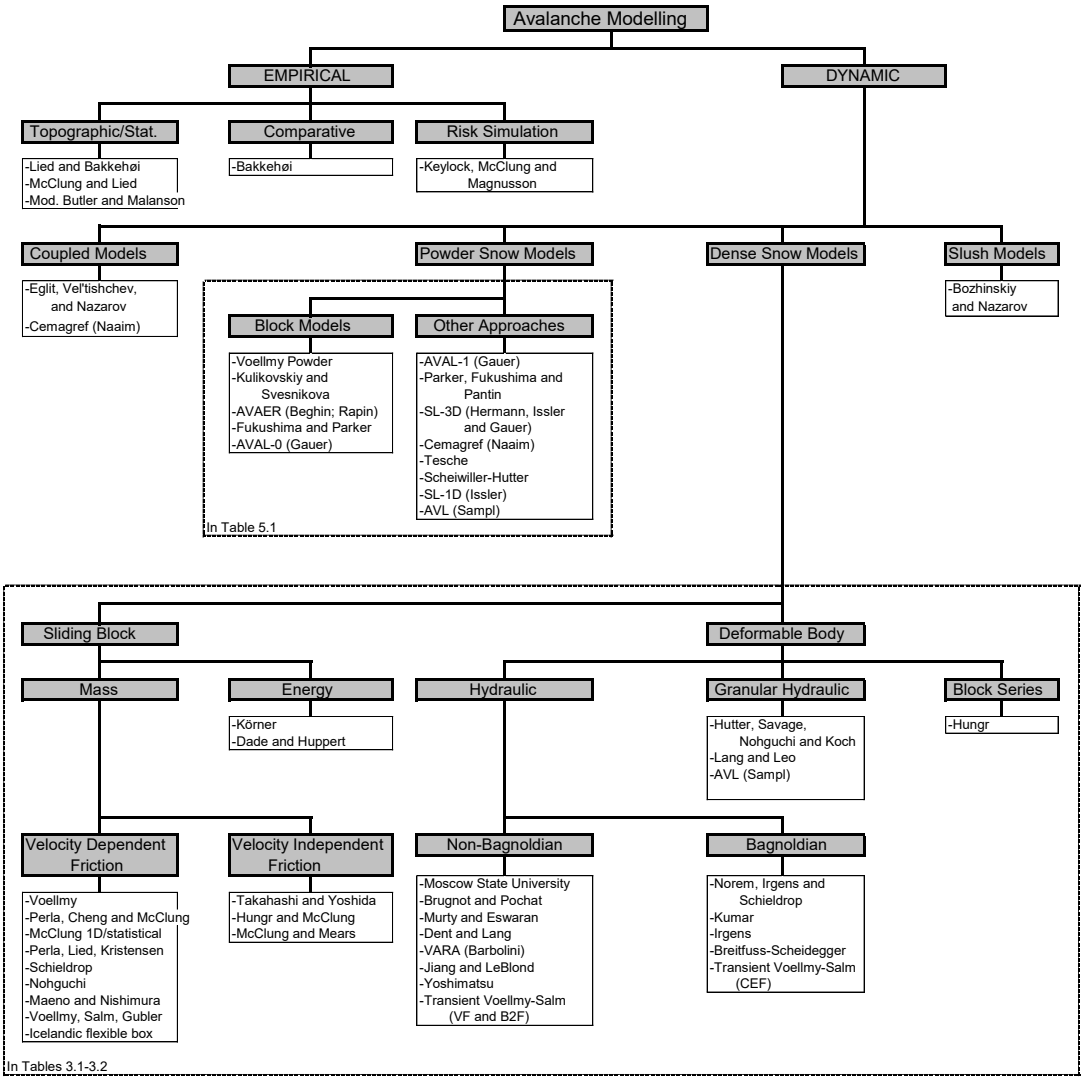

Figure 1.1: Overview of avalanche computational models.

Dynamics snow avalanche models can be divided into three groups, see Fig. 1.1:

1. The sliding block (or lumped mass) dense snow avalanche model describes the avalanche as a rigid body on a linear slope or as a flexible body (“blanket”) following the terrain. Alternatively, the motion can be described by a centre-of-mass consideration, incorporating the sum of external forces acting on the body.
2. Deformable body models describe the dense snow avalanche as a continuum. In the granular models, the flow is described as a cohesionless material, normally treated as an incompressible Coulomb (dry friction) medium that transmit no tensile but only compressive stresses. The main supporting force is attributed to grain-to-grain interaction.
3. Powder snow avalanche models describe the airborne turbulent particle flow as a block or by other approaches such as density current models or binary (solid-fluid) mixture models.

A few combinations of these, i.e. coupled models including both the dense and the powder snow part of the avalanche do also exist, in addition to a few models for slush avalanches.

To limit the extent of the report, papers on material properties or physical experiments of dense snow avalanches, release mechanisms, impact pressure, defence structures, descriptions of case studies or other related topics are omitted when not including any aspects of dynamics modelling or runout distance calculations. For further studies, the following review papers are referred: Hopfinger (1983), Hutter (1991), Mellor (1978), Norem (1992a, 1995b), Perla (1980) and Scheiwiller and Hutter (1982). Keylock (1997) employs a climatological framework to examine the mechanisms by which snow avalanches occur. This is followed by a discussion of the hydrologic and geomorphic aspects of avalanches. A previous, less extensive review of avalanche models was presented by Kleemayr (1996). Mathematical and physical modelling of powder snow avalanches in Russia is described by Eglit (1998a), and mathematical modelling of dense snow avalanches in Russia with examples of calculations is presented by Eglit (1998b).

With other parameter values or minor modifications, many of the models originally designed for other kinds of slide motion (rock slides, debris flows, etc.) should also be applicable for avalanches. A survey of computational models for rock slide and debris flow motion is given by Harbitz (1996).

2 EMPIRICAL DENSE SNOW AVALANCHE MODELS

(C.B. Harbitz and C.J. Keylock)

Empirical procedures for snow avalanches are based on statistical and comparative models for estimation of avalanche runout distance. In topographical/statistical models the runout distance relations are normally found by regression analysis. Comparative models are based on methods for evaluating the similarity between path profiles. An alternative approach is to present pure limiting criteria for flow behaviour, as recognised from considerations of subaerial debris flow behaviour (e.g. Benda & Cundy (1990), Cannon (1993), Fannin & Rollerson (1993), Fannin & Wise (1995)).

Empirical procedures are normally applied to dense flows. However, in principle there is no reason why they could not be applied to slush flows, dense and coupled avalanches (and perhaps even powder snow avalanches with data of sufficient quality) if new coefficients were derived. Thus, these procedures are treated separately in Fig. 1.1. A brief review of the current state of research as regards predicting maximum avalanche runout and avalanche risk is presented by Keylock (1997). Jóhannesson (1998a) provides an in-depth comparison of two of the commonly emplyed topographic models (the α/β and the runout ratio models).

2.1 The use of statistics in avalanche research

(C.J. Keylock)

A flowing snow mass is an extremely complex phenomenon to investigate. A detailed study would have to consider all of the following processes operating at a micro-scale: Fluctuations in particle size and temperature due to inter-granular collisions; changes in collision frequency

with position (relatively few collisions occur in a powder cloud compared to the dense core), and local changes in the mass balance as snow is eroded and deposited.
In order to produce a workable model of an avalanche one must make some important simplifications. These simplifications commonly involve averaging and thus, an informal application of statistics. For example, the Voellmy block model (Voellmy, 1955) assumes that on average, the effect of individual snow particles interacting with the bed results in a Coulomb friction for bed resistance. The VARA continuum models (Nettuno, 1996) assume that the Boussinesq coefficients take a value of unity. This results in a uniform velocity profile. In other words, just the first moment (the average value) of the vertical velocity distribution is considered relevant. Higher moments such as the variance, skewness and kurtosis are neglected. Thus, the assumptions underlying many dynamics models imply an informal application of statistics. In fact, it is also true that purely statistical methods based upon joint probability density functions are a classical technique for modelling turbulent flows (Pope, 1985).

An avalanche will only occur after a snowpack of sufficient depth has accumulated. One could adopt a deterministic approach to resolving the expected snow accumulation in an avalanche path. The expected precipitation level in the avalanche path of concern could be derived from the prevailing meteorological conditions through the use of nested meteorological models. A broad-scale model would be employed to obtain a general characterisation of meteorological parameters, which would then be used as input to a more local model. This ‘scaling down’ would continue until one arrived at the individual avalanche path scale. An alternative approach is statistical; one fits a statistical model (e.g. a regression equation) to past measurements of precipitation levels in the path, obtained with concurrent information on broader scale meteorological data. Then, given a particular meteorological regime, one should be able to predict (with associated levels of confidence) an appropriate precipitation level.

In order to state on a given day whether or not an avalanche will occur, and if so, how far it will travel, both types of information given above need to be coupled, together with information concerning snowpack metamorphism. Statistical and deterministic methodologies are compatible in this situation and have different strengths and weaknesses. Consequently, a robust analysis will employ a mixture of techniques.

However, a different and important problem for avalanche engineers is the design and location of settlements to resist an avalanche of a particular recurrence interval (return period), typically in the order of 100 years or so. In this case, one is not concerned with direct prediction in the sense discussed above (a specific event at a particular time). Instead, one considers how often, on average, that an avalanche exceeds a specific runout distance. As the length of observation (T) tends to infinity, the number of avalanches attaining or exceeding the 100 year return period position will converge upon T / 100. The consideration of return period drives any risk assessment exercise, whether formal or informal. Knowledge of probable degree of damage is a secondary factor. For example, one could envisage a situation where it is estimated that the peak pressures (for the 100 year avalanche) at the 25 year avalanche stopping position and the 50 year avalanche stopping position are similar. The fact that avalanches reach one of the locations twice as often as the other is the more important consideration.

As soon as one begins to discuss return periods, one is operating within a statistical framework. The advantage of statistical methods is that the existence of uncertainty in our measurement and modelling of physical processes is acknowledged and may be quantified. This quantification occurs through a distribution fitting procedure (although this may be implicit within

the statistical technique). The two most well known statistical models in avalanche work are the α/β model (Lied and Bakkehøi, 1980) and the runout ratio model (McClung and Lied, 1987). Both attempt to predict the location of the stopping position of the 100 year avalanche given knowledge of the location of the starting zone and the β point (the point on the path profile where the local slope angle attains 10°). Error is quantified directly by the runout ratio model through the Gumbel distribution of runout ratios and indirectly by the α/β model by the implicit assumption of a Gaussian distribution of error in a simple least-squares regression model. It is the error distribution rather than the simple first moment prediction (i.e. the mean value) that should be the focus of attention for the mathematical modeller who wishes to compare numerical results to a statistical model. Statistical models are based upon real avalanches and consequently provide a very useful validation tool for the mathematical modeller. They subsume the complexities of avalanche flow into a single, important parameter (the stopping position) and then provide an expected distribution of this variable.

An experienced modeller working with a complex mathematical model of avalanche flow will have to select appropriate ranges of values for various model parameters that act as initial and boundary conditions. The selected set of parameter ranges for an extreme avalanche (100 year return period) will, when implemented in the model, yield a range of predicted runout distances. The diligent modeller should compare the distribution of runout distances obtained from a number of simulations using various parameter combinations to the error range of the statistical models. Ideally, the two distributions should have similar moments (again, one should examine more than the first moment). Where this is not the case, there are two possibilities: either the statistical model performs poorly (likely to occur if the topography of the particular path is different to that of events in the database); or particular parameter values or parameter combinations are inappropriate. If the latter is the case, the modeller will have to re-inspect and re-think the appropriate parameter ranges. To eliminate the first possibility it would seem to make sense to first apply the mathematical model to a path where an extreme avalanche has been recorded and used in the development of the statistical model and which was not an outlier in this event database.

In this way, the statistical models can be seen as complementing the dynamics models. They provide an estimate of error based upon a sample of real events. By tuning the numerical model to this error range, the modeller can then go beyond the information contained in the statistical models and give predictions for velocities, impact pressures and related phenomena. It is important to note that of the two statistical models, the runout ratio model gives a positively skewed distribution of runout distances, while the α/β model is symmetrical. Thus, certain parameter combinations may be tolerated by one model and not the other.

An important criticism of statistical models is their inability to examine how return period varies along a given avalanche path – the models are developed for a specific return period. However, there are currently methods emerging that attempt to develop statistical models appropriate for this situation (Keylock *et al.*, in press; McClung, in preparation) and this advance will hopefully improve the utility of the statistical methodology, giving error estimates for a range of return periods.

Multivariate statistics in avalanche research are commonly employed in a nearest-neighbour fashion (Buser *et al*, 1987; Bakkehøi and Norem, 1993). Essentially, the procedure is to formulate a multi-dimensional space with axes consisting of the relevant parameters for the prediction of the dependent variable (degree of avalanching or runout distance for the two

references given above respectively). Coupled to this multivariate space is a look-up table of known values for the dependent variable. Then, given knowledge of the independent parameters, one should be able to place a new event (for which the dependent variable is unknown) into this space, find its nearest neighbour in the space and then use the look-up table to derive an appropriate value for the dependent variable.

Of critical importance in this type of work is an appropriate formulation of the multivariate space. This should be done in such a way that there is no particular bias towards any specific variable, unless such an effect is intended or is suggested by theory. Variables may be normalised to similar ranges, or emphasised in the analysis, through the application of appropriate weighting factors or by explicit standardisation. If one has no *a priori* knowledge of the significance of different variables then it is generally recommended that variables are standardised to prevent the variable with the largest dispersion having a disproportionate effect. The usual distance measures employed for measuring dissimilarity in multivariate spaces are the classic Euclidean distance and the city block or Manhattan distance. Given n variables and objects i and j, the Euclidean and city-block distance measures are respectively:

$$d(i,j) = \sqrt{\sum_{p=1}^{n} \left(x_{ip} - x_{jp} \right)^2}$$

$$d(i,j) = \sum_{p=1}^{n} \left| x_{ip} - x_{jp} \right|$$

Standardisation of the variables is attained by the following transformation:

$$z_{ip} = \frac{x_{ip} - m_p}{s_p}$$

where m_p is the mean value for the p'th variable and s_p is an appropriate measure of dispersion (median absolute deviation, mean absolute deviation or standard deviation). The choice of dispersion measure is dependent upon the nature of the data. If the data strongly conforms to Gaussian assumptions then the standard deviation may be best, while the other, more robust measures reduce the impact of outliers upon the dispersion value.

An alternate distance measure to the Euclidean metric may be preferable if there is correlation between variables and an appropriate variance-covariance matrix is available (from a preceding discriminant analysis for example). McClung and Tweedy (1994) provide an example of this situation for numerical avalanche prediction in Canada. The strategy used was to employ the Mahalanobis distance, which reduces to the Euclidean metric if there is no correlation between variables, but otherwise is given by:

$$\left[d(i,j) \right]^2 = \left(X_i - X_j \right)' S^{-1} \left(X_i - X_j \right)$$

where X_i and X_j are vectors of length n containing the predictor values for the i'th or j'th observation and S^{-1} is the inverse of the pooled variance-covariance matrix.

2.2 The Lied and Bakkehøi statistical α/β-model

(C.B. Harbitz and C.J. Keylock)

The statistical α/β-model (Lied and Bakkehøi, 1980, Bakkehøi *et al*., 1983, Lied and Toppe, 1988, Bakkehøi and Norem, 1994) was developed at NGI and governs maximum runout distance solely as a function of topography. The runout distance equations are found by regression analysis, correlating the longest registered runout distance from 206 avalanche paths to a selection of topographic parameters. The parameters that have proved to be most significant are presented in Tab. 2.1, cf. Fig. 2.1:

Table 2.1 Topographic parameters governing maximum runout distance

Symbol of parameter:	Parameter description:
β (deg.)	Average inclination of avalanche path between starting point and point of 10^o inclination along terrain profile.
θ (deg.)	Inclination of top 100 vertical meters of starting zone.
H (m)	Total height difference between starting point and lowest point of best-fit parabola $y=ax^2+bx+c$.
y'' (m^{-1})	Related to curvature of avalanche path.

The β-angle is empirically found to be the best characterisation of the track inclination, and the regression analysis revealed that the β-angle is also the most important topographic parameter. In fact, in general it would appear that β is the only statistically significant terrain parameter. A β-point is accepted only if it is inside the section of the profile where the angle between the tangent of the best-fit parabola and the horizontal plane is between 5^o and 15^o.

The inclination θ of the top 100 vertical metres of starting zone indirectly governs the rupture height, and thereby the slide thickness, which is greater in gentle slopes than in steep slopes. Hence smaller values of θ give longer runout distances or smaller average inclination of the total avalanche path, α. The topography, the width and the degree of lateral confinement in the starting zone, as well as the drifting snow transport into the starting zone, have little influence upon the runout distance (Lied and Bakkehøi, 1980, Lied *et al*., 1995). As opposed to what was presumed, no tendency was found that an avalanche with a wide rupture zone, which is channelled into a narrow track, has a longer reach than an avalanche following an unconfined path.

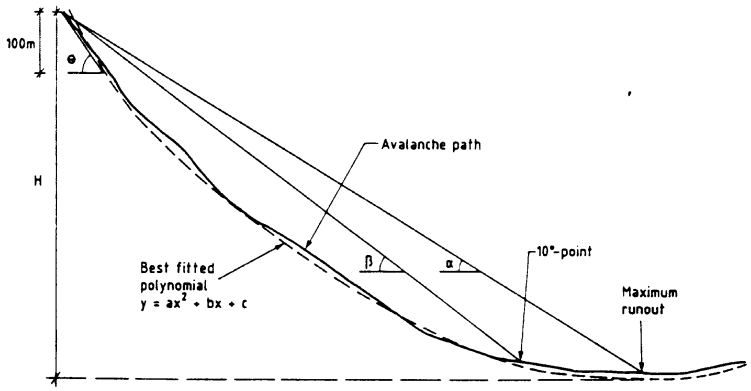

Figure 2.1: Topographic parameters describing terrain profile (after Lied and Toppe, 1988)

In Norway most avalanche paths might be approximately described by the parabola $y=ax^2+bx+c$. For a parabolic slope, the β-angle is determined by $\beta = \tan^{-1}\left(\sqrt{\frac{Hy''}{2}} + \frac{\tan 10^\circ}{2}\right)$, where the second derivative $y''=2a$ is related to the curvature. Smaller values of the product Hy'' mean smaller values of β. This results in theoretically smaller values of α, because the avalanches run with smaller velocity, and the velocity-dependent frictional transformation of potential energy into heat is reduced. Hence, the avalanches have an apparently lower coefficient of friction. The result of the regression analyses is referred in Tab. 2.2.

Table 2.2 Results of regression analysis (translated from Bakkehøi and Norem, 1994) with standard deviations (SD) and correlation coefficients (R). [H] represents the numerical value of H

Assumption	No. of avalanches	Regression equation, α=	Accuracy		Standard deviation (m) H=1000m, horizontal runout		
			SD (deg.)	R [-]	α (deg.)	-ΔL (m)	ΔL (m)
$\beta \le 30°$	68	$0.89\beta + 0.035\theta - 2.2° \cdot 10^{-4}[H] - 0.9°$	1.49	0.84	25	138	154
$30° < \beta \le 35°$	59	$1.15\beta - 2.5° \cdot 10^{-3}[H] - 5.9°$	2.50	0.53	30	162	189
$\beta > 35°$	79	$0.81\beta + 0.036Hy''\theta + 3.2°$	2.67	0.62	36	127	144
$\beta \le 30°$, $H \ge 900$m		$0.94\beta + 0.035\theta - 2.6°$	1.02	0.90	25	96	103
All avalanches	206	$0.96\beta - 1.4°$	2.30	0.92			
All avalanches	206	$0.92\beta - 7.9° \cdot 10^{-4}[H] + 0.024Hy''\theta + 0.04°$	2.28	0.92			

The model is most appropriate for travel distance analysis along longitudinally concave profiles. The calculated runout distances are those that might be expected under snow conditions favouring the longest runout distances. The authors have no explanation as to why there is such a small correlation in the data for $30^o < \beta \le 35^o$.

Lied and Toppe (1988) redefine the starting zone as the part of the path lying between the starting point and the point of 30^o inclination along the terrain profile. The average inclination

of this zone is termed γ. Identification of the γ-point on the avalanche path is performed by the same procedure as used for the β-point above (the tangent angle interval of acceptance for this point is between 25° and 35°). They further describe the automatic computation of the avalanche parameters. Applying the relation $\alpha = f(\beta, \gamma)$ for 113 avalanches, the equation $\alpha = 0.91\beta + 0.08\gamma - 3.5^{\circ}$ gives R=0.94 and SD=1.4°, which is a small improvement to the relation between α and β in Tab. 2.2. Lied and Toppe (1988) also present combinations of the lengths of the starting zone, the avalanche track and the runout zone, L_1, L_2 and L_3 respectively, as well as the area A of the starting zone (evaluated subjectively from local topography as a substitute for the avalanche volume). The best relation is $L \equiv L_1 + L_2 + L_3 = 0.93L_1 + 0.97L_2 + 0.61\text{m} \cdot [\text{A}] + 182\text{m}$, with R=0.96 and SD=137m ([A] represents the numerical value of A [m^2]). Using L_3 alone as the dependent variable does not give R- and SD-values that enable sufficiently accurate calculations of runout distance. The prediction of path lengths will give runout distances independent of steepness of path, as opposed to the more realistic α/β-relations. McClung and Lied (1987) show that the avalanches with the 50 highest values of the ratio $L_3/(L_1 + L_2)$ give a very good fit to an extreme value distribution.

The assumption of small variations in the physical snow parameters giving the longest runout distance is only valid within one climatic region (McClung *et al*., 1989). Martinelli (1986) and McClung *et al*. (1989) have applied the basics of the statistical α/β-model in mountain regions outside Norway.

The avalanche database of NGI is constantly extended, and contains at present 230 events. Both the statistical and the dynamics models are occasionally recalibrated. The usual form of the α/β-model is that of a simple linear regression relation: $\alpha = m\beta + c$, where *m* and *c* are regression parameters. The comparison with the best-fit parabola to avoid local 10°-points is omitted, as this parabola is really not needed with only the simple regression equation without y″ and H. Local 10°-points are now avoided by selecting with some caution the lowest 10°-point along the path. More complex forms of the model are usually overfitted (see final row of Tab. 2.2). For the Norwegian dataset, the values of *m* and *c* are 0.96 and -1.4.

An analysis of 45 paths in Iceland with reliable records (25 0f which terminate on land and 20 in the sea) was used to produce an Icelandic α/β-model. A least-squares regression analysis found that the intercept term was not statistically significant and it was dropped from the model to $\alpha = 0.85\beta$. This equation had a standard error of 2.3° and a correlation coefficient (*R*) of 0.71 (Jóhannesson, 1998a).

The regression analysis for the α/β-model has also been accomplished in Austria, see Tab. 2.3.

Table 2.3 Results of regression analysis for Austrian avalanches (from Lied et al., 1995) with standard deviations (SD) and correlation coefficients (R). [H] represents the numerical value of H (m).

Assumption	Regression equation, α=	Accuracy	
		SD (deg.)	R [-]
β<25°	$1.14\beta - 4.66^o$	0.87	0.88
$25^o \le \beta < 30^o$	$0.89\beta + 0.5^o$	1.3	0.70
β ≥30°	$1.05\beta - 4.47^o$	1.7	0.93
All avalanches	$0.946\beta - 0.83^o$	1.5	0.96
All avalanches	$0.97\beta - 0.7 \cdot 10^{-1}\theta - 0.32 \cdot 10^{-1} y'' + 0.6 \cdot 10^{-6} Hy''\theta + 1.54^o$	1.3	0.97

The Austrian four-parameter equation may be improved by classifying the avalanches according to β-ranges.

2.3 The McClung and Lied Runout Ratio Model

(C.J. Keylock)

The runout ratio model of McClung and Lied (1987) is a statistical model based on the same parameters as the α/β-model, but including an additional term, δ, defined as the angle from the α-point to the β-point. Thus, the topography of the runout zone (which is likely to be of some importance in runout studies) is explicitly incorporated. The runout ratio itself is defined as:

$$\frac{\Delta x}{X_\beta} = \frac{\tan\beta - \tan\alpha}{\tan\alpha - \tan\delta}$$

where Δx is the horizontal distance from the β-point to the α-point and X_β is the horizontal distance from the starting zone to the β-point.

When a set of runout ratios from a mountain range are analysed, a distribution is fitted by a maximum likelihood procedure, using a plotting position formula derived by McClung and Lied (1987):

$$P_i = \frac{r_i - 0.4}{N}$$

where P_i is the non-exceedance probability of occurrence of the i'th largest extreme avalanche in the dataset (the data are ranked in ascending order), r_i is the rank of the i'th value of the runout ratio and N is the number of extreme events used in analysis.

The analysis of data from several mountain ranges shows a high degree of fit to an Extreme Value Type I or Gumbel distribution as one would expect from theoretical considerations. The cumulative distribution function for this distribution is given by:

$$F(x) = \exp\left\{-\exp\left[-(x-u)/b\right]\right\}$$

where u is alocation parameter and b is a scale parameter of the distribution. Tab. 2.4 provides parameter values, degree of fit (assessed by r^2), standard error values and the number of extreme events used in analysis for various mountain ranges.

The model can be used for land-use planning purposes by specifying a standard value for p and from this, a value for the runout ratio $\Delta x/X_\beta$. For example, one might decide to specify a value of $p = 0.95$. For Iceland this yields a runout ratio of 0.53 and leads to the statement that on 95% of avalanche paths, extreme events (with a return period between 50 and 300 years) are not expected to exceed a runout ratio of 0.53.

Table 2.4 Parameter values, degree of fit (assessed by r^2), standard error values and the number of extreme events used in analysis for various mountain ranges

Mountain Range	u	b	r^2	Standard Error	Number of Paths
Canadian Rockies (Censored Data)	0.079	0.070	0.98	0.012	79
British Columbia Coast Mountains	0.107	0.088	0.97	0.020	31
Western Norway	0.155	0.072	0.98	0.010	54
Colorado Rockies	0.118	0.236	0.97	0.046	42
Sierra Nevada	0.266	0.199	0.95	0.052	20
Iceland	0.128	0.135	0.97	0.029	45

2.4 The KMM Statistical Avalanche Risk Model

(C.J. Keylock)

The KMM statistical avalanche risk model (Keylock et al., in press) employs historical information in order to evaluate the risk (at a general level) to people inhabiting structures in avalanche-prone terrain. The modular structure permits more detail to be included as the historical records improve. While the specific distribution parameters (and indeed the actual distributions) may differ for other mountainous areas, the overall approach has general validity.

Risk may be defined as the probability of death or losses and is the product of three subcomponents, each of which takes values between 0 and 1:
(1) The *encounter probability* is defined by the spatial and temporal exceedance probability of avalanching as a function of location.
(2) The *exposure* is the proportion of time that the objects or people that one is concerned with are under threat.
(3) *Vulnerability* is the proportion of damage that is caused to the exposed objects or persons.

For avalanche risk mapping at a regional scale, the encounter probability is of primary importance. Consequently, this model focuses upon this component of risk. The model is of use when there is insufficient historical information upon one path to evaluate the encounter probability directly. In this case, it is possible to artificially develop a probable event record based upon avalanche runout information from other paths in the same general region.

Avalanches of different magnitudes cause varying degrees of damage. Consequently, the model is formulated for nine avalanche sizes defined by the five main sizes of the Canadian avalanche classification (McClung and Schaerer, 1993) and the four half sizes. The avalan-

ches in the historical record are allocated to one of these sizes and for each the runout distance [expressed using the runout ratio (McClung and Lied, 1987) to permit inter-path comparison] and the maximum width of the deposit is recorded. Furthermore, the deviation of this avalanche from an average travel direction for avalanches is calculated. This is done by assuming that the plan view of the constructed avalanche path profile represents the mean travel direction for the path.

This deviation in avalanche direction is simply the ratio between:

1. The perpendicular distance of the centre of the front of the avalanche deposit from the average travel direction;
2. The horizontal component of the distance along the most frequently travelled direction until it intersects with 1.

Consequently, it is a dimensionless parameter.

It is then necessary to determine frequency distributions for the avalanche width and runout distances for each size. The Central Limit Theorem would suggest that a normal distribution is appropriate for the runout distances, and this was borne out in Iceland. The mean and variances of the runout distances for all sizes are such that there is no danger of a physically meaningless value (runout ratio less than or equal to zero) occurring. However, this is not the case for the avalanche widths and, consequently, a gamma distribution was considered more appropriate for the width data.

If there is insufficient information to evaluate these distributions for each size class explicitly, then parameter values are extrapolated from regression curves fitted to the evaluated sizes. In practice it is highly unlikely that there will be a large enough number of records of both small (size 1), and very large (size 5) avalanches for their parameters to be evaluated directly. This is because small events are rarely recorded owing to their short runout distances and the low levels of damage they cause, while large events have a low frequency. Fortunately, both these avalanche sizes are less important in terms of risk (low vulnerability and encounter probability values respectively).

The deviation distribution has a mean of 0 (deviation is measured from the average direction). The measurements of deviation (standardized with respect to down-profile travel distance) should permit the characterization of a single variance value for a normal distribution of avalanche deviation (σ_{dev}^2).

One more distribution is required before the encounter probability may be evaluated, this gives the relative frequency of different sized avalanches. Ideally, this would make use of records from a continuously monitored location. In Iceland, there is no such location and consequently, the avalanche records from Rogers' Pass, Canada were used to obtain the relative frequency of the smaller avalanches which escape detection in Iceland due to the short winter days. The relative frequency of the larger sizes is generally better known because of the impact these events have upon local communities. The Canadian data for small events were combined with the Icelandic records for the larger sizes to derive the final distribution.

For an avalanche of a given size *n*, the encounter probability (*E*) is given by:

$$E_n = f.r_n.P(T_x)_n.P(T_y)_n \qquad (1)$$

where f is the average avalanche frequency (events per year) upon the path, r is the relative frequency of the given size and $P(T)$ denotes the probability of an event reaching a target point T, with co-ordinates (T_x,T_y), where x is distance along the plan view of the constructed path profile and y is a cross-slope distance perpendicular to this.

All of the terms on the right-hand side of equation 6, except $P(T_y)_n$, can be evaluated directly from the derived distributions and relations once the distance T_x has been converted into an appropriate runout ratio. The evaluation of $P(T_y)_n$ is somewhat more complicated in that one must account for the combined effect of avalanche width and deviation from the average avalanche direction, as both contribute to lateral variation in avalanche extent:

$$P\left(T_y\right)_n = \int_{i=-\infty}^{\infty}\left[P\left(\psi_i\right).P\left(w_i\right)_n\right]d\psi \qquad (2)$$

where $P(\psi_i)$ is the probability of the avalanche deviating from the centre-line by ψ_i metres and $P(w_i)_n$ is the cumulative distribution function that defines the probability of an avalanche of size n attaining the required width w_i defined as:

$$w_i = 2\left|T_y - \psi_i\right| \qquad (3)$$

$P(\psi_i)$ is obtained from the normal distribution for the avalanche deviation. This distribution has a mean of 0 and a standard deviation σ:

$$P\left(\psi_i\right) = \frac{1}{2\pi\sigma}e^{\frac{-\psi^2}{2\sigma^2}} \qquad (4)$$

$$\sigma = \sigma_{dev}.T_x \qquad (5)$$

where σ_{dev} is the standard deviation of the avalanche deviation derived from data and found to equal 0.053 in Iceland. This was defined to be independent of avalanche travel distance (see above), hence it must be re-converted into an appropriate value for the travel distance of the particular avalanche to be examined.

$P(w_i)_n$ is found from the cumulative gamma distribution for a size n avalanche:

$$P\left(w_i\right)_n = 1 - \int_0^{w_i}\frac{\lambda^a w_i^{a-1}e^{-\lambda w_i}}{\Gamma(a)}dw_i \qquad (6)$$

where a and λ are the shape and scale parameters of the gamma and where the delta function is evaluated as:

$$\Gamma(a) = \int_0^{\infty} w_i^{a-1}e^{-w_i}dw_i \qquad \text{for a} > 0 \qquad (7)$$

To evaluate equation 2, it is necessary to establish some physical limits upon i. Size 5 avalanches tend to have the largest widths. In Iceland, an 1100 m wide (550 m half-width) size 5 avalanche has a probability in the order of 10^{-6} and thus a solution of equation 2 using this half-width value as a maximum for w_i will be precise to five decimal places, sufficient for our purposes. Consequently, a fairly conservative recommendation for avalanche evaluation in Iceland is that limits are placed on equation 2 as given in equation 8. This equation can then solved numerically.

$$P\left(T_y\right)_n = \int_{i=T_y-550}^{T_y+550}\left[P\left(\psi_i\right).P\left(w_i\right)_n\right]d\psi \qquad (8)$$

Having derived the encounter probability at the target point for each avalanche size, the other two components of risk, vulnerability and exposure can now be evaluated. Owing to a lack of information in the avalanche literature on the precise nature of avalanche damage, vulnerability functions were estimated from information available in Iceland, as well as international reports of earthquake damage. One may express the vulnerability in terms of the household inhabitants (proportion of fatalities) or the damage to the buildings as a proportion of cost of replacement. This may be assessed for both reinforced and unreinforced structures. The final vulnerability values for each avalanche size are given in Tab. 2.5 below. We have constrained our analysis to building damage and to fatalities within buildings. An investigation into the risk to people while they are outside would require different vulnerability and exposure functions.

Exposure was simply set to unity for risk to constructions (buildings are stationary objects) and to 0.5 for individuals (who spend roughly half of their time at home).

Having obtained values for encounter probability, exposure and vulnerability for each avalanche size, the degree of risk attributed to each size is obtained as the product of these three values. The overall risk at a given point in the terrain is the sum of the size-specific risk values.

A computer program linked to a Geographic Inforamtion System (GIS) was written to solve the model for selected points in the terrain. From here, one can readily proceed to construct risk contours, although if the runout zones of two different avalanche paths overlap, the risk at a given target point should be the sum of the risk values for the separate paths. This will not result in risk values greater than 1, because this could only occur if both starting zones overlapped significantly, in which case it is not clear that one has two separate paths.

The risk values obtained using the model are difficult to explicitly validate because there was insufficient data to maintain a control sample. However, the risk values are in quite strong agreement with independent, more vulnerability-oriented calculations performed at the Icelandic Meteorological Office.

It is also the case that approximately 50 people have been killed in the last 25 years in Iceland from avalanches in the towns most at risk. Approximately 5 000 people inhabit at risk areas, and 20 % of these are at a high risk. Thus, in a given year, assuming all deaths have occurred in the high risk zone, the annual probability of death for an individual living in a high risk zone is approximately 0.002 [no. of deaths / (no. of years × no. of residents)]. Construction of a risk map using the model developed here clearly places the 0.002 contour line in the designated high-risk zones.

Table 2.5 Vulnerability expressed as specific loss or proportion of fatalities for two different construction materials

	Low Quality Constructions		Reinforced Concrete Structures	
Avalanche Size	Specific Loss (Percentage)	Fatalities (Percentage)	Specific Loss (Percentage)	Fatalities (Percentage)
1	0	0	0	0
1.5	0	0	0	0
2	7	0	4	0
2.5	12	3	7	2
3	20	7	12	4
3.5	30	13	18	8
4	39	21	24	13
4.5	66	33	40	20
5	82	50	50	30

2.5 The Bakkehøi comparative model

(C.B. Harbitz)

Buser (1983) and Buser *et al*. (1987) developed a method to evaluate the similarity between two meteorological situations. Thus they were able to compose an avalanche hazard warning for the actual day by finding the earlier days with the most similar conditions, and studying the registered avalanche activity on those days.

Bakkehøi and Norem (1993, 1994) use the same method to estimate avalanche runout angle α (average gradient of the avalanche path) along a certain path profile. The actual profile is compared with registered path profiles of more than 200 previous avalanche events. The average inclination of the avalanche path between starting point and point of 10^o inclination along terrain profile, β, is considered the most important parameter governing the runout angle. Thus avalanche path profiles in the register with β-values differing more than two degrees from the actual profile, are excluded from the investigation. Each remaining avalanche path profile and its best fit parabola y(x) are described by the characteristic parameters presented in Tab. 2.6 (cf. the statistical α/β-model above). All parameters are weighted by suitable coefficients w_i.

When comparing the actual profile with a profile from the avalanche data register, the seven parameters in Tab. 2.6 will take different values for the two paths, x_{i1} and x_{i2}, i=1,2,...,7, respectively. The similarity between the two paths is expressed by the 7-dimensional weighted distance

$$d = \sqrt{\sum_{i=1}^{7} w_i (x_{i1} - x_{i2})^2}$$

where a small value of d indicates a high degree of similarity. The actual runout angle is finally calculated as the average of the runout angles of the five most similar registered avalanche path profiles.

Table 2.6 Parameters describing avalanche path profile

Symbol of parameter x_i:	Parameter description:	Weight coefficient w_i:
θ	Inclination of starting zone.	0.3
y''	Shape factor, $y''=2a$. Describes curvature of best fit parabola $y=ax^2+bx+c$.	0.3
H	Total height difference between starting point and lowest point of best fit parabola $y=ax^2+bx+c$.	0.04
z	Altitude of runout area (m.a.s.l).	0.03
H y''	Determines β angle for a parabolic slope by $\beta = \tan^{-1}\left(\sqrt{\frac{Hy''}{2}} + \frac{\tan 10^\circ}{2}\right)$	0.7
σ	Standard deviation of best fit parabola from the co-ordinates ot the given path profile.	1.0
Q	Standard deviation of variation of deviation of best fit parabola from the co-ordinates of the given path profile. Q expresses the roughness of the path profile.	2.0

Evaluation of the method is accomplished by Bakkehøi and Norem (1994). The standard deviation of the calculated runout angle from the observed runout angle for all the registered avalanches is 1.86°. This is better than the standard deviation for both the statistical α/β-model (Sec. 2.2) and the NIS model (Sec. 3.18), which is 2.2° and 2.3° for the whole avalanche register respectively.

The comparative model also gives the opportunity to study the background material of the most similar registered avalanche events with regard to topographical conditions, regional climate, and accuracy of return period. Hence it is possible to attach greater importance to selected registered events.

2.6 The modified Butler and Malanson Excessive Travel Distance energy line block model

(C. Keylock)

Butler and Malanson (1992) draw upon the energy line approach of Heim (1932) and Hsü (1975), (see also Körner, 1980; Sec. 3.1) to formalise a definition of excessive travel distance (a greater than expected runout distance). There are several flaws in the original paper, and the authors do not extend the technique so that it can be employed operationally. However, with a few modifications a model can be developed that is similar in form to the runout ratio model of McClung and Lied (1987), Sec. 2.3.

Hsü (1975) in his study of sturzstroms (catastrophic debris streams) employed an effective coefficient of friction of tan 32° to define the energy-line of the flow. Excessive travel distance was then simply (p. 138):

> *'the horizontal displacement of the tip ... beyond the distance one expects from a frictional slide down an incline with a normal coefficient of friction of tan 32° (0.62)'*

Thus, the expected travel distance is that point on the profile that intersects a line drawn from the starting zone with an angle to the horizontal of 32°. Excessive travel distance is the horizontal displacement of the tip of the avalanche debris beyond this point. Butler and Malanson 'tentatively adopt' the same value for the coefficient of friction as used by Hsü in order to perform their analysis and present results for 6 avalanche events. The excessive travel distance L_e varied from –310 m for a dry avalanche to 970 m for a wet snow avalanche.

It is somewhat surprising that the wet avalanches ran further than the dry events. However, it must be recognised that firstly, just the flowing component of the dry avalanche was recorded and secondly, Butler and Malanson do not define what they consider to be a wet avalanche. Thus, a large dry event which produces some free-water because of the heat generated during granular collisions may have been classified as wet. Conversely, they may have observed a slush event, although this is unlikely given the location of the field site.

Use of the energy-line to delimit avalanches with long runout distances is certainly an important concept. However, several changes are needed for this method to become usable. Firstly, it is highly likely that 32° is too high an angle for the friction term if one is concerned with larger events. McClung and Schaerer (1993) present data that show that dry avalanches can be released from slope angles as low as 25°. Körner (1980) states that the average slope of large avalanches (equivalent to the energy line in its simplest formulation) is usually between 22° and 27°. As a first approximation, a coefficient of friction of tan25° would seem more reasonable for dry events.

Secondly, Butler and Malanson use the same coefficient of friction for wet and dry avalanches; thus, it is not surprising that wet events tend to have higher excessive travel distances. At the limit case for wet avalanches (the slush avalanche), Nobles (1966) notes that flows can be sustained upon slope angles of less than 5°. It is more correct to analyse dry, wet and slush avalanches separately.

Thirdly, comparisons between paths such as those given by Butler and Malanson are not valid because of the inherent scale effect that paths with a greater elevation will tend to produce events with longer travel distances. This effect can be eliminated (or at least substantially reduced) by non-dimensionalising the excessive travel distance by the horizontal distance from the starting zone to the expected travel distance point.

This gives a formulation directly analogous to the runout ratio, with the difference that the runout ratio defines a β-point based on the local terrain angle and the technique elaborated here (the travel distance ratio) uses an energy-line approach to find such a point.

The similarity between the two ratio techniques suggests that the travel distance ratio could be employed operationally in a similar way to the runout ratio (through fitting to a Gumbel distribution).

The excessive travel distance approach is described in a form valid for operational use for the first time in this paper. No validation of this method has yet been performed. However, it is likely that its performance would be approximately similar to the runout ratio technique.

3 DENSE SNOW AVALANCHE DYNAMICS MODELS

(C.B. Harbitz and C.J. Keylock)

While empirical procedures may permit an assessment of runout distance, the more advanced dynamics models give much additional information concerning th enature of the sliding event (flow heights, velocities, etc.). This information is crucial for improved understanding of avalanche dynamics, and for the calculation of (amongst others) the impact pressure upon obstacles. At present, impact pressures are calculated only in the VSG model, while the pressure distribution at a point, which varies through time as the avalanche passes by, is not calculated in any model.

Depth-averaged models for an avalanche in a three-dimensional terrain exist, but all models in common use are either one-dimensional rigid body models (lumped mass or sliding block on a linear slope or in two-dimensional terrain) or two-dimensional depth-averaged deformable body models (two-dimensional continuum in a two-dimensional terrain).

There may be some confusion in the terminology concerning the dimensionality of models. In Tab. 3.1-3.2, dimensions are given separately for the flow and the terrain. Hence, block models moving in a three-dimensional terrain are considered to be of dimension 0,3. In order to characterise the centre-of-mass models further, one may talk about variable-height, variable-width, variable-length, variable-cross-section, or variable-size models if the characteristic extension of the avalanche in the respective dimension(s) is determined by an additional dynamical equation.

The basic dimensionality of the deformable body models is the number of space dimensions in the dynamics equations. The term "quasi two-dimensional model" means one-dimensional equations with depth or width averaging. "Quasi three-dimensional model" is ambiguous since it could mean a one-dimensional model with height and width averaging, or a two-dimensional model with height averaging. A depth-averaged deformable body model that uses a profile plus transects is said to have dimension 2.5,2.5 (the flow is described down and across the slope, but the height of the eflow isn’t all there, while the terrain is not quite fully three-dimensional).

The existing dynamics models can be divided into sliding block models and deformable body models, Fig. 1.1. A more detailed overview of the computational models for dense snow avalanche motion is presented in Tab. 3.1-3.2.

Table 3.1: Summary of characteristic features of the described dense snow avalanche dynamics models. Dimensions are given as 'flow, terrain' where a flow dimension of 0 represents a block model. Non-integer flow dimensions represent averaging over a dimension, while non-integer terrain dimensions mean that there is limited inclusion of the additional dimension.

Model Name / Author(s)	*Dimension*	*Friction/material parameterisation*	*Snow entrainment*	*Numerical scheme*	*Validation*
Körner	0, 1	dry friction f_r	No	None	Compared to field observations by Blagoveshchenskiy (1991)
Dade and Huppert	0, 1	Const. resisting shear stress ≈ yield strength	No	None	None specified
Voellmy	0, 1.5	turbulent friction ξ and Coulomb friction μ	No	None	Buser and Frutiger (1980) discuss values of the coefficients.
PCM (Perla, Cheng & McClung)	0, 1.5	Coulomb friction μ. M/D for terms proportional to v^2	Lumped into M/D but not resolvable	None	Bakkehøi et al (1981) discuss the values of the coefficients. Compared to field observations by Blagoveshchenskiy (1991). Alean (1984) tests the model against ice avalanche data.
McClung 1D/statistical	0, 1.5	Coulomb friction μ. M/D for terms proportional to v^2. See 'validation'	No	None	By definition consistent with field measurements, speed-dependent friction defined by statistical methods
Perla, Lied and Kristensen particle model	1, 1.5	Varying Coulomb friction μ and M/D for terms proportional to v^2. Random term determined by Monte-Carlo simulation	At the avalanche front	Finite-difference Monte-Carlo	Simulations of Ryggfonn avalanche
Schieldrop	0, 2	similar to PCM model	No	4th order Runge-Kutta	Compared to field observations and Irgens model by Irgens *et al.* (1998), Domaas and Harbitz (1998).
Nohguchi	0, 3	similar to Voellmy model	No	Runge-Kutta	Numerical simulation of real avalanches
Maeno & Nishimura	0, 3	Coulomb friction μ, Viscous term B, Turbulent term C	Related to velocity by an exponential function.	Runge-Kutta	Maseguchi avalanche
VSG (Voellmy, Salm & Gubler)	0, 1.5	Voellmy coefficients with internal friction parameter λ	No	None	Tested by Gubler (1987) and Lied et al (1995)
Icelandic "flexible" box	1.5, 2	See PCM	Experimental	4th order Runge-Kutta	None specified
Transient Voellmy-Salm (Bartelt & Gruber)	1.5, 2.5	Various for the 3 flow laws: Voellmy, Bingham, and modified CEF	None or at a rate equal to airborne powderisation	Galerkin f.e. / upwind f.d (no damping)	Flow laws evaluated against known events (Aulta). Also comparison with experiments (Hutter *et al*, 1995) and with Voellmy-Salm and McClung-Mears
Dent & Lang	1.5, 2	Friction through viscosity terms	No	f.d. scheme	Coefficients evaluated by fitting to experimental results. Successful validation for slow avalanches
MSU dense (Grigoryan, Eglit & Yakimov)	1.5, 2.5	Coulomb with an upper limit. Hydraulic turbulent friction k. (v^2 and v dependent)	Ostroumov (1972) extended entrainment to the whole flow.	Not specified	Numerical exploration coupled with calculations for real events
Hungr	1.5, 2.5	Various rheological models can be selected.	Assumed to be a constant % of the cross-sectional area per unit displacement	Lagrangian centred f.d. explicit scheme	Model compared to other models and experiment, as well as flow slides from coal waste dumps by Kent and Hungr (1995). The lateral pressure coefficient is very important
Breitfuss-Scheidegger	1, 1	Friction is a result of particulate collision or flow field deformation	No	Not Specified	Suggested parameter values are provided by the authors
Yoshimatsu	1, 1	dynamic and static dry friction coefficients	No	f.d. schemes	The author suggests from experiment that the ratio of the dynamic to the static coefficient = 0.8
NIS (Norem, Irgens & Schieldrop)	1.5, 2	modified CEF	Only theoretically described, not in numerical model	Eulerian f.d. in space and 4th order Runge-Kutta in time.	Widely tested against avalanches, submarine slides and rockslides. Also compared with laboratory experiments
Irgens	1.5, 2.5	modified CEF	No	See NIS model	Numerical simulation of real avalanche

Table continues on following page.

Table 3.1: Continued.

Model Name / Author(s)	*Dimension*	*Friction/material parameterisation*	*Snow entrainment*	*Numerical scheme*	*Validation*
VARA (Nettuno & Barbolini)	2, 2.5	Coulomb bed friction and an 'inertial regime' granular resistance.	No	Various types of f.d. scheme	Validation limited by a lack of data. However, comparisons with the transient Voellmy-Salm model
Murty & Eswaran	1.5, 2.5	dry, laminar and turbulent friction	No	MacCormack method	???
Kumar	1.5, 2.5	Coulomb friction	No	MacCormack method	None specified
Brugnot & Pochat	1.5, 2.5	dry friction and dynamic drag coefficients	At the leading edge	Not specified	Tested against the Voellmy model and experiments
Hutter, Savage, Nohguchi & Koch	1.5, 1.5	Coulomb internal friction	No	Lagrangian f.d. scheme with numerical diffusion	Comparisons made with laboratory experiments
AVL	2.5, 3	Coulomb internal and basal friction	No	Lagrangian finite volume	Comparisons with observations
Lang &Leo	2.5, 3	granular media with a Coulomb yield criterion. Basal Coulomb friction and boundary drag ($\propto v^2$)	No	Lagrangian f.d. scheme with numerical diffusion	Comparison with the experimental results of Lang *et al.* (1989)
Hungr & McClung	1, 1	Just a Coulomb basal resistance (no turbulent drag)	No	None	Tested by experiment (Chu *et al.*, 1995) and comparisons made to real events
Jiang & LeBlond	1.5, 1	Bingham	No	None	Comparison with the snow flow test of Dent's experiment
Naaim	2, 3	Various rheological models can be selected.	No	Finite Element	None specified

Table 3.2: Summary of quality, potential and limits of dense snow avalanche dynamics models described in the SAME model survey report.' +' is a point in the model's favour and '–' a weakness. 1) but see McClung and Mears (1995); 2) depends on the rheological model chosen.

Model Name / Author(s)	*Validation successful against real events?*	*All model parameters are physically-based?*	*Parameter values are relatively well constrained*	*The model is readily transferable to other locations?*	*Model is informed by snow mechanics considerations?*	*The approach can be extended to higher flow dimensions?*	*Model results include runout distance and flow height, respectively*
Körner	not known	+	+	+	–	–	+ –
Dade and Huppert	–	–	+	+	–	–	+ –
Voellmy	–	+	–	+	–	–	+ –
PCM (Perla, Cheng & McClung)	–	–	–	+	–	–	+ –
McClung 1D/statistical	+ (by definition)	–	+	+	–	–	+ –
Perla, Lied and Kristensen particle model	+	–	–	+	–	–	+ +
Schieldrop	+ (small/slow events)	–	–	+	–	–	+ –
Nohguchi	not known	+	–	+	–	–	+ –
Maeno & Nishimura	not known	–	–	–	–	–	+ –
VSG (Voellmy, Salm & Gubler)	Validation results not described	–	–	–	–	–	+ –
Icelandic “flexible” box	not known	–	–	+	–	–	+ +
Transient Voellmy-Salm (Bartelt & Gruber)	+–??	+	–	+	+	+	+ +
Dent & Lang	+ (slow events)	+	+	+	–	–	+ –
MSU dense & hydraulic (Grigoryan, Eglit & Yakimov)	not known	+	–	–	–	+	+ +
Hungr	+	+	+ – [2]	+	–	–	+ +
Breitfuss-Scheidegger	not known	+	+	+	+	–	– –
Yoshimatsu	+	+	+	–	+	–	+ –
NIS (Norem, Irgens & Schieldrop)	+	+	+	+	+	+	+ +
Irgens	+	+	+	+	+	+	+ +
VARA (Nettuno & Barbolini)	–	+	–	+	+	+	+ +
Murty & Eswaran	not known	+	–	+	–	+	+ +
Kumar	not known	–	+	–	+	+	+ +
Brugnot & Pochat	+	–	–	–	–	+	+ +
Hutter, Savage, Nohguchi & Koch	–	+	+	+	+	+	+ +
AVL (Sampl)	+	+	+	+	+	+	+ – +
Lang &Leo	–	–	–	–	+	+	+ +
Hungr & McClung	+	+	+	+	– [1]	–	+ +
Jiang & LeBlond	+	+	+	+	–	+	+ +
Naaim	not known	+	not known	+	+– [2]	+	+ +

The sliding block (also called lumped mass or rigid body) model describes the avalanche as a rigid body on a linear slope or as a flexible body ("blanket") following the terrain. Alternatively, the motion can be described by a centre-of-mass consideration, incorporating the sum of external forces acting on the body. These models describe the slide initiation well. Due to their simplicity they are also widely applied to the rest of the avalanche motion. Only the translation of the mass centre, not the deformation, is described. Back-calculated friction coefficients tend to be low compared with measured values. The rigid body models termed 'mass' employ the centre-of-mass considerations, while the models termed 'energy' represent energy considerations.

Deformable body models describe the dense snow avalanche as a continuum. Difficulties arise in choosing convenient constitutive equations, boundary conditions, and initial conditions, and in solving the equations.

Most dense snow avalanche dynamics models are rooted in hydraulic theory, although granular flow models utilising various geotechnical methods from soil mechanics have also been developed. Hydraulic deformable body models are distinguished by the use of depth-averaged equations of motion similar to those used for calculating unsteady flood waves (from an analogy with open-channel hydraulics). Both wet snow and dry snow avalanches involve a high internal deformation and are more or less in a liquid state. For wet snow avalanches, solid concentrations are high (inertial regime), and energy dissipation is caused mainly by particle interactions. In dry snow avalanches, energy dissipation is caused mainly by particle interactions at high solid concentrations, and by viscosity in the interstitial air at low concentrations (macro-viscous regime, more or less gaseous state). Both flow regimes give rise to a dynamic shear and to a dispersive pressure normal to the flow direction reducing internal friction, as described by Bagnold (1954, 1956). In the macro-viscous regime the dispersive pressure is caused by the influence of the grains on the flow patterns of the fluid around neighbouring grains

The more simple non-Bagnoldian models normally contain a turbulent (dynamic drag) friction proportional to the velocity squared or a Bingham (viscoplastic) fluid), while Bagnoldian models include the concept of a dispersive pressure, which implies a velocity dependent reduction of friction.

The main problems of dense snow avalanche dynamics models are related to the understanding and description of material properties that in the first place differ considerably during the flow and after deposition.

3.1 The Körner energy line block model

(C.B. Harbitz and V.P. Blagoveshchenskiy)

The Körner (1980) energy line model describes a rigid body that slides along a path with constant coefficient of dry friction, f_r. The energy line results from the graphical representation of the law of conservation of energy, which states that the sum of potential energy plus kinetic energy plus energy losses that occur, is constant along the path. When the energy losses are due to dry friction only, the energy line corresponds to the straight line between the position of rest of the centres of gravity of the sliding mass before and after the movement, Fig. 3.1.

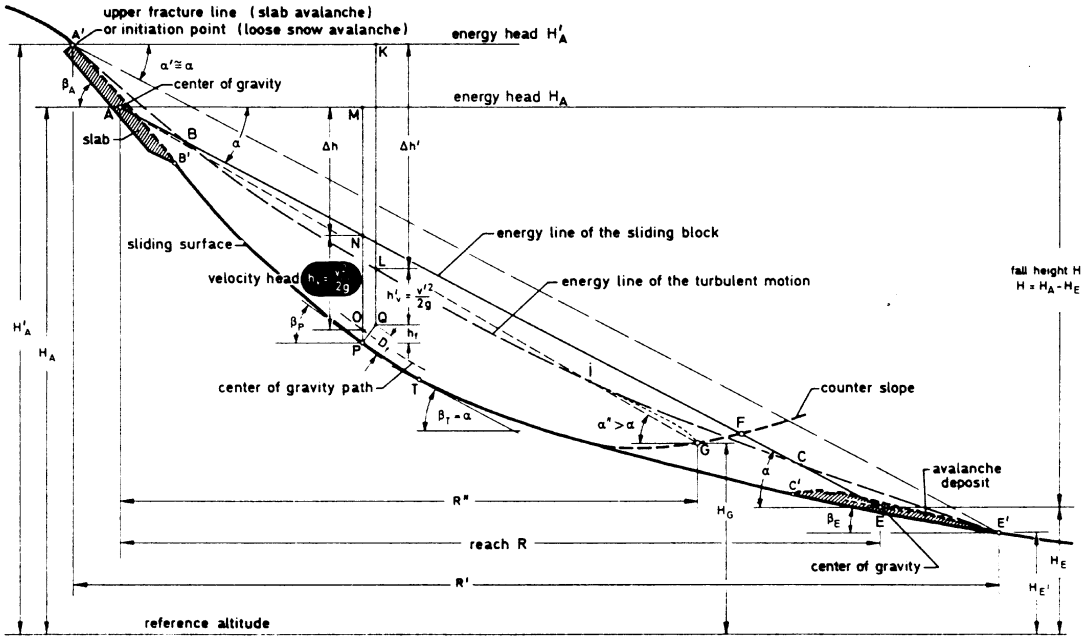

Figure 3.1: Avalanche-path profile with the energy lines (after Körner, 1980)

The slope angle of this line is given by

$$\tan\alpha = \frac{H}{R} = \frac{\text{fall height}}{\text{reach}} = f_r$$

Empirical values of α can be used to determine the reach by plotting the energy line from the starting point. The terminal point of the movement is always where the centre-of-gravity path A-E (or the slide path as an approximation) intersects the energy line.

The velocity v of the block for every point along the path is determined by

$$v = \sqrt{2gh_v}$$

where h_v is the distance between the path of the centre of gravity and the energy line, and g is the acceleration of gravity.

Körner (1976, 1980) also discusses how the energy line model can be applied to determine the two coefficients μ and ξ of the Voellmy model described below. An example of application is included.

Zenke and Hildebrandt (1983) extend the method to include a coefficient of friction varying along the path. The coefficient values at each path segment represent the regression coefficients and are multiplied by the relative length of each segment in a linear regression equation expressing the calculated overall friction coefficient. The coefficients are determined by minimising the difference between the calculated overall friction coefficient and the

observed friction coefficient expressed by tanα. Calculated coefficients of friction are presented as functions of both avalanche cross-sections along the path and avalanche scar area.

A similar energy line approach was proposed by Kozik (1962), who determined avalanche runout distance by use of the ”total drag coefficient” r only. Blagoveshchenskiy (1991) describes how the value of r depends on certain characteristics of the avalanche site and volume. His analysis is based on data from more than 300 avalanches in Tien-Shan. For channelised avalanche sites he finds that

$$r = tg\alpha + (0.25 - 0.012\alpha)\ln V + 0.2H^2$$

while the corresponding expression for non-channelised avalanche sites is

$$r = tg\alpha + (0.007 - 0.005\alpha)\ln V + 0.1H^2$$

where α is the mean slope of avalanche path from the starting zone to the point where the slope inclination becomes less than 20^o [deg], H is the total height difference of the avalanche site [km], and V is the avalanche volume [m^3]. The standard error of calculation of the runout distance in Tien-Shan by using these formulas is 10%.

3.2 The Dade and Huppert long runout energy line block model

(C.J. Keylock)

Dade and Huppert (in press) consider the problem of long running debris flows and similar phenomena via an energy-balance approach:

$$mgH - W = 0 \qquad (1)$$

If the work done (*W)* is given by a simple Coulomb resistance with constant resisting force acting over the length *L* (Eq. 2), it can be simply shown that the ratio *L/H* should be independent of event size, a fact that is clearly not the case for phenomena such as debris flows and large dry snow avalanches. This has led to the postulation of additional flow properties that may enable a reduction in friction in larger flows. For example, Melosh (1979) suggests that acoustic fluidisation of the flow could reduce the friction between particles.

$$W = FL = mgkL \qquad (2)$$

In this paper the authors employ an alternative friction law employed by Knopoff (1958) for the relaxation of stress during earthquakes:

$$W = \tau AL \qquad (3)$$

where τ is the modulus of resistance during runout. It is related to the internal deformation and friction at the lower boundary of the flow. $A = \lambda L^2$ is the total area overrun by an event, where λ is the ratio of average width to length of an event. By substituting equation 3 into equation 1 and rearranging, the authors obtain the following expression for the area covered by an avalanche:

$$A = \lambda^{1/3} (mgH/\tau)^{2/3} \qquad (4)$$

A problem with this scaling relation is determining a suitable value for the average resisting stress τ. The view put forward in this paper is that τ corresponds to the yield strength τ_y of unconfined debris in transport. The mass of debris is therefore presumed to flow in a 'plastic-like state' with a constant resisting shear stress that is approximately equal to τ_y. Separating the dynamic terms from those expressing the geometric properties of the flow leads to the definition of a friction number (N_f) given by equation 5. If one assumes that an upper bound for the square of the flow velocity scales with gH, the friction number can be considered to represent a ratio of inertial to plastic resistance forces. It is therefore analogous to a Hampton number. According to Middleton and Southard (1984), a maximum value for N_f should be approximately 10^3 for non-turbulent conditions.

$$N_f \equiv \rho gH/\tau = A^{3/2}/\lambda^{1/2}V \qquad (5)$$

From equation 5 and using the result from Middleton and Southard quoted above, if one plots deposit area against volume and introduces contours for the term $\lambda^{1/2}/N_f$, events plotting beneath the 10^3 contour can be attributed to a non-turbulent flow regime. Those events that plot beyond this value can be distinguished as belonging to a different flow regime population.

3.3 The Voellmy block model

(C.B. Harbitz)

Voellmy's (1955) model is a one-dimensional block model for the calculation of avalanche runout distance.

The sliding mass is considered as an endless fluid of height H reaching a terminal velocity by equilibrium of gravitational forces and shear forces on an infinitely long slope of constant inclination θ_1. Based on hydraulic theory, the shear forces are represented by a dynamic drag proportional to the terminal velocity squared on the free, upper surface and a combination of a similar dynamic drag and a Coulomb friction proportional to the normal forces along the bed. Hence the terminal velocity is expressed by the two-parameter formula

$$V_t = \left[\xi\, H(\sin\theta_1 - \mu\cos\theta_1)\right]^{1/2}$$

where density and drag coefficients are lumped together into the "coefficient of turbulent friction", ξ [m/s^2], and μ is the Coulomb friction coefficient. To account for lateral confinement, H is replaced by the hydraulic radius (flow cross-sectional area divided by wetted perimeter).

The deceleration starts at a certain reference point, normally located where the actual slope inclination equals $\tan^{-1}\mu$. From this point the runout distance on a slope of constant inclination θ_2 is computed by energy considerations:

$$S = V_t^2\left[2g(\mu\cos\theta_2 - \sin\theta_2) + V_t^2 g/(\xi\, H_D)\right]^{-1}$$

H_D is the mean depositional depth accounting for the energy loss due to pile-up of debris and g is the acceleration of gravity.

The computed runout distance is based on the assumption that terminal velocity is reached, and depends strongly on the selected location of the reference point, as well as on the values of the input parameters.

The values of μ and ξ are discussed by Buser and Frutiger (1980) and by Martinelli *et al*. (1980).

3.4 The PCM block model

(C.B. Harbitz and V.P. Blagoveshchenskiy)

The 2-parameter PCM-model (Perla *et al*., 1980) is a further development of Voellmy's model above. The avalanche is described as a one-dimensional block of finite mass moving on a path of varying curvature. The reference point is the initial rest position of the block's centre of mass. The equation of momentum includes Coulomb friction, centrifugal force due to curvature of the path, dynamic drag and inertia resistive ploughing. The Coulomb friction term consists of an adjustable friction coefficient μ multiplied by the normal force along the bed. The latter three terms are all proportional to v^2, the tangential velocity squared, and hence lumped together into one term consisting of v^2 divided by the second adjustable parameter interpreted as a mass-to-drag ratio, M/D [m]. The result is a linear differential equation in v^2:

$$\frac{1}{2}\frac{dv^2}{ds} = g(\sin\theta - \mu\cos\theta) - \frac{D}{M}v^2$$

where θ is the local inclination, s is the slope position and g is the acceleration of gravity. However, the inclination and perhaps the adjustable parameters are not constant along the path. An iterative solution procedure is described, dividing the slope into small segments of constant inclination and parameter values. To compensate for the absence of curvature along the linear segments, the velocity is corrected for conservation of linear momentum at each segment transition. For constant inclination and parameter values along an infinitely long slope, the result is analogous to that of Voellmy.

The usefulness of the model depends on a knowledge of the two adjustable parameters that can vary considerably. For avalanches, these values have been limited to some extent by testing the model statistically on 136 extreme paths in Northwest USA and Norway (Bakkehøi *et al*., 1981) and on 206 extreme paths in Norway (Bakkehøi *et al*., 1983).

Alean (1984, 1985) has analysed nineteen ice avalanches to establish parameter values and test whether the PCM-model might be applicable for such events. He concludes that deviations between model predictions and observations are "disappointingly high", and that a one-parameter model leads to only slightly worse predictions of runout distances for ice avalanches.

In vulnerability estimation and hazard zoning in Iceland, the model is first applied to known events where some fracture line and deposit size information can permit an estimation of M/D (Keylock, pers. comm., 1997). It is then permissible to obtain a value for μ. The values of the parameters are not adjusted downslope, but are kept constant upon a path. These same parameters can then be used to simulate an avalanche along a standard avalanche path for Iceland, found from average path profile geometry. The horizontal distance from the starting zone to the stopping position along this standard path is used to index model simulations. For example, if the avalanche ran a horizontal distance of 1400 m on the standard path, this gives an index of 14. It is then possible to move to a path where no events have been accurately recorded and to again run the model using the same parameter values. The stopping position on this path will have an index value of 14.

By choosing so called 'long', 'medium' and 'short' running known events, the runout index can be used to guide planning decisions and hazard mapping on paths where avalanches are undocumented.

Moskalev (1977) developed a two-parameter model similar to the PCM model, with a drag coefficient b [1/m] instead of the inverse mass-to-drag ratio D/M. By use of data from about 120 avalanches in Tien-Shan, Blagoveshchenskiy (1991) found that μ and b vary during the avalanche motion, and depend on avalanche type, volume and velocity. The dependency for dry avalanches is expressed as

$$\mu = 0.1 + 0.4e^{-0.048v}$$
$$b = 0.13V^{-0.35}$$

while the corresponding expression for wet avalanches is

$$\mu = 0.36 - 0.13\ln V + (0.65 - 0.23\ln V)e^{-0.12v}$$
$$b = 0.006 + 0.15V^{-0.3}$$

where V is the avalanche volume [m^3]. The standard error of the calculation of the avalanche velocity and the runout distance in Tien-Shan by using these formulas is 5%.

3.5 The McClung one-dimensional model for scaling avalanche speeds

(C.B. Harbitz and C.J. Keylock)

McClung (1990) combine avalanche speeds, runout distances, and the concepts from dense granular flows in a model for prediction of speeds along the incline. Field measurements indicate that speeds and runout distances are nearly independent of path steepness once a suitable length is chosen to scale them. Application of granular-flow concepts explains these results: the higher rate of basal shearing compensates for the increased driving force on steeper paths by increasing the dynamic friction.

The proposed model defines the extreme avalanche runout distance by statistical methods as described in Sec. 2.3, field observations or a combination of these, and calculates approximate expected speeds for one type of avalanche: the dry avalanche, which is that characterised by minimum friction and maximum speed. Since the model requires avalanche runout as input and since it is calibrated from field measurements of maximum avalanche speed, it is (by

definition) consistent with these field measurements. The speed model appears mathematically similar to simple models like Voellmy (Sec. 3.3) and PCM (Sec. 3.4), but its application is entirely different: the runout distance and avalanche-speed data are used to define the granular (speed-dependent) friction.

The most important feature of the model (and the speed data) is the steep gradient of speeds in the runout zone. These results emphasise the need for high precision in runout prediction when construction or defences are contemplated.

3.6 The Perla, Lied and Kristensen one-dimensional particle simulation model

(C.B. Harbitz)

Perla *et al.* (1984) have developed an alternative to the PCM model. The continuum model is abandoned and instead an avalanche is modelled as a collection of $\approx 10^3$ particles. The particles move randomly and independently subjected to gravity and resistive forces that have a random fluctuation computed by Monte-Carlo simulation. Each particle is allowed to move with only one degree of freedom along straight-line segments. In essence, the model uses the equation of motion for each particle mass-centre, and in no way requires that the particles, taken together, form a continuum within a defined boundary. The model includes entrainment at the avalanche front where new particles are introduced into the avalanche, when the front arrives at the next slope segment. The relative amount of entrainment is determined by pre-setting the number of injected particles in comparison to the original number of particles released from the starting segment. The applied particle model also forces entrainment-deposition to have a strong dependence on slope angles. Furthermore, the model includes the possibility of varying resistive parameters with speed and slope position.

On any slope increment a particle may experience randomly either a positive or a negative force, for simplicity modelled using only the linear term $b_1 V$. Hence, the only new parameter in the PCM momentum equation above is the random $\pm b_1 / M \cdot V$, which seemed to improve the distributions, but was introduced in an ad hoc manner and appears to lack a physical interpretation. b_1/M has units s^{-1} which physically could be interpreted in terms of collision frequency. The sign is determined by Monte-Carlo simulation.

Particle statistics computed for the 20 April 1982 Ryggfonn avalanche in Norway provide a reasonable simulation of recorded speeds and debris distribution.

3.7 The Schieldrop centre-of-mass model for avalanche motion on deflecting dams

(C.B. Harbitz)

A centre-of-mass model for avalanche motion along the side of a retaining dam was developed by Schieldrop (Irgens et. al, 1998) in co-operation with the Norwegian Geotechnical Institute. Strictly speaking, the centre-of-mass is that of a representative frontal part of the slide projected onto the terrain (the total avalanche centre-of-mass may not even reach the dam). As in the model of Nohguchi (1989) for centre-of-mass motion on a three-dimensional surface of arbitrary configuration, the equations are derived from classical mechanics, including a resistance force represented by a dynamic drag and a Coulomb friction (as in the Voellmy (1955) model). However, a lumped mass consideration does not include

any dynamics effects of the avalanche extension. Hence, the model results will be encumbered with obvious restrictions. For these reasons, it was preferred to perform a simplified geometry study of the influence of avalanche impact velocity, terrain inclination, dam configuration, and dam orientation on avalanche course deflection and run-up height along a deflection dam. An additional advantage of a simplified geometry study is that the deflecting dam does not have to be superimposed on a complex digital terrain.

The simplified dam geometry consists of a plane terrain of inclination β and the upper plane wall of the deflecting dam, oriented by its angle relative to the terrain, ψ, and the angle between the base line of the wall (the *x*-axis) and the terrain contour lines, φ, Fig. 3.2.

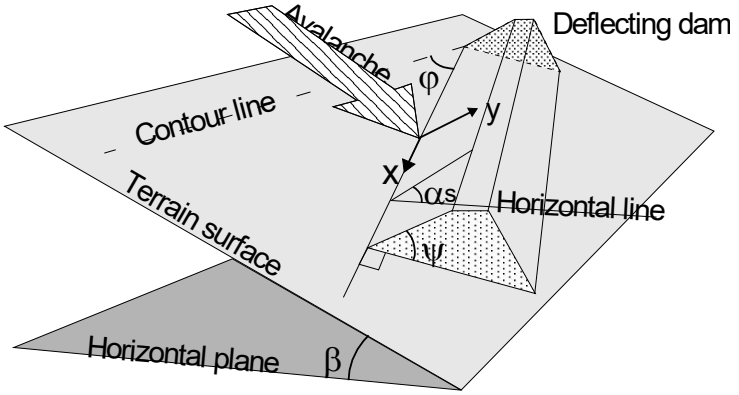

Figure 3.2: Simplified geometry configuration for centre-of-mass model.

The tangential and normal components of the centre-of-mass momentum equations are

$$\frac{dv}{dt} = g_x \cos\gamma - g_y \sin\gamma - \mu g_z - D/M \cdot v^2 \qquad (1)$$

and

$$\frac{v^2}{R} = g_x \sin\gamma + g_y \cos\gamma \qquad (2)$$

respectively, where v is the centre-of-mass velocity at time t, $g_x = g\sin\beta\sin\varphi$, $g_y = -g(\cos\beta\sin\psi - \sin\beta\cos\varphi\cos\psi)$, and $g_z = -g(\cos\beta\cos\psi + \sin\beta\cos\varphi\sin\psi)$ are components of the gravitational force per unit mass, g, in the upper wall plane, g_x along and g_y normal to the base line respectively, while g_z is the component normal to the wall plane. γ is the angle between the centre-of-mass path tangent line and the base line, μ is the dry friction coefficient, *M/D* is the mass-to-drag ratio described by Perla *et al*. (1980) and R is the radius of curvature of the centre-of-mass path line on the wall. By means of the kinematic condition $v^2/R = -v\cdot(d\gamma/dt)$ and the transcription $dv/dt = (dv/d\gamma)\cdot(d\gamma/dt)$, eqs. (1) and (2) can be combined into:

$$\frac{dv}{d\gamma} = -\left(g_x \cos\gamma - g_y \sin\gamma - \mu g_z - D/M \cdot v^2\right)v / \left(g_x \sin\gamma + g_y \cos\gamma\right), \qquad (3)$$

which is solved numerically by a fourth order Runge-Kutta procedure. The angle γ is reduced by constant increments $d\gamma$ throughout the simulations. For each new pair of (v,γ) values, the centre-of-mass is moved a distance $ds = v\cdot dt$ along the upper wall in the direction determined by the value of γ. The time increment $dt = -v\cdot d\gamma/(g_x\sin\gamma + g_y\cos\gamma)$ is found by combining eq. (2) and the kinematic condition above.

Also the effects of energy loss due to impact may be investigated by the deflecting dam model. The angle between the centre-of-mass path tangent line on the upper dam wall and the dam base line is $\gamma_0 = \tan^{-1}\left[\left(\cos^2\varphi\cos^2\psi + k^2\cos^2\varphi\sin^2\psi\right)^{1/2} / \sin\varphi\right]$, where k is the coefficient of restitution. The initial centre-of-mass velocity on the upper dam wall (in the direction determined by γ_0), is $v_0 = v_T\left(\sin^2\varphi + \cos^2\varphi\cos^2\psi + k^2\cos^2\varphi\sin^2\psi\right)$. Without any loss of energy (k=1), the initial values are $\gamma_0 = \pi/2 - \varphi$ and $v_0 = v_T$, respectively. If the centre-of-mass velocity component normal to the upper dam wall is completely lost during the impact (k=0), initial values are $\gamma_0 = \tan^{-1}\left(\cos\psi / \tan\varphi\right)$ and $v_0 = v_T\left(\sin^2\varphi + \cos^2\varphi\cos^2\psi\right)^{1/2}$. v_T is found by running the PCM model.

Comparisons with field observations and with the Irgens model, Sec. 3.19, are found in Irgens *et al*. (1998) and Domaas and Harbitz (1998). In the latter paper, the relation between the maximum calculated centre-of-mass run-up heights and the observed total run-up heights is elaborated upon for various categories of slide volumes. A best-fit line between the observed and the calculated run-up heights is suggested for practical dam design. The model is in practical use at NGI.

A similar approach for terrain deflection of avalanches is described by Jóhannesson (1998b).

3.8 The Nohguchi centre-of-mass path model

(C.B. Harbitz)

The Nohguchi (1989) model is a three-dimensional model for mass centre motion of an avalanche on a surface of arbitrary configuration. The equations describing the motion are derived from classical mechanics, including the restriction force on the flowing mass from the ground, and a resistance force represented by dynamic drag and Coulomb friction (as in the Voellmy model). The point mass is constrained to the surface by requiring that the vertical component of the normal force from the ground is directed upwards.

The equations are solved numerically by the Runge-Kutta method. Numerical simulations of real avalanches are presented. For suitable choices of the parameter values of ξ, H and μ (determining the terminal velocity, cf. Voellmy's model) the avalanche follows the observed path. However, the simulated travel path of the avalanche is strongly dependent on the parameter values. The deviation from the steepest path through the curves increases with increasing terminal velocity.

Simulations of real travel paths can be used to determine appropriate parameter values.

3.9 The Maeno and Nishimura centre-of-mass path model

(K. Nishimura)

Similar to the Nohguchi model (1989), this model (Maeno and Nishimura, 1987; Nishimura 1991) treated the motion of a centre-of-mass of an avalanche, but substantial improvements were made in many points; for example, velocity dependence was considered in the terms

representing friction and the rate of snow entrainment, and viscous resistance was automatically computed at every point on a given real three-dimensional topography. A short explanation of the model is given in the following:

1) The motion of the centre-of-mass of an avalanche on a given plane, $z = f(x,y)$ is projected and treated in a horizontal xy-plane; z-axis is vertical. Equations of motion are as follows:

$$m\frac{du}{dt}=F_x-R_x-u\frac{dm}{dt}, m\frac{dv}{dt}=F_y-R_y-v\frac{dm}{dt}, \frac{dx}{dt}=u, \frac{dy}{dt}=v$$

where m is the mass of the avalanche, F and R are the driving and resistive forces respectively, and u and v are the velocity components in the x and y directions. The z-component, w, is written as $w = u f_x + v f_y$, where $f_x = \partial f/\partial x$ and $f_y = \partial f/\partial y$. Analytical expressions of F and R are:

$F_x = -mf_xG, \quad F_y = -mf_yG, \quad R_x = u/V, \quad and\ R_y = vR/V$

where

$$G=\frac{f_{xx}u^2+2f_{xy}uv+f_{yy}v^2+g}{1+f_x^2+f_y^2}, \quad V=(u^2+v^2+w^2)^{1/2},$$

$f_{xx} = \partial^2 f / \partial x^2, \quad f_{yy} = \partial^2 f/\partial y^2, \quad f_{xy} = \partial^2 f / \partial x\, \partial y$

and g is the acceleration of gravity

2) The snow entrainment is taken into account as follows:

$k = dm / dr = (1/V)\ (dm / dt)) = \alpha\rho DW$

where ρ, D and W are the density, depth and width of the fresh snow to be entrained in the avalanche respectively. The entrainment rate, α, is dependent on the velocity such that:

$\alpha = \alpha_\infty (1 - exp(-V/V_m)),$

where α_∞ is the rate at large velocity and V_m is a constant. The constants k and α were estimated for a large dry snow avalanche, which occurred at Maseguchi on January 26, 1986, as k = (2.4 - 7.0) x 10^3 kg/m and α = 0,12 - 0,47.

3) Three resistive forces were considered: $R = \mu N + BV + CV^2$, where the first term is the Coulomb force, μ is the friction coefficient, N is the normal force $(= mG)$, BV is the viscous force and CV^2 is the turbulence force.

The friction coefficient of the Coulomb force was assumed to decrease with velocity as:

$\mu = \mu_\infty + (\mu_0 - \mu_\infty) \exp(-V/V_\mu)$

where μ_0 and μ_∞ are the friction coefficients at velocities of *0* and infinity respectively, and V_μ is a constant. Viscous force appearing in the boundary shear-layer near the bottom is important, although it has been neglected in most numerical computations. The constant B was the order of Sv/λ, where S is the area of the avalanche bottom, and λ and ν are the height and kinetic viscosity of the shear layer respectively. The value of B was estimated to range from 10^{-3} to 10^4 kg/s. The turbulence force includes air drag, internal turbulence and snow ploughing and compaction, and the constant C is of the order of 10 - 10^5 kg/m.

4) The above equations of motion were solved by a numerical computation (Runge-Kutta method), its time step being 0.1 and 0.2 s in most cases. The initial condition $(u_0, v_0, x_0, y_0, m_0)$, the topography $f(x,y)$ and the various parameters must be given before operation; in the computation on real mountainous slopes, heights are digitised on a map and input to a computer program.

It should be noted that the turbulence coefficient C (set to be 100 kg/m) must be much smaller than values frequently used if the viscous force is taken into account, B having been set to 3 000 kg/s.

3.10 The VSG refined block model

(C.B. Harbitz)

The VSG-model (Voellmy, 1955, Salm *et al*., 1990, Salm, 1993 and Gubler, 1993) is the most commonly used model for calculation of avalanche motion in Switzerland and Austria.

The model assumptions are incompressibility of flow along the whole path, steady flow and small variations of flow height along the track (i.e. between starting and runout zones) and non-steady quasi-rigid body movement in the runout zone. The model is quasi two-dimensional as it to some extent incorporates the average width of the starting zone, the track and the runout zone separately, as well as the cross-sectional shape of the track.

The computed velocity v_0 of the mass centre leaving the starting zone is computed in correspondence with the terminal velocity of Voellmy's model (for avalanches a default value of initial flow height d_0 is presented based on statistical analysis of precipitation data from Swiss mountain areas). Given the width of the starting zone, W_0, the model computes the flow rate $Q = W_0 d_0 v_0$. The terminal velocity at the bottom of the track

$$v_p = \left[\frac{Q}{W_p} \xi \, (\sin \psi_p - \mu \cos \psi_p) \right]^{1/3}$$

is based on the average width W_p of a "control section" of a few hundred meters (theoretical length as suggested by Gubler (1993)) at the lower end of the track, μ and ξ are the same coefficients as in Voellmy's model, and ψ_p is the inclination of the control section. For laterally confined tracks the terminal velocity is given by

$$v_p = \left[R\xi\,(\sin\psi_p - \mu\cos\psi_p)\right]^{1/2}$$

where R is the hydraulic radius. The numerical model also returns dynamic pressure on obstacles along the track.

The runout zone is said to begin where the inclination equals $\tan^{-1}\mu$. (Thus the runout zone starts on more gentle slopes for larger avalanches because the assumed μ values are smaller). By time-dependent modelling of the movement of the avalanche front, and assuming a linear decrease of the velocity squared

$$v^2 = d_s\xi\,(\mu\cos\psi_s - \sin\psi_s)$$

in a runout zone of average inclination ψ_s, the length of the runout zone is

$$s = \frac{d_s}{2g}\ln\left(1 + \frac{v_p^2}{v^2}\right)$$

where g is the acceleration of gravity and deposit height $d_s = \frac{Q}{W_p v_p} + \frac{v_p^2}{4\lambda g}$. The internal friction parameter of the avalanche mass, λ, determines the transfer of kinetic energy (particle speed) to potential energy (flow height). According to Harbitz (1995), the model results are not very sensitive to the value of λ (equals 2.5 for wet, dense snow avalanches). The runout zone might be divided into small segments for adjusting the parameter values and computing the velocity along the slope. The numerical program returns both the limit of the red zone (i.e. where the dynamic pressure exceeds 30 kPa) and the total runout distance.

An alternative runout model is also included (Salm, 1993), applicable when there is no enlargement of the flow width in the runout zone. In this case, the flow is modelled as a flexible sliding sheet with high internal friction. The model results in lower (more realistic) deposit heights and a faster decrease of flow speed in the runout zone. This runout model is more dependent on the value of the internal friction parameter (Harbitz, 1995).

The results of the VSG-model are critically dependent on the input values of width, length and inclination of the starting zone, initial flow height h_0, friction coefficients, cross-section of the track and inclination of the track and the runout zones. A default value of the initial flow height is presented according to the Swiss guidelines (Salm *et al*., 1990), based upon the altitude of the fracture line, the return period of the avalanche and the climatic region.

The model has been tested for avalanches by Buser and Frutiger (1980), Föhn and Meister (1982), Gubler (1987) and Lied *et al*. (1995). The latter concluded that the uncertainties for the VSG-model are as great as for the PCM- and NIS-models.

3.11 The Icelandic ”flexible box” model

(T. Jóhannesson and C.B. Harbitz)

Jóhannesson (1998b) describes a centre-of-mass model developed at the Icelandic Meteorological Office, which has been extended to include simple parameterisations of variations in the length of the avalanche due to longitudinal stress gradients and entrainment/deposition of snow by the avalanche as it flows down the path. In principle, the physical basis of the model is similar to the PCM model (Perla *et al.*, 1980) and to the Voellmy-Salm-Gubler model, that is used in the Swiss Guidelines (Salm *et al*., 1990), in that the friction is parameterised as a combination of a Coulomb-type friction component proportional to the overburden or the weight of the avalanche and a turbulent friction component proportional to the velocity squared. The parameterisation of entrainment/deposition is experimental and primarily intended for experimentation rather than for operational use.

The model computations are carried out in a curvilinear co-ordinate system that is aligned along the avalanche path. The definition of the longitudinal co-ordinate for the computations ensures that the length of the avalanche is parallel to the path along which the avalanche is flowing and no length changes are induced by movement of the avalanche over path segments with different slopes. The model considers the avalanche as a “flexible box” described by its thickness, length and width, which change as the avalanche flows down the path in response to changes in path width, entrainment/deposition and internal forces within the avalanche. The dimensional parameters are approximate scales rather than exact values, which determine the magnitude and gradients of internal stresses that lead to internal deformation of the avalanche. The width is typically predetermined and considered as a part of the definition of the path geometry. Width changes below a certain reference position in the path can, however, be dynamically calculated in a similar way as changes in the length of the avalanche. This corresponds to the situation when the avalanche spreads to the sides under its own weight. The thickness is initially treated as depending on the curvilinear co-ordinates. In the final model equations, the motion of the avalanche is, on the other hand, described by the movement of its centre-of-mass and time-dependent changes in the length and width scales of the moving avalanche body. It is assumed that the gradients of the avalanche thickness with respect to the curvilinear co-ordinates vanish near the centre-of-mass and that the shape of the avalanche may be approximated by an inverted parabola in a central main part within the dense core of the moving avalanche. At the ends of this central main part, the thickness is assumed to be one half of the thickness at the approximate location of the centre-of-mass. Similarly, the width at the approximate location of the centre-of-mass is interpreted as a scale for the width of the avalanche as it moves down the path. The assumption of a parabolic shape of the avalanche is only used to compute internal forces within the avalanche and effects of the longitudinal and transverse shape of the avalanche on the conservation equations for mass and momentum are ignored. Snow propagating outside the central region is not treated explicitly by the model, except that it is assumed that it contributes to the volume of the avalanche.

Velocity variations in the vertical and the transverse directions are ignored so that the avalanche is assumed to flow as a plug with a uniform velocity in the longitudinal direction, which is a function of distance along the path only. The transverse velocity is assumed to be determined by extension or compression in the transverse direction. Inertial or centrifugal

forces induced by the movement along a curved path, which affect the Coulomb-type friction component and the internal stresses, are included in the model. Other effects of path curvature are ignored.

The model is implemented by solving the systems of equations and initial conditions with a fourth order Runge-Kutta algorithm with a fixed step size in time. The spatial derivatives of the path geometry are computed with an adaptive smoothing algorithm based on a weighted average of the path geometry over the length scale of the avalanche. This algorithm fits a local weighted least squares second order polynomial to the path geometry at each location where the slope and the curvature are needed. The applied definition of weights limits the region that influences the slope and curvature to that where the avalanche is located at each point in time. The gradient of the width of the path, which is also sometimes needed in the computations, is found in a similar way. The choice of a least squares method for the computation of gradients in the path geometry was made because direct interpolation of the path using for instance splines or Bessel interpolation turned out to be subject to fluctuations in case of a non-uniform spacing of the points used to describe the path. Furthermore, one may also for physical reasons want to let the centre-of-mass of the avalanche respond to changes in the slope and curvature of the path averaged over the length scale of the avalanche rather than using point values. The least squares method for the computation of gradients turns out to be insensitive to small wiggles in the path geometry, which are sometimes introduced by digitisation errors when the path is derived from a topographical map. Due to the simplifications introduced and the least squares method for the computation of gradients, the model is not applicable to paths with path geometry gradients equal to or less than the length scale of the avalanche. The model assumes no loss of momentum when the avalanche flows over a terrain with slope changes and is unable to represent sharp features such as catching dams in the path geometry.

3.12 The SFISAR quasi two-dimensional model

(P. Bartelt and U. Gruber)

In recent years a numerical, depth-averaged, quasi two-dimensional, continuum model (Bartelt and Gruber, 1997; Sartoris and Bartelt, 1997; Bartelt *et al*. 1997a, 1997b) has been developed to supplement the Voellmy-Salm model (Salm *et al*. (1990), Salm (1993)) which is officially used to dimension hazard zones in Switzerland.

The numerical model tracks the motion of the avalanche from initiation to runout. The shape of the mass deposition is predicted. The model allows the implementation of different flow laws and is based on the following assumptions:

1. Flowing snow is modelled as a fluid continuum of mean constant density.
2. Flow is unsteady and non-uniform.
3. Motion is described by the mean flow velocity.
4. The vertical pressure distribution is hydrostatic. It remains hydrostatic even on steep slopes.
5. The flow width is known.
6. The flow height is the average flow height across the section, i.e. the flow height is level over the flow width.
7. A free, clearly defined top flow surface exists. A drag force can be postulated which acts on this surface; however, in the following, surface drag is neglected.
8. An avalanche track segment is flat. Centripetal pressures which modify the hydrostatic pressure distribution are not accounted for.
9. The rates of mass loss due to airborne powderisation of snow and mass increase due to input from the ground (snow pick-up) are zero, or, equal to each other.

The conditions listed above yield the following depth-averaged, one-dimensional equations for balance of mass and momentum, respectively:

$$\frac{\partial A}{\partial t} + \frac{\partial Q}{\partial x} = 0$$

$$\frac{\partial Q}{\partial t} + \frac{\partial}{\partial x}\left(\alpha \frac{Q^2}{A}\right) + \lambda\, g\, A \frac{\partial h}{\partial x} \cos\varphi = g A\left(S_0 - S_f\right)$$

where x is the distance along avalanche path, A(x,t) the cross-sectional flow area, Q(x,t) the flow discharge, α(x,t) the velocity profile factor, h(x,t) the flow height, φ(x) the slope angle, λ the active-passive pressure coefficient, g the gravity, S_0(x) the acceleration slope and S_f(x,t) the friction slope.

To date, three different flow laws have been implemented. These are a Voellmy-fluid (VF) with an active-passive pressure (adapted from Salm *et al*. (1990)), a cohesionless CEF fluid (Criminale-Ericksen-Filby, 1958) with n=2 power law viscosity coefficients (adapted from Criminale *et al*. (1958) and Norem *et al*. (1989)), and a two regime Bingham flow model (B2F) (adapted from Dent and Lang (1983). The VF model assumes that no shear strains exist within the avalanche flow plug. Shear resistance is concentrated at the base of the avalanche. Non-rectangular velocity profiles, implying shear deformations within the avalanche flow body, are simulated in the CEF and B2F models. Flow cohesion is contained in the B2F, but not in the CEF law. Longitudinal straining in all cases is governed by the active-passive pressure. The values of α, S_f and λ are given in Tab. 3.3 for all three flow laws.

Table 3.3 Velocity profile factor α, friction slope S_f and active-passive pressure values λ for the three flow laws VF, CEF and B2F

Law	α	S_f	λ
VF	1	$b\cos\varphi + \frac{sU^2}{\rho g h}$	$\lambda_a = \tan^2\left(45 - \frac{\phi}{2}\right)$ $\lambda_p = \tan^2\left(45 + \frac{\phi}{2}\right)$
CEF	$\frac{5}{4}\left[\frac{9u_h^2 + 6u_h u_0 + 5u_0^2}{(3u_h - 2u_0)^2}\right]$	$S_f = b\cos\varphi + \frac{su_0^2}{\rho g h} - \frac{9\nu_1}{8h^2}\frac{\partial}{\partial x}\left[(u_h - u_0)^2\right]$ $R = \frac{u_h}{u_0} = \left[1 + \frac{2h}{3}\sqrt{\frac{s}{\rho(m - b\nu_2)}}\right]$ $u_0 = \frac{5U}{(3R+2)}$	$1 + \frac{9\nu_1(u_h - u_0)^2}{8gh^3\cos\varphi}$
B2F (I)	1	$b\cos\varphi + \frac{su_0^2}{\rho g h}$	$\lambda_a = \tan^2\left(45 - \frac{\phi}{2}\right)$ $\lambda_p = \tan^2\left(45 + \frac{\phi}{2}\right)$
B2F (II)	$\frac{3h}{5}\left[\frac{15h - 7h_c}{(h_c - 3h)^2}\right]$	$\frac{c}{\rho g h} + b\cos\varphi + \frac{2mu_p}{gh_c h}$	

U is the depth-averaged mean velocity, λ_a is the active pressure coefficient, applied for $\frac{\partial U}{\partial x} > 0$, λ_p the passive pressure coefficient, applied for $\frac{\partial U}{\partial x} \le 0$, ϕ the internal friction angle, ρ the snow density, u_h the velocity at the top flow surface, u_0 the basal sliding velocity, u_p the plug velocity and h_c the fluidized layer height.

The Voellmy-fluid friction coefficients are the dry sliding friction b (equals μ of the classical Voellmy-Salm model) and the turbulent friction s (equals $\frac{\rho g}{\xi}$ of the classical Voellmy-Salm model).

The friction coefficients for the CEF fluid model are m, ν_1, ν_2, b and s, where m is the shear viscosity, ν_1 and ν_2 are normal stress viscosities, b is the dry sliding friction and s is the viscous sliding friction.

The two regimes of the Bingham model are defined as follows: B2F (I) is used for $\tau < \tau_y$ (Plug) and B2F (II) is used for $\tau \ge \tau_y$ (Bingham), where: τ is the shear stress and τ_y is the yield stress. The yield stress is defined by $\tau_y = c + bp$, where c is the cohesion and p is the overburden pressure.

The coefficients for the B2F (I) plug regime are the dry sliding friction, b, and the viscous sliding friction, s. For the B2F (II) Bingham regime, the coefficients are cohesion, c, internal friction, b, and shear viscosity, m.

The governing differential equations are numerically solved using either a Galerkin finite element method with numerical damping (Bartelt and Gruber, 1997) or upwinded finite differences without numerical damping (Sartoris and Bartelt, 1997). In both cases the spatial grid is fixed, i.e. an Eulerian approach is implemented. The numerical program is embedded in a GIS (geographical information system) to allow the efficient specification of real

avalanche tracks. The digital terrain model of the Swiss Federal Office of Topography is used for case studies. The terrain model has a spatial resolution of 25 m. The numerical program is provided with a graphical user interface to display simulation results (Gruber, 1998).

A numerical procedure to treat catching dams is implemented. This procedure assumes that the dams are rigid, straight and placed at right-angles perpendicular to the ground. Snow can flow over the dam, but not around it, once the height of the dam is reached. In case of an overflow, snow flows over the stationary backfill mass stopped by the dam.

The advantages in comparison to the traditional Voellmy-Salm model are:

1. *Real Terrain Description Without Point P:* No point P must be determined and it is also no longer necessary to determine, by iteration, the mean slope angle above point P. The slope of the avalanche track is determined now directly from the digital terrain model of the Swiss Federal Office of Topography. Thus, several modelling assumptions that must be made by the Voellmy-Salm model are no longer required.
2. *Visualisation from Initiation to Runout:* The graphical display of numerical results from initiation to runout allows a detailed analysis of the simulation data. For example, flow velocities and flow heights at different locations along the avalanche track can be carefully examined. In turn, this allows a better comparison to observations and a better evaluation of the quality of the simulations.
3. *Extendibility into a two-dimensional Model:* Since the model is based on an Eulerian description of flow, the model can be extended into a fully two-dimensional model. The main advantage of such a model is that the avalanche width no longer needs to be specified. A first version of such a two-dimensional model is presently being tested.

Some of the weaknesses of the classical Voellmy-Salm model also occur in the numerical model:

1. Runout distance is sensitive to the initial fracture height and length. These initial conditions are often unknown and have to be estimated.
2. The width of the avalanche from the top release zone to the runout zone must be specified in the one-dimensional model.

The flow laws are being evaluated using field studies (e.g. Examples of the Swiss Guidelines, Mettlenruns, Aulta, Leontica) and laboratory experiments described in Hutter *et al*. (1995). Theoretical comparisons are being made to the traditional Voellmy-Salm and McClung-Mears models (McClung and Mears, 1995). Detailed results of these evaluations are given in Bartelt and Gruber (1997), Bartelt *et al*. (1997a, 1997b).

It is now possible to recommend parameter combinations for different types of avalanche events. However, more experimental results are needed in order to apply the newly developed numerical models - with confidence - in practice. Therefore, in Switzerland, the legal avalanche hazard mapping procedure is still based on the classical Voellmy-Salm model. Over the next few years the numerical model will be applied to actual avalanche hazard mapping problems in parallel to the official procedure. In this way, more experience will be gained using the numerical model and, in addition, avalanche hazard experts will have a tool that provides more detailed insights into a specific avalanche problem.

3.13 The Dent and Lang biviscous quasi two-dimensional modified Bingham model

(C.J. Keylock and C.B. Harbitz)

Dent (1982) and Dent and Lang (1983) model avalanches as a combination of two linear-viscous fluids, one of which (that at the base) has a very high viscosity relative to the other. The model operates in one horizontal dimension (along the profile) and vertically within the dense core of the avalanche. The model has three parameters and assumes incompressibility of the flow, a no-slip boundary condition between flowing and stationary flow surfaces, and the exclusion of air-drag, ploughing and entrainment effects.

In a conventional Bingham fluid, the constitutive relation is in two parts, divided by a threshold stress intensity τ_0. Below this value no deformation occurs, while above it deformation is proportional to the degree to which the stress intensity τ exceeds τ_0:

$$\tau = \frac{\partial u}{\partial y} + \frac{\partial v}{\partial x} = 0 \qquad \tau < \tau_0$$

$$\tau = \mu\left(\frac{\partial u}{\partial y} + \frac{\partial v}{\partial x}\right) + \tau_0 \quad \tau \geq \tau_0$$

where u and v are velocity components in the x and y directions parallel and normal to the slope respectively, and μ is a dynamic viscosity constant.

To ease the process of determining a correct value for τ_0 (one of the model parameters) the biviscous modified Bingham model of the fluid permits small deformations within the rigid part of the flow. The high viscosity for this part of the flow regime makes any deformation negligible compared to that occurring in the area above, but because stresses may be calculated throughout the flow, the identification of the part of the flow where $\tau = \tau_0$ is simple. The new model has the form:

$$\tau = \mu'\left(\frac{\partial u}{\partial y} + \frac{\partial v}{\partial x}\right) \qquad \tau < \tau_0$$

$$\tau = \mu\left[\left(\frac{\partial u}{\partial y} + \frac{\partial v}{\partial x}\right) - \frac{\tau_0}{\mu'}\right] + \tau_0 \qquad \tau \geq \tau_0$$

where μ' and μ (the two other parameters of this model in addition to τ_0) are the dynamic viscosities in the lower and upper parts of the flow respectively. τ_0 / μ' appears as a corrective term, necessary because the velocity gradient is not zero at $\tau = \tau_0$.

The model is solved by implementing a finite-difference scheme. Stresses are calculated at cell nodes and the finite difference approximation to the momentum-balance equation when applied to these stresses yields the time flow field.

An examination of the influence of the parameters found that μ and τ_0 had a dominating effect upon the runout distance, velocity profile and motion of the leading edge. Values for these two parameters were not found from physical arguments, but were chosen to best-fit both the

runout distance and the velocity profile found from experiment. The parameter μ' had little effect on leading edge motion, a small influence on the velocity profile, but a major impact upon the distribution of debris. Its value was also found by fitting to experimental results. In the final equations for balance of momentum, the parameters always appear as a ratio to the density of the flowing masses. Hence the parameter values were selected as:

$$\mu/\rho = 0.002 \text{ m}^2 \text{ s}^{-1}$$
$$\mu'/\rho = 0.10 \text{ m}^2 \text{ s}^{-1}$$
$$\tau_0/\rho = 2.20 \text{ m}^2 \text{ s}^{-2}$$

These gave good results when compared to the experimental data for avalanches with a velocity less than 20 m s^{-1}.

3.14 MSU one- and two-dimensional models

(M.E. Eglit)

MSU - models of dense avalanches were developed by researchers of Moscow State University (the first papers were those by Grigoryan, Eglit, and Yakimov, 1967; Eglit, 1968). They are based on the fact that usually the characteristic length of an avalanche is much larger than its thickness. It is therefore possible to use an approach analogous to that applied in shallow-water theory or in hydraulics: the continuity and momentum equations are averaged over the coordinate perpendicular to the bottom (for avalanches on wide slopes) or over cross-section (for avalanches in chutes) and the acceleration component normal to the slope is neglected.

In MSU-models the coupled partial differential equations for an avalanche flow are similar to those for an unsteady flow in a river or on a slope. The essential difference are: 1) inclusion of dry component of friction together with hydraulic one; 2) special conditions at the leading edge of an avalanche taking into account that properties of the snow in an avalanche differ from those in the snow cover ahead of it.

One-dimensional model: The simplest variant of equations for a one-dimensional motion on a wide slope has the form

$$\frac{\partial h}{\partial t} + \frac{\partial hv}{\partial x} = 0$$
$$\frac{\partial v}{\partial t} + v\frac{\partial v}{\partial x} = g\sin\psi - \frac{1}{2h}\frac{\partial}{\partial x}\left[h^2\left(g\cos\psi + \frac{v^2}{R}\right)\right] - \left(f_1 + f_2\right) \qquad (1)$$

Here $f_1 = \mu\left(g\cos\psi + \frac{v^2}{R}\right)\text{sign}v$ and $f_2 = k\frac{v^2}{h}\text{sign}v$ denote the dry and hydraulic friction respectively, t and x are the time and the coordinate along the slope; $v(x,t)$ and $h(x,t)$ are the velocity and thickness (depth) of the flow; $\psi(x)$ is the slope angle; $R(x)$ is the radius of curvature of the path; μ is the coefficient of dry friction, and k is the coefficient of hydraulic turbulent friction.

Boundary conditions for the equations (1) are conditions (2) and (3) on the leading $(x = x_f)$ and tailing $(x = x_0)$ edges of the avalanche.

The zone of the avalanche leading edge where the snow cover is disrupted and incorporated into the body of the avalanche is modelled by a "hydraulic" jump. Snow parameters on an avalanche front $x = x_f$ satisfy the relations (the mass and momentum conservation laws)

$$\rho \bar{h}(w - \bar{v}) = \rho_0 h_0 w$$

$$\rho_0 h_0 w \bar{v} = \frac{1}{2}\rho h^2 \left(g\cos\psi + \frac{v^2}{R} \right) - \sigma_* h_0 \equiv v \qquad \text{at} \quad P \geq 0 \qquad (2)$$

Here w is the speed of the avalanche front, $\bar{h}$ is its height and $\bar{v}$ the snow velocity on the front; σ_* is the compressional strength of the layer of snow cover torn off by the avalanche, and ρ and ρ_0 are densities of snow in the avalanche and in the snow cover. If $P<0$, i.e., the force acting from the side of the avalanche on the snow cover is insufficient to disrupt it, then in place of the second relation (2) one of the following conditions can be used that mean, respectively, stopping of the avalanche front, motion with entrapment of only part of snow cover, and motion over the snow cover without entrapment of snow:

$$w = \bar{v} = 0; \quad h_0 = \frac{\rho \bar{h}^2 g\cos\psi}{2\sigma_*}; \quad w = \bar{v}; \quad \bar{h} = h_0 = 0$$

At the tailing edge the condition

$$v = 0 \qquad (3)$$

is assumed.

Later model extensions: The two - dimensional motion of an avalanche was considered (Kulikovsky and Eglit, 1973; Mironova, 1985). The lateral spreading of an avalanche can be calculated by this model.

The equations for motion in chutes with different cross-sections were written and investigated (Ostroumov, 1972; Danilova and Eglit, 1977a).

Additional terms connected with the curvature of the slope were included into the equations (Eglit, 1982, 1983).

Entrainment of snow by all parts of an avalanche (not only by the front part) was included (Ostroumov, 1972).

Modified expressions for the friction force were suggested concerning both dry and hydraulic friction components.

The Coulomb law for dry friction was modified by introduction of an upper limit for the value of dry friction: the shear stress τ at the base is equal to μp, where μ is the friction coefficient and p is the pressure at the base, if μp is not larger than the shear strength τ_* of the material over which the avalanche moves. Otherwise it is equal to τ_* (Grigoryan, 1979).

Furthermore, it was taken into account that the friction force for stopped parts of an avalanche (on the stopping section of the avalanche path) should be taken equal to an active force - the sum of gravity force and pressure gradient (Eglit, 1983).

The hydraulic friction was taken to be proportional to the square of velocity at Reynolds number *Re* larger than Re_{cr} and to velocity at $Re < Re_{cr}$ (Eglit, 1983).

Analytical solutions for avalanche motion on long homogeneous slopes: Analytical investigation of the equations was made. In particular conditions for instability of an avalanche flow and formation of rolling waves on the avalanche body were obtained. These conditions should be taken into account when one choose a numerical method for calculation of avalanche dynamics parameters.

Some analytical solutions were constructed for motion on long homogeneous slopes and in long homogeneous chutes (Bakhvalov and Eglit, 1970, 1973; Danilova and Eglit, 1977a, b; Mironova, 1987). These solutions provide approximate formulae for dynamics parameters of avalanches moving along slowly varying paths. Besides they can be used for controlling numerical calculations.

Below the examples of analytical formulae for the avalanche front height $\overline{h}$ and its speed *w* are given for avalanches moving down long homogeneous slopes.

i) An avalanche moving without entrainment of snow from the slope.

$$\overline{h} = \frac{3V}{x_f}, \quad w = \sqrt{\frac{3Vg(\sin\psi - \mu\cos\psi)}{kx_f}}$$

where x_f is the coordinate of the avalanche leading edge and *V* is the volume of the avalanche per unit width.

ii) An avalanche involving snow from the slope. In this case the front velocity on a long homogeneous slope tends to a constant value w_0. The thickness of the layer of snow cover involved into the avalanche is h_0. The slope is steep, $\tan\psi > \mu + 4k$; the avalanche is not too large so that the limit shear stress τ_* is not reached: $\mu\rho gh < \tau_*$. Then

$$w_0 = \sqrt{gh_0\cos\psi}\left(1 + \sqrt{\frac{\tan\psi - \mu}{k}}\right)^{3/2}$$

iii) An avalanche involving snow from the slope. The slope is not very steep $(\mu < \tan\psi < \mu + 4k)$. Then $w \to w_0 = \sqrt{gh_0\cos\psi}\sqrt{6.75(\tan\psi - \mu)/k}$

Numerical investigation for avalanche motion on inhomogeneous slopes: Appropriate software was created for calculating the motion on inhomogeneous slopes. Numerical investigation of the models were performed. The influence of different terms and coefficients of the equations as well as the initial conditions was studied. The possible ranges of model coefficients were found. Calculations of avalanches on real mountain slopes were performed (Ostroumov, 1972; Grigoryan and Ostroumov, 1975a,b; Eglit and Sveshnikova, 1980; Blagoveshchenskiy and Eglit, 1985; Volodicheva *et al*., 1986; Mironova, 1987; Mironova and Eglit, 1988; Blagoveshchenskiy *et al*., 1995).

Below one example of the modified equations is given. These equations include a more precise account of the slope curvature.

$$\left(1-\frac{h}{R}\right)\frac{\partial h}{\partial t}+\frac{\partial hv}{\partial x}=0$$

$$\frac{\partial v}{\partial t}+\left(1+\frac{h}{2R}\right)v\frac{\partial v}{\partial x}=g\sin\psi-\frac{1+\dfrac{h}{2R}}{2h}\frac{\partial}{\partial x}\left[h^2\left(g\cos\psi+\frac{v^2}{R}\right)\right]-\left(f_1+f_2\right)$$

Dry friction f_1 is defined by different formulae in moving ($v\neq 0$) and stopped ($v=0$) parts of an avalanche:

$$f_1=\begin{cases}0 & \left(f_{11}<0\right),\\ f_{11}\operatorname{sign}v & \left(0\le f_{11}\le f_{12}\right),\\ f_{12}\operatorname{sign}v & \left(f_{11}>f_{12}\right),\end{cases}\qquad \text{at } v\neq 0;$$

$$f_1=\begin{cases}f_{13} & \left(|f_{13}|<\min\left(|f_{11}|,|f_{12}|\right)\right),\\ f_{11}\operatorname{sign}f_{13} & \left(|f_{13}|\ge f_{11},\ f_{11}<f_{12}\right),\\ f_{12}\operatorname{sign}f_{13} & \left(|f_{13}|\ge f_{12},\ f_{12}<f_{11}\right),\end{cases}\qquad \text{at } v=0;$$

where

$$f_{11}\equiv\mu\left(1+\frac{h}{R}\right)\left(g\cos\psi+\frac{v^2}{R}\right),\qquad f_{12}\equiv\left(1+\frac{h}{R}\right)\frac{\tau_*}{\rho h},\qquad \text{and}$$

$$f_{13}\equiv g\sin\psi-\frac{1+\dfrac{h}{2R}}{2h}\frac{\partial}{\partial x}\left[h^2\left(g\cos\psi+\frac{v^2}{R}\right)\right].$$

Formulae for hydraulic bottom friction f_2 are

$$f_2=\begin{cases}\dfrac{\lambda v}{h^2}\left(1+\dfrac{h}{R}\right) & \left(\dfrac{vh}{\upsilon}<\mathrm{Re}_{cr}\right),\quad \lambda=3\upsilon\\ \dfrac{kv^2}{h}\left(1+\dfrac{h}{R}\right) & \left(\dfrac{vh}{\upsilon}\ge\mathrm{Re}_{cr}\right).\end{cases}$$

where υ is the viscosity coefficient of the avalanche snow.

3.15 The Hungr quasi two-dimensional multi-material deformable body model

(C.B. Harbitz)

Hungr (1995) has developed a deformable body model for simulating the characteristics of non-steady rapid flowslides, debris flows and avalanches. The model is quasi two-dimensional based on vertically integrated equations of the balance of mass and linear momentum and with a simplified lateral confinement. The slide mass is represented by a number of blocks contacting each other, free to deform and retaining fixed volumes of material along a vertically curved path.

The block representation leads to a Lagrangian centred finite difference explicit numerical solution referenced to curvilinear co-ordinates and a moving mesh. The momentum equation is applied to narrow columns of the flow, called "boundary blocks". The continuity equation for balance of mass is applied to "mass blocks" of fixed volume separating the boundary blocks. All interpolations are predicated on the assumption that both flow surface and path are reasonably smooth. Spline function fitting ensures smoothness of the path profile.

The driving force, F, acting on each boundary block of heights H_i and widths B_i, i=1 to n, consists of the tangential component of weight, the basal resisting force, T (described below), and the tangential internal pressure resultant, P:

$$F = \gamma\ H_i B_i ds\ \sin\alpha + P - T$$

where γ is the bulk unit weight and α is the inclination (the nominal length ds of the boundary block, measured in the direction of the curvilinear co-ordinates, cancels out in the equations, once all the forces are evaluated).

The new velocity, v_i, of each boundary block at the end of a time step is obtained from the old velocity, v_i', by numerical integration of Newton's second law:

$$v_i = v_i' + \frac{g(F\Delta t - M)}{\gamma\ H_i B_i ds}$$

where Δt is the time increment, and g is the acceleration due to gravity. The term M is a momentum flux resulting from material deposition (M=0) or entrainment ($M=\Delta m \cdot v$, where Δm is the mass increment entrained during the time step). The erosion or deposition rates of each boundary and mass block are assumed constant percentages of the cross-sectional area per unit displacement. The volume changes are applied only in designated zones along the path.

A second integration is used to obtain the curvilinear displacements, S_i, of the boundary blocks following the time step (old displacements primed):

$$S_i = S_i' + \frac{\Delta t}{2}(v_i + v_i')$$

The new positions of the boundary blocks are now known. The average depth of the flow in the mass blocks, h_j, j=1 to n-1, is determined so as to maintain their constant volume, V_j:

$$h_j = \frac{V_j}{(S_{i+1} - S_i)(B_{i+1} + B_i)/2}$$

The new height of each boundary block is calculated as the mean of the depths of the adjacent mass blocks:

$$H_i = \frac{h_{j-1} + h_j}{2}$$

while the end mass blocks are assumed to be triangular:

$$H_1 = \frac{h_1}{2} \qquad H_n = \frac{h_{n-1}}{2}$$

A lateral pressure coefficient k reflects the longitudinal rigidity of the flowing mass. It depends on the tangential compressive strain, and is defined both for the boundary blocks, k_i, and for the mass blocks, k_j. Under hydrostatic conditions k equals 1, and for a dry granular material with friction, it may range between the active and passive coefficients k_a and k_p. The longitudinal pressure gradient at each boundary block is obtained as the average for the two adjacent mass blocks using the following equation (s_j values are the curvilinear displacements of the mass block centres):

$$k_i \frac{dH}{ds} = \frac{1}{2}\left[\frac{k_j(h_j - H_i)}{s_j - S_i} + \frac{k_{j-1}(H_i - h_{j-1})}{S_i - s_{j-1}}\right]$$

The coefficient k_j is increased or decreased by a value equal to the incremental strain multiplied by a stiffness coefficient, as shown in Fig. 3.3:

$$k_j = k'_j + S_{cu}\Delta\varepsilon_j$$

where the stiffness coefficient S_{cu} is taken as $S_c = (k_p - k_a)/0.05$ for compression and $S_u = (k_p - k_a)/0.025$ for unloading. The minimum and maximum values that k_j can reach correspond to the active and passive states. The incremental strain in each mass block during a time step, $\Delta\varepsilon_j$, is calculated from the displacements of the adjacent boundary blocks:

$$\Delta\varepsilon_j = \frac{(S_{i+1} - S_i) - (S'_{i+1} - S'_i)}{S'_{i+1} - S'}$$

Now the longitudinal pressure differential on each boundary block may be determined as:

$$P = k\gamma \frac{dH}{ds}\left(1 + \frac{a_c}{g}\right) H_i B_i \cos\alpha \; ds$$

based on the assumption that the flow lines are approximately parallel to the bed and that the pressure parallel to the path increases linearly with depth. $a_c = v_i^2 / R$ is the centrifugal acceleration, dependent on the vertical curvature radius of the path, R.

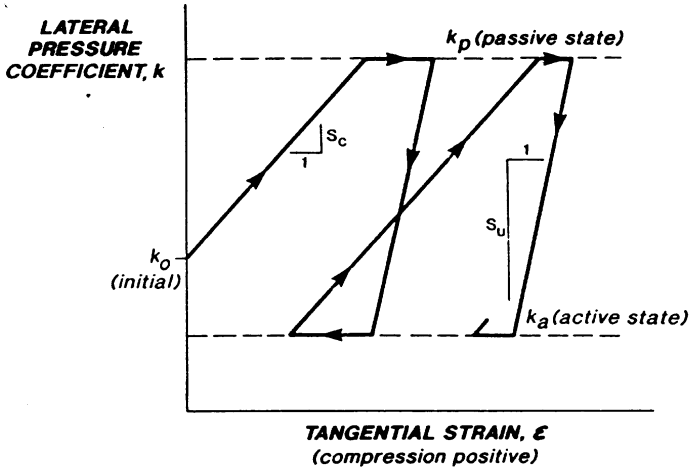

Figure 3.3: Method of calculating the lateral pressure coefficient k in a mass element as a function of changing tangential strain. Initially, k is equal to an "at rest" coefficient k_0, usually 1.0. As each mass block expands or contracts during motion to maintain geometric compatibility, k changes following a path similar to that shown in the diagram. Stiffness coefficient: S_c, compression; S_u, unloading (after Hungr, 1995).

The functional relationship between T and other parameters of the flow is based on the assumption that the shear stress on tangential planes increases linearly with normal depth. This, together with a given rheological constitutive equation, determines a velocity-depth distribution profile and an equation for T.

The model allows the selection of seven material rheological functions (the boundary block base A_i=ds B_i):

1. *Plastic flow*: This flow is controlled by a constant shear strength, such as the steady state undrained strength, c, of liquefied material:

$$T = cA_i$$

2. *Friction flow*: T is a function only of the effective normal stress on the base of the flow. This stress depends on flow depth, bulk unit weight and pore pressure:

$$T = A_i \gamma \; H_i \left(\cos\alpha + \frac{a_c}{g} \right) (1 - r_u) \tan\phi$$

where r_u is the pore pressure coefficient (ratio of pore pressure to the total normal stress at the base of the block) which might be a function of location or elapsed time (drainage). The friction angle, ϕ, can be a function of displacement to simulate the decay of strength from peak to residual.

3. *Newtonian laminar flow*: T is a linear function of velocity with a dynamic viscosity μ. The flow resistance term is determined by the Poiseuille equation:

$$T = \frac{3A_i v_i \mu}{H_i}$$

4. *Turbulent flow*: T is a function of velocity squared. For water flow, the Manning equation with the roughness coefficient n can be used:

$$T = A_i \gamma \; v_i^2 n^2 H^{-\frac{1}{3}}$$

5. *Bingham flow*: The resisting force is a function of flow depth, velocity, constant yield strength, τ, and Bingham viscosity, μ. As for the Newtonian laminar flow, the mean flow velocity is derived from an assumption of a linear increase of shear stress with depth:

$$v_i = \frac{H_i}{6\mu}\left(\frac{2T}{A_i} - 3\tau + \frac{\tau^3 A_i^2}{T^2}\right)$$

   The determination of T requires a solution of the cubic equation above. The velocity profile associated with this formulation contains a rigid plug, riding on a zone of distributed shear. The thickness of the plug equals $\tau \; H_i / T$.

6. *Coulomb viscous flow*: The Bingham yield strength in the equation above, is made dependent on the normal stress:

$$\tau = \gamma \; H_i\left(\cos\alpha + \frac{a_c}{g}\right)(1 - r_u)\tan\phi$$

7. *Voellmy fluid*: The expression for T contains a Coulomb friction coefficient, μ, and a "turbulent friction" coefficient, ξ, as introduced by Voellmy (1955):

$$T = A_i\left[\gamma \; H_i\left(\cos\alpha + \frac{a_c}{g}\right)\tan\phi + \gamma\frac{v_i^2}{\xi}\right]$$

The rheological function and the material parameter values can vary along the slide path, or within the slide mass, for overriding of liquefiable soil or changes in pore pressure. The model allows for internal rigidity of relatively coherent slide debris moving on a thin liquefied basal layer.

To approximate a three-dimensional flow with an irregular cross-section, B_i can be taken as the top surface width and H_i is the hydraulic depth, defined as the ratio of the flow cross-sectional area divided by the top width. The surface width along the slide path is a prescribed input function. The flow resistance is assumed to act on the channel base only, while in reality it acts on the wetted perimeter of the channel. The value of the resulting error normally remains less than 10%. A second error results from the use of a constant width at any location, irrespective of the current flow depth. This error will affect the flow front and tail profile in cross-sections with sloping sides where the surface width should vary with depth. Given the moderate overall accuracy of runout predictions, possible improvements are not considered productive. According to the author, the model represents a reasonable approximation to the

three-dimensional confinement effects for all but very narrow channels. However, energy losses due to sudden constrictions or abrupt changes of cross-section or flow direction are not presently accounted for.

The importance of the lateral pressure coefficient, k, is clearly demonstrated by simulating a rock slide moving against a steep adverse slope. As observed by Hungr, "the model is shown to compare favourably with results of controlled laboratory experiments and other analytical tools (i.e. numerical models) for several different materials and problem configurations (including sudden breach of a tailings dam)" (the comments within parentheses are those of the writer). Several examples, also including practical use, are presented. Kent and Hungr (1995) have calibrated the model for flowslides from coal waste dumps.

3.16 The Breitfuss-Scheidegger one-dimensional dispersive pressure model

(C.B. Harbitz)

The model of Breitfuss and Scheidegger (1974) was originally developed for calculation of the shear velocity of debris flow motion. However, it is included in the present survey of avalanche models as it elucidates the distinction between the inertial and the macro-viscous regime, and because it is a particle model including "dispersive pressure". All these terms are of importance in the understanding of avalanche motion (cf. the NIS and Kumar models below).

Breitfuss and Scheidegger (1974) state that the mechanism of debris flow is an intermediate process between bed load transport flow in rivers and suspension flow of, for example, powder snow avalanches. They state that the fluidisation mechanism of debris flows is the one described by Bagnold (1954), where a "dispersive pressure" is present normal to the shearing direction because of particle interactions (inertial regime) or because of the influence of the grains on the flow patterns of the fluid around neighbouring grains (macro-viscous regime). It is the dispersive pressure that counteracts gravity and thus holds a mixture of water and debris in a fluidised state.

According to Bagnold (1954), one has a macro-viscous regime when

$$N = \frac{\lambda^{1/2} \sigma \, D^2 \, dU / dy}{\eta} < 40$$

and an inertial regime when $N > 450$, with a transition zone for $40 < N < 450$.
$\lambda = \left((c_0 / c)^{1/3} - 1 \right)^{-1}$ is a measure of "packing", c is the actual and c_0 the maximum possible volume concentration of the grains (equals 0.74 for spheres), D and σ is the diameter and the density of the grains respectively and η is the kinematic viscosity of the continuous phase consisting of the water including the fine suspensions; dU / dy is the shear velocity.

Assumption of steady flow conditions for a balance between shear stresses due to the dispersive stresses parallel to the slope as expressed by Bagnold (1954) and shear stresses due to gravity, yields for the shear velocity at distance y above the bed in the inertial regime

$$\frac{dU}{dy} = \frac{1}{\lambda D}\left(\frac{\rho + (\sigma - \rho)c}{0.0128\sigma} g(h - y)\sin\beta\right)^{1/2}$$

and in the macro-viscous regime

$$\frac{dU}{dy} = \frac{[\rho + (\sigma - \rho)c]g(h - y)\sin\beta}{(1 + \lambda)(1 + \lambda/2)\eta}$$

where h is the flow height, g is the acceleration of gravity, β is the slope angle and ρ is the density of the continuous phase.

Examples for computation of dU/dy, and for the velocity U at the surface, are presented with actual choices of parameter values for the inertial regime. A check for whether the regime is indeed the inertial one is also included.

3.17 The Yoshimatsu one-dimensional energy dissipation resistance model

(C.B. Harbitz)

The Yoshimatsu (1991) model is originally a deformable body model for calculation of the vertical velocity profile of soil movement. However, it is included in the present survey of avalanche models because it is a particle model including the concept of "dynamic shear", which is also important in the understanding of avalanche motion (cf. the NIS and Kumar models below). The included shear stresses are caused by interparticle friction and inelastic collision of particles, i.e. dynamic shear. The former is proportional to the normal stresses (dry friction approach) while the latter is derived from a particle array model describing the energy dissipation by particle collision (Bagnold, 1954). Assumption of steady flow conditions by balance between shear forces and gravitational forces, yields for the velocity of dry sand in a distance y normal to the slope

$$u(y) = \frac{2}{3}\left(\frac{cg(\sin\theta - \mu\cos\theta)}{\frac{\pi\sigma}{12b}\sin^2\alpha\,(1 - e^2)D^2}\right)^{1/2}\left(H^{\frac{3}{2}} - (H - y)^{\frac{3}{2}}\right)$$

whence the mean velocity is

$$\bar{u} = \frac{2}{5}\left(\frac{cg(\sin\theta - \mu\cos\theta)}{\frac{\pi\sigma}{12b}\sin^2\alpha\,(1 - e^2)D^2}\right)^{1/2} H^{\frac{3}{2}}$$

where c is the volume concentration of the particles, g is gravitational acceleration, θ is the inclination of the slope, μ is the dynamic dry friction coefficient, H is the flow height, b is the average ratio of the distance between adjacent grains to the diameter D of the grains, α is some unknown angle determined by the collision conditions including grain rotation, σ is the density of the grains and e is the coefficient of restitution for the particle collisions.

Yoshimatsu (1991) also presents experimental methods to measure the static dry friction coefficient, and proposes that the ratio of the dynamic dry friction coefficient to the static dry friction coefficient is 0.8. He also discusses observed velocity and concentration distributions. The latter distributions are used to express the value of b in terms of c.

The numerical simulations presented for runout distance and depositional shape are based on one-dimensional (depth-integrated) equations of continuity and momentum including erosion, where the shear stresses are implemented as described above. The equations are solved by finite differentiation.

Comparisons between experimental and calculated velocity profiles are presented, and according to the author "a satisfactory degree of coincidence was observed for the sedimentation process of dry sand through comparison with experimental results".

From Bagnold (1954), Sholtz *et al.* (1997) arrive at

$$\bar{u} = \frac{2}{3}(0.165)(g \sin \beta)^{1/2} \frac{H^{3/2}}{D}$$

which could be easier to interpret than the equations above. Assuming a fully developed avalanche propagating steadily along a constant slope, $D \sim H^{3/2}$ and $\bar{u} \sim H^{3/2}/D$. This means that the only way to have thicker and thicker avalanches is to have larger and larger grain sizes. It is questionable whether an avalanche really behaves this way (R. Perla, pers. comm., 1998).

3.18 The NIS quasi two-dimensional visco-plastic deformable body model

(C.B. Harbitz)

The NIS-model (Norem, Irgens and Schieldrop, 1987, 1989, Norem and Schieldrop, 1991) was originally developed for avalanches and has also been applied to submarine flowslides. Thus it is constructed to treat both kinds of energy dissipation regimes described in Sec. 1 and 3.16. The mathematical deformable body model describes a quasi two-dimensional, non-steady shear flow of varying height with slip or no-slip velocity. The shear flow moves along an arbitrary path producing centrifugal forces. The constitutive relations comprise the viscosity and visco-elasticity of a CEF fluid (Criminale-Ericksen-Filby, 1958), combined with plasticity for a cohesive material, yield (as depicted in Fig. 3.4) for the normal stresses σ_x and σ_y parallel and normal to the slope respectively, and for the shear stress τ_{xy}:

$$\sigma_x = p_e + p_u - \rho\,(\upsilon_1 - \upsilon_2)\left(\frac{dv_x(y)}{dy}\right)^r$$

$$\sigma_y = p_e + p_u + \rho\,\upsilon_2\left(\frac{dv_x(y)}{dy}\right)^r$$

$$\tau_{xy} = a + p_e \tan\varphi + \rho\, m\left(\frac{dv_x(y)}{dy}\right)^r$$

where p_e is the effective pressure (all normal compressive stresses have a positive sign according to soil mechanic practice), p_u is the pore pressure, ρ is the average density of the flowing material, υ_1 and υ_2 are the normal stress viscosities, $dv_x(y) / dy$ is the shear velocity parallel to the slope at a height y above the bed, a is the cohesion, φ is the internal friction angle, m is the shear stress viscosity and r is an exponent preliminary suggested equal to 2 for rock slides and avalanches (inertial regime) and 1 for debris flows of low concentration and submarine flowslides (macro-viscous regime).

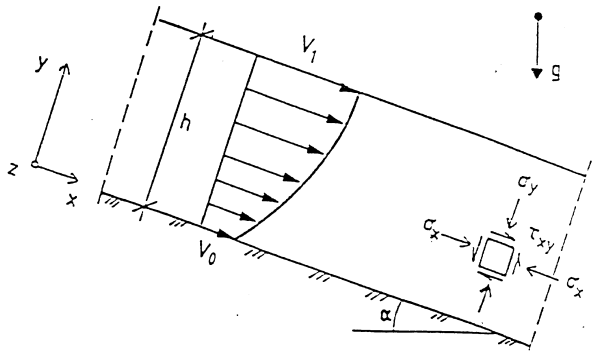

Figure 3.4: Definition of steady flow geometry (after Norem, Locat and Schieldrop, 1989)

As the viscometric functions are represented by power laws, they express flow induced dispersive pressure and dynamic shear, as described by Bagnold (1954). The model is quasi two-dimensional as the vertical velocity profile is assumed to be identical in form to the steady shear flow profile. Cohesion and/or upper surface shear stress induce a plug flow velocity profile, as opposed to the parabolic flow profile of a non-cohesive material with zero shear stress along the upper surface.

Cohesion, upper surface shear stress and erosion are omitted in the numerical model. The resulting partial differential equations for balance of mass and linear momentum are solved by a Eulerian finite difference mid-point scheme in space and a fourth-order Runge-Kutta procedure in time.

The rear and frontal grid cells in the finite-difference representation of the avalanche are considered equal to the other cells in between. Each time the accumulated volume (i.e. volume flux integrated in time) passing through the contemporary avalanche front (i.e. the foremost "wall" of the frontal grid cell) matches the volume of the grid cell ahead of the avalanche (i.e. product of contemporary avalanche front height and grid distance), the avalanche is said to advance one grid distance. Similarly, the rear grid cell is empty and neglected when the accumulated volume flowing out of the cell equals the volume contained in the cell when it was first defined to be the rear one, as the one behind was emptied.

To simplify comparison with other models, four program options are implemented:
- varying flow height and slip velocity conditions
- varying flow height and no-slip velocity conditions
- varying flow height and uniform profile
- constant flow height and velocity profile

The latter is approximately equal to the Voellmy or PCM models.

Several input parameters are required, the most important are the material friction coefficient (equals tanφ) and the initial flow height h of the avalanche. For avalanches a default value, h_{crit}, is presented for the latter (Bakkehøi and Norem, 1994), based upon the fact that an unstable situation occurs when the actual shear stress, $\tau = \rho g h \sin\theta$ equals the yield strength, $\tau_y = a + \tan\varphi \rho g h \cos\theta$, of the snow:

$$h_{crit} = \frac{a}{\rho g(\sin\theta - \tan\varphi \cos\theta)}$$

where g is the gravitational acceleration due to gravity and θ is the slope angle. The cohesion is eliminated by introducing a known reference height, h_{40}=1.3m, for a slope angle of 40°:

$$h_{crit} = h_{40} \frac{\sin 40 - \tan\varphi \cos 40}{(\sin\theta - \tan\varphi \cos\theta)}$$

A value of tanφ=0.3 (φ=17°) is applied in the computations.

Bakkehøi and Norem (1994) also suggest that the length of the initial avalanche slab should equal one sixth of the total height difference of the slide path, with a maximum of 100 m.

The numerical results are verified by comparing with laboratory (Norem *et al*., 1992) and full-scale experimental data of avalanches (Norem, Irgens and Schieldrop 1989, Norem, 1992b), submarine slides (Norem, Locat and Schieldrop, 1989) and rock slides (Locat *et al*., 1992). For avalanches and submarine slides, the front velocity and the runout distance are simulated well by the model. With varying flow height, the program is less sensitive to the shape of the path, and the computed deposits in the runout zone also agree fairly well with experimental data.

It is an admitted weakness by the authors that the model does not include effects of temperature and volume changes due to altering arrangements of the grains. Neither is the effect of active and passive earth pressure included. However, this effect is probably not significant as the internal friction is low due to the dispersive stress (Norem, pers. comm., 1995).

3.19 The Irgens one-dimensional deformable body model for three-dimensional avalanche flow

(F. Irgens and C.B. Harbitz)

The Irgens (Irgens *et al*., 1998) one-dimensional deformable body model model for three-dimensional avalanche flow is an extension of the NIS-model above. The avalanche channel path is approximated by a set of volume elements with varying widths, compensating for converging and diverging effects in a real avalanche flow. Furthermore, horizontal centrifugal effects due to the curvature of the horizontal projection of the path are taken into account. The main feature of the model is the fact that the centre line of the avalanche is a space curve, which is determined by the terrain and also by the dynamics of the flowing material. This is

in contrast to the three-dimensional model of Sassa (1988) and Lang and Leo (1994), where the centre line is a curve in a vertical plane.

A representation of the three-dimensional avalanche topography is shown in Fig. 3.5. The geometry of an avalanche channel is defined by a preliminary centre line space curve and terrain profiles in cross sections perpendicular to this line. The centre line is specified by a selected number of path points, Q_1, . . , Q_n, at the bottom of the profiles and defined by Cartesian co-ordinates (X,Y,Z). The projections of the centre line in the XY- and XZ-planes are replaced by cubic splines. The centre line is then subdivided into a chosen number of sub-segments by station points, P_1, . . , P_m. The cross sectional terrain profile at each path point Q_i is approximated by a circle of radius $R_i(X)$ as shown in Fig. 3.6. The radii R_1, . . , R_m of similar profiles at the station points, P_1, . . , P_m are found from a cubic spline through points with Cartesian co-ordinates (X,R) for the path points, Q_1, . . , Q_n. By this procedure the real avalanche channel is replaced by a set of elements between the cross sectional profiles. The avalanche of the flowing material is defined by a subset of these elements filled with snow. The height of the snow is given by $h_i(X,t)$ at the station points P_i. The circular terrain profile shown in Fig. 3.6 represents the terrain profile both at the path points, Q, . . , Q_n and the station points, P_1, . . , P_m.

The profile of the flowing material through the cross section is approximated by a circular segment. Due to centrifugal forces the trace of the free surface in the cross section will be inclined with respect to the horizontal plane. The angle of inclination θ defines the origin of the local co-ordinate systems xyz and $x\bar{y}\bar{z}$ as shown in Fig. 3.6. The x-axis is tangent to the path curve, and the $x\bar{y}$-plane is vertical. The origins are taken to be adjusted station points $\bar{P}_i$ with new global co-ordinates (X_i, Y_i, Z_i) for the calculated centre line of the avalanche. The circular segment cross section of the flowing material is further replaced by a rectangular cross section of height h and computational width w, and with the same cross sectional area A as the circular cross section. The assumption of a circular segment profile implies an interdependence between the flow width $w_1(X,t)$ and the flow height $h(X,t)$. The slope α_X and the curvature κ_{XZ} in the horizontal XZ-plane, and the slope ϕ and the curvature $\kappa_{x\bar{y}}$ in the vertical $x\bar{y}$-plane are all computed from the co-ordinates of the stations $\bar{P}_i$ and based on central difference formulas.

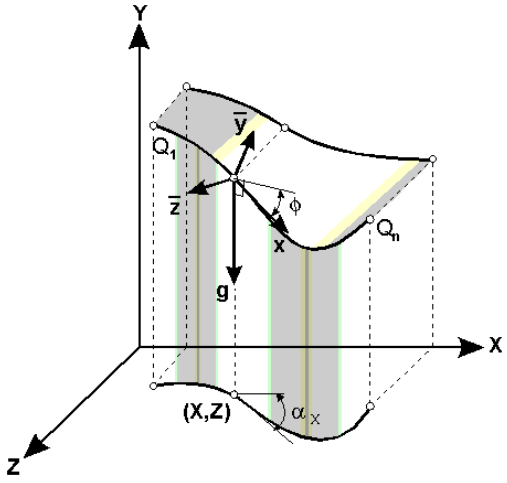

Figure 3.5: Centre line of three-dimensional avalanche. Q_1, ..., Q_n are the path points defining the centre line. XY is a vertical plane, and XZ is a horizontal plane. The x-axis is in the direction of the flow. The $x\bar{y}$-plane is vertical. ϕ is the angle of flow inclination with respect to the horizontal plane. α_X is the slope of the projection of the avalanche centre line in the XZ-plane with respect to the X-axis. g is the gravitational force per unit mass.

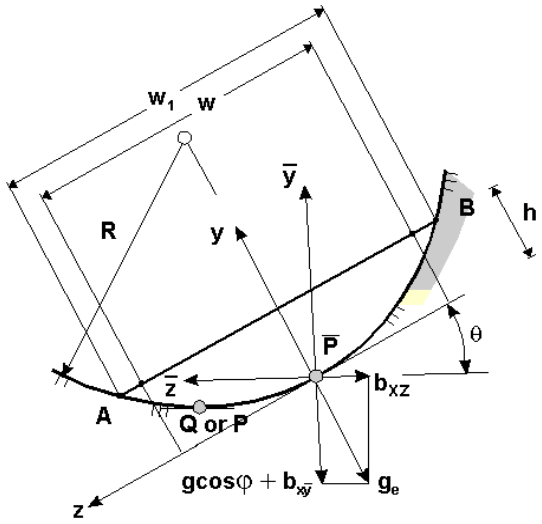

Figure 3.6: Circular segment cross sectional profile at a path point Q or a station point P. $\bar{P}$ is the adjusted station point. θ is the angle of inclination of the profile, b_{XZ} is the centrifugal force per unit mass in the XZ-plane, h is the height of the flow and is determined by the flow. w is the computational width of the corresponding rectangular profile, and is determined by h and the radius R. w_1 is the width of the circular segment.

The projected curved motion of the flowing material in the *XZ*-plane is responsible for a horizontal centrifugal force component b_{XZ} per unit mass.

$$b_{XZ} = (v_a \cos\phi)^2 \kappa_{XZ} \qquad (4)$$

where v_a is the average velocity through the cross section of the flow. Due to this centrifugal force the free surface of the flowing material will be inclined with respect to the horizontal $\bar{z}$-axis at each station profile. The gravitational force g per unit mass has a driving component $g \cdot \sin\phi$ in the x-direction and a component $g \cdot \cos\phi$ in the $\bar{y}$-direction. To the latter component we add a centrifugal force component in a vertical plane

$$b_{x\bar{y}} = (v_a \cos\phi)^2 \kappa_{x\bar{y}} \qquad (5)$$

The effective gravitational force, g_e, in the $\bar{y}\bar{z}$-plane is the resultant of these forces

$$g_e = \sqrt{(g\cos\phi + b_{x\bar{y}})^2 + b_{XZ}^2} \qquad (6)$$

This body force defines the angle of inclination θ of the free surface of the avalanche, which is determined from

$$\theta = \arctan\left(\frac{b_{XZ}}{g\cos\phi + b_{x\bar{y}}}\right) \qquad (7)$$

This angle determines the directions of the coordinate axes y and z in the $\bar{y}\bar{z}$ -plane. The flow is now considered to be two-dimensional with the velocity field given by the two components $v_x(X,y,t)$ and $v_y(X,y,t)$.

For the sake of simplicity the complete version of the simulation model presents two special options as alternatives: 1) For highly cohesive material extensional flow with a uniform streamwise velocity $v_x = v_o(X,t)$ is assumed. The constitutive equations contain terms representing active and passive pressure contributions; 2) When cohesion may be neglected, shear flow and the no-slip condition $v_x = 0$ on the bed surface $y = 0$ are assumed. On the free surface, $y = h(X,t)$, the normal stress must be equal to the atmospheric pressure, which is assumed to be equal to the pore pressure p_u, and the shear stress must be zero. The constitutive equations do not produce active and passive pressure terms in this case.

The constitutive model is similar to the one for the NIS-model above, and is described together with the numerical simulation procedure, comparison with field observations and results of the Schieldrop model (Sec. 3.7) in Irgens *et al*. (1998). At present the model has not been used for practical applications.

3.20 VARA one- and two-dimensional models

(M. Barbolini and L. Nettuno)

Introduction: VARA continuum models for simulation of snow avalanche flows have been derived in the Department of Hydraulic and Environmental Engineering of the University of Pavia, Italy, between 1993 and 1996 following an hydraulic approach, in the sense that the equation used in the models are similar to that originally derived and commonly applied for open channels flow problems. In this respect they refer only to flowing snow avalanches. The main assumption of the models are:
- the avalanche is assumed to behave (at macroscopic level) as an homogeneous one-phase continuum media;
- the interaction (exchange of mass, stresses) between the avalanche and the upper boundary (atmospheric air) is assumed to be negligible;
- the media is assumed to be incompressible;
- the flow is assumed to be shallow in the sense that H/L<<1 (Fig. 3.7). From this assumption it follows that the variation with respect to the spatial coordinate of the component of the velocity normal to the slope (Vz) can be neglected;
- the effects of vertical acceleration are neglected, so that the vertical distribution of pressure is hydrostatic;
- the sliding surface is assumed to be fixed

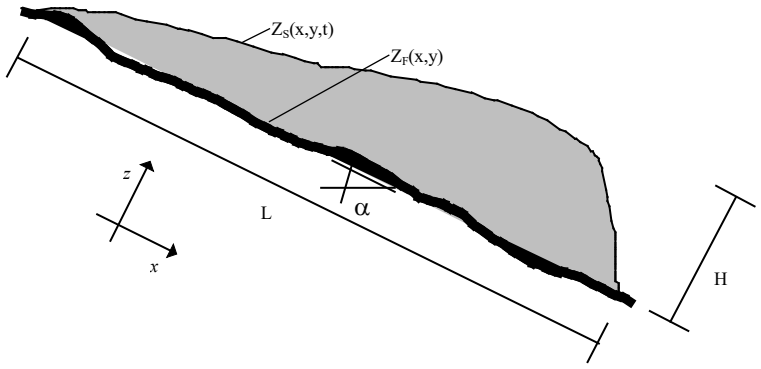

Figure 3.7: Sketch of a section of dense avalanche; H and L are two characteristic lengths.

Two-dimensional formulation: From this assumption the integration of the differential balance of mass and momentum along the normal to the slope leads to the following set of equations for the two-dimensional model (Nettuno, 1996) :

$$\frac{\partial h}{\partial t} + \frac{\partial h\bar{u}}{\partial x} + \frac{\partial h\bar{v}}{\partial y} = q_f \qquad (1a)$$

$$\frac{\partial h\bar{u}}{\partial t} + \frac{\partial(\alpha_{xx}\bar{u}^2 h)}{\partial x} + \frac{\partial(\alpha_{xy}\bar{u}\bar{v}h)}{\partial y} = g\varepsilon_x h + gh\varepsilon_z\left(-K_{ap}\frac{\partial h}{\partial x} - \frac{\bar{u}}{\|\bar{\mathbf{U}}\|}J\right) + \frac{\partial T_{xy}}{\partial y} - u_f q_f \qquad (1b)$$

$$\frac{\partial h\bar{v}}{\partial t} + \frac{\partial(\alpha_{yy}\bar{v}^2 h)}{\partial y} + \frac{\partial(\alpha_{xy}\bar{u}\bar{v}h)}{\partial x} = g\varepsilon_y h + gh\varepsilon_z\left(-K_{ap}\frac{\partial h}{\partial y} - \frac{\bar{v}}{\|\bar{\mathbf{U}}\|}J\right) + \frac{\partial T_{yx}}{\partial x} - v_f q_f \qquad (1c)$$

where $\bar{u}$ and $\bar{v}$ are the average values along the vertical of the two components of the velocity V_x and V_y; h is the local flow depth; q_f is the flow rate through the sliding surface, which permits the representation of fthe snow erosion - deposition processes along the track; α_{xx} , α_{yy} , α_{xy} are the Bousinnesq coefficients, with values related to the shape of the vertical velocity profile; ε_x , ε_y , ε_z are coefficients that are a function of local slope and which allow one to account for the component of gravity in the flow plane; K_{ap} is the pressure coefficient that accounts for the anisotropy of normal stresses, which are a function of internal and bed friction angles; $T_{xy} = \int_{z_f}^{z_S} t_{xy}\,dz$ and 0 $T_{yx} = \int_{z_f}^{z_s} t_{yx}\,dz$ are two terms which synthesise the whole dissipation within the flow (t_{ij} is the general component of the stress tensor **t**); J is the dynamic friction coefficient at the flow bed (rate between normal and shear stress), which incorporates the dissipation at the snow-snow cover interface (or snow-ground in the case of full depth snow avalanches).

The model is closed by this following further hypothesis:
- the terms T_{xy} and T_{yx} are neglected, assuming the internal dissipation to be negligible with respect to the boundary effects;

- the Boussinesq coefficients α_{xx} , α_{yy} , α_{xy} are actually set to unity (hypothesis of uniform velocity profile), and so is the pressure coefficient K_{ap}, (hypothesis of isotropy of normal stresses);
- the effect of deposition and erosion of snow along the avalanche track are not considered, i.e q_F=0;
- for the coefficient of dynamic friction on the wall the following empirical relationship is adopted at present:

$$J = \mu + n^2 \frac{\|\mathbf{U}\|^2}{h} \tag{2}$$

according to the structure of the resistance term most commonly employed in literature for the simulation of real scale events. The first term on the right-hand side of Eq. (2) is interpreted as representing the Coulomb Friction at the bed, while the second term is interpreted with reference to the resistance developed in a granular material within the "inertial" flow regime; in this sense the n coefficient should be strictly related to the physical characteristics of the material (density, diameter of snow particles) and to its flow regime (volumetric concentration), even if its evaluation is actually empirically based.

From these simplifications, which can be verified once more experimental information about the mechanical behaviour of the material is available, the following final form of the two-dimensional model equations may be derived (Nettuno, 1996):

$$\frac{\partial h}{\partial t} + \frac{\partial h\bar{u}}{\partial x} + \frac{\partial h\bar{v}}{\partial y} = 0 \tag{3a}$$

$$\frac{\partial h\bar{u}}{\partial t} + \frac{\partial(\bar{u}^2 h)}{\partial x} + \frac{\partial(\bar{\bar{u}}\bar{\bar{v}}h)}{\partial y} = g\varepsilon_x h - gh\varepsilon_z\left(\frac{\partial h}{\partial x} + \frac{\bar{u}}{\|\bar{\mathbf{U}}\|}J\right) \tag{3b}$$

$$\frac{\partial h\bar{v}}{\partial t} + \frac{\partial(\bar{v}^2 h)}{\partial y} + \frac{\partial(\bar{\bar{u}}\bar{\bar{v}}h)}{\partial x} = g\varepsilon_y h - gh\varepsilon_z\left(\frac{\partial h}{\partial y} + \frac{\bar{v}}{\|\bar{\mathbf{U}}\|}J\right) \tag{3c}$$

One-dimensional Formulation: With the same approach and hypothesis of the two-dimensional formulation, the fully one-dimensional formulation of the problem (Nettuno, 1996), able to describe flow on open slope, is obtained. This neglects the y velocity components and the y derivatives:

$$\frac{\partial h}{\partial t} + \frac{\partial \bar{u}h}{\partial x} = 0 \tag{4a}$$

$$\frac{\partial h\bar{u}}{\partial t} + \frac{\partial(\bar{u}^2 h)}{\partial x} = g\varepsilon_x h - gh\varepsilon_z\left(\frac{\partial h}{\partial x} + \frac{\bar{u}}{|u|}J\right) \tag{4b}$$

In the case of channelled flow a formulation able to take in account for gradual variation of cross section is also derived In this case the integration is performed on the cross section area instead of the normal to the slope. The resulting set of equations is written (Nettuno, 1996):

$$\frac{\partial A}{\partial t} + \frac{\partial Q}{\partial x} = 0 \qquad (5a)$$

$$\frac{\partial Q}{\partial t} + \frac{\partial \left(Q^2/A\right)}{\partial x} = g\varepsilon_x A - g\ \varepsilon_z A \frac{u}{|u|} J - g\ \varepsilon_z \frac{\partial I_1}{\partial x} + g\varepsilon_z I_2 \qquad (5b)$$

where A is the wetted cross sectional area; Q is the flow rate; *b* is the cross section width for a given flow depth; $I_1 = \int_{z_f}^{z_s} [h - z] b dz$ and

$I_2 = \int_{z_f}^{z_s} [h - z] \left[\frac{\partial b}{\partial x}\right]_{z=\cos t} dz$ are the two terms describing the pressure force variation in the flow direction and on the banks respectively.

Numerical schemes: All the presented mathematical models (equation 3a-b-c, 4a-b, 5a-b) are numerically solved with explicit finite difference schemes; at present the following different types of such schemes have been adopted to solve the equations in one- and two-dimensional forms:

- A first order modified Lax type scheme proposed by Natale and Savi (1992);
- A popular two step variant of the Lax-Wendroff explicit second order scheme proposed by MacCormack (1969), and applied to these models by Galbiati and Savi (1996);
- A second order scheme of the family of the recent high resolution Gudunov schemes in a similar form to one proposed by Nujic (1994), applied to these models by Nettuno (1996).

The one-dimensional version of these schemes have been recently compared, with respect to the numerical accuracy of the model in relation to the adopted grid spacing (Natale *et al*., 1996). This analysis, performed on the basis of analytical solutions, experimental results and real scale data, showed that the scheme's validation does not really require small spatial steps. This is because when treating real-scale problems and using the grid spacing allowed by the related cartography, the schemes appear to be highly inaccurate. To allow a satisfactory accuracy of such numerical schemes in dealing with real scale events, the fully one-dimensional models include the possibility of perform the simulation on a "virtual" grid which is automatically derived in the code on the basis of the original input topography, with a user-defined spatial discretisation.

Degree of calibration: The degree of model validation is still very low due to the lack of appropriate experimental full scale data. Also a complete calibration of the parameters of the models, represented by the drag coefficients μ and *n,* is still far from being reached; anyway, in the few applications of the model to real events (Natale *et al*., 1994; McClung *et al*., 1994; Barbolini, 1996; Nettuno, 1996) we have observed a situation similar to that observed by Swiss researchers in applying their new transient V-S model (Bartelt and Salm, 1996), that uses an analogous form for the drag term: it appears necessary for big events to allow the coefficient *n,* relating the resistance to the square of velocity (*n* is equivalent to the ζ of Voellmy-Salm model; $n^2 = 1/\zeta$), to become lower with respect to the classical values listed in the Swiss Guidelines. This work has shown the potential of models that adopt the integral continuum approach for describing the main characteristics of such flows (runout distance,

front velocity along the slope, final distribution of debris) and to treat a wide range of practical problems (avalanche risk mapping, identification and design of structural defense works) (Barbolini and Nettuno,1996).

At present, the main weakness of the models appears to be related to:
- the form adopted for the bed resistance (in particular it does not appear to be possible to properly reproduce a certain event from release to runout using constant values for the drag coefficients μ and *n);*
- the omission of an erosion term;
- the assumption of incompressibility.

Special attention is currently directed towards overcoming this weakness, but results will be achieved only when more experimental information about the mechanical behaviour of the material and quantitative data related to the exchange of mass is available.

3.21 The Murty and Eswaran quasi two-dimensional internal energy hydraulic model

(C.B. Harbitz)

Murty and Eswaran (1994a) describe the avalanche as a quasi two-dimensional hydrostatic flow (deformable body) along a gully, the geometry of which is described by the cross-sections perpendicular to the line of greatest inclination. Resistance to the flow is assumed to include both dry, laminar and turbulent (dynamic drag) friction. With these assumptions they derive the following one-dimensional equations for conservation of mass, momentum and energy respectively (Murty and Eswaran, 1994b):

$$\frac{\partial S}{\partial t} + \frac{\partial P}{\partial x} = 0$$

$$\frac{\partial P}{\partial t} + \frac{\partial}{\partial x}\left(\frac{P^2}{S}\right) + gS\cos\psi\,\frac{\partial h}{\partial x} = gS\sin\psi - f_r$$

$$\frac{\partial}{\partial t}(Su) + \frac{\partial}{\partial x}(Pu) = Vf_r$$

where t and x refer to time and distance along the path of inclination ψ, g is the acceleration due to gravity, h is the avalanche thickness, V is the snow speed, S is the cross-sectional area multiplied by density, P =SV is the mass-flow rate and u is the specific internal energy of the snow. All the dependent variables, h, V, S, P and u, are functions of x and t. The frictional term f_r is

$$f_r = f_d gS\cos\psi + f_l g\frac{P}{R^2} + f_t g\frac{P^2}{SR}$$

where f_d, f_l and f_t are the coefficients of dry, laminar and turbulent friction respectively, and R is the hydraulic radius (equal to cross-sectional flow area divided by wetted perimeter).

In general the geometrical relationship between cross-sectional flow area and h, the equation of state between u and temperature, and an equation that models the density as an empirical function of other flow variables such as velocity, temperature, etc. have to be added to the

equations above. However, so far the authors assume that the density does not vary. Furthermore, in the presented example, f_l=0.0 (while f_d=0.2 and f_t=0.02).

The equations are solved numerically by the MacCormack method which is an explicit, second order and two level predictor corrector scheme capable of capturing shocks without isolating them. A no-flux boundary condition is imposed on the upstream end of the avalanche path, and a continuity boundary condition is applied at the downstream end.

3.22 The Kumar quasi two-dimensional internal energy hydraulic model

(C.B. Harbitz)

Kumar (1994) presents an extension of the Murty and Eswaran-model, incorporating the aspects of dispersive pressure and dynamic shear as in the NIS-model. The velocity at a distance y above the bed is given by

$$V(y) = V_1 - (V_1 - V_0)(1 - \frac{y}{h})^{1.5}$$

where V_1 is the velocity at the surface of the avalanche flow, V_0 is the slip velocity along the bed and h is the avalanche thickness. The effect of compressibility might be considered by prescribing the density in the equations in accordance with Brugnot and Pochat (1981), cf. sec. 3.23.

Hence the equations of balance of mass, linear momentum and energy expressed in terms of maximum velocity V_1 are:

$$\frac{\partial(\rho A)}{\partial t} + \frac{\partial(\rho A V_1 \alpha_1)}{\partial x} = 0$$

$$\frac{\partial(\rho A V_1 \alpha_1)}{\partial t} + \frac{\partial(\rho A V_1^2 \alpha_2)}{\partial x} + \rho A\left[g\cos\theta - \frac{9\upsilon_1}{4R_h^3} V_1^2 (1 - R_v)^2 \right]\frac{\partial h}{\partial x}$$
$$= \rho g A \sin\theta - b\rho g A \cos\theta - \frac{9\rho A}{4R_h^3}(m - b\upsilon_2)V_1^2(1 - R_v)^2$$

$$\frac{\partial(\rho A u)}{\partial t} + \frac{\partial(\rho A V_1 u \alpha_1)}{\partial x} = V_1\alpha_1(b\rho g A\cos\theta + \frac{9\rho A}{4R_h^3}(m - b\upsilon_2)V_1^2(1 - R_v)^2$$

where A is the cross-sectional area of the path, u is the specific internal energy and ρ is the snow density at time t and position x along the path of inclination θ, while g is the gravitational acceleration, m is the shear viscosity, υ_1 and υ_2 are the normal stress viscosities, b is the Coulomb friction coefficient, R_h is the hydraulic mean radius and R_v=V_0/V_1. According to the author, introduction of the correction factors $\alpha_1 = (\int_A V(y)dA) / V_1 A$ and

$\alpha_2 = (\int_A V^2(y)dA) / V_1^2 A$ for mass flow rate and momentum respectively, gives more realistic values for these variables.

The third term on the left-hand side of the momentum equation represents the normal force over the cross-section due to effective and dispersive pressure, while the two latter terms on the right hand side represent shear force due to Coulomb friction and dynamic shear.

The equations are solved numerically in the same way as in the preceding Murty and Eswaran-model.

3.23 Other quasi two-dimensional hydraulic unsteady flow models

(C.B. Harbitz)

The quasi two-dimensional hydraulic flow (deformable body) models by Kulikovskiy and Eglit (1973), Grigoryan and Ostroumov (1977) and Brugnot and Pochat (1981) (all discussed by Hopfinger, 1983) were originally used for dense-avalanche flow. Depth-averaged and one-dimensional equations similar to those used for calculating unsteady flood waves have been developed by utilising the analogy with open-channel hydraulics. The assumptions of hydrostatic pressure and a horizontal free surface in the cross-stream direction, yield the following one-dimensional continuity and momentum equations including the possible effects of channelling, slope changes and entrainment:

$$\frac{\partial P}{\partial t} + \frac{\partial Q}{\partial t} = 0$$

$$\frac{\partial Q}{\partial t} + \frac{\partial (Q^2 / P)}{\partial x} + gP\frac{\partial h}{\partial x}\cos\theta = gP\left(\sin\theta - \mu\cos\theta - \frac{fQ^2}{P^2R}\right)$$

where $P = \rho A$ is the concentration (A is the cross-sectional area), $Q = PU$ is the flux at position x and time t, U is the depth-averaged velocity, h is the flow depth, g is the acceleration of gravity, μ is the dry friction coefficient and f is the dynamic drag coefficient.

The jump conditions at the front are described as an hydraulic jump. In a reference frame fixed in a front moving with velocity U_f, assuming that the shock thickness (in the moving direction) is small so that pressure forces dominate gravitational forces, continuity and momentum give

$$U_f(P - P_s) = Q$$

$$Q(U_f - U) = \frac{g\cos\theta}{n+1}(Ph - P_s h_s)$$

where θ is the slope inclination, n=1 for unconfined flow and n=2 for semicircular or triangular gullies. Subscript ‘s’ refers to the incorporated snow cover ahead of the leading edge (Brugnot and Pochat, 1981).

Brugnot and Pochat (1981) test the following form of snow density variation:

$$\rho = \frac{\rho_0}{1 + \alpha(U - U_0)}$$

where ρ_0 is the density at rest, U_0 is the threshold speed at which ρ varies and α is the coefficient of variation. Subsequently they include a sensitivity analysis of the model and conclude that the results vary extremely, depending on the selected friction value, while the sensitivity of density is less distinctive. Widening and narrowing of the gully do not effect the avalanche velocity significantly, in contrast to breaks in slopes. Depth of entrainment largely determines the zone in which the avalanche stops. Comparisons with the Voellmy model and experimental *in situ* studies produce satisfactory results.

3.24 The Hutter, Savage, Nohguchi and Koch quasi two-dimensional granular deformable body model

(C.B. Harbitz)

Hutter and Koch (1991) describe a model to predict the flow of an initially stationary mass of cohesionless granular material (rock, ice and dense flow avalanches) obeying a Coulomb-type internal friction down a rough curved bed. They apply the depth-averaged non-linear one-dimensional equations of balance of mass and linear momentum (Savage and Hutter, 1990), which in dimensionless forms are written

$$\frac{\partial h}{\partial t} + \frac{\partial (hu)}{\partial x} = 0,$$

$$\frac{\partial u}{\partial t} + u\frac{\partial u}{\partial x} = \sin\zeta - \tan\delta\,\mathrm{sgn}(u)(\cos\zeta + \lambda\kappa u^2) - \varepsilon K_{ap}\cos\zeta\frac{\partial h}{\partial x}$$

The first equation is exact, while the latter one introduces relative errors of order ε^2=(depth scale/longitudinal length scale)^2; u is the depth-averaged velocity at position x and time t, h is the flow height, ζ is the slope angle, δ is the (non-constant) bed friction angle, λ= (longitudinal length scale/scale for the radius of curvature of the bed profile), κ is the curvature and K_{ap} is the earth pressure coefficient that can take active or passive values according to whether $\partial u / \partial x$ is positive or negative. When tanδ and/or λ are smaller than order $\varepsilon^{1/2}$, and u does not become too large (upper limit not specified), then the term in the momentum equation due to centrifugal effects may be dropped. Since ζ may still vary with position, some weak curvature effects are still implicitly incorporated. The equations are solved numerically by a Lagrangian finite difference scheme that incorporates numerical diffusion (Savage and Hutter, 1989). Hutter and Koch (1991) analyse the reliability of this scheme when the numerical diffusion is varied (a conventional Eulerian finite difference scheme was first unsuccessfully attempted).

For granular flows which start as parabolic piles, the governing equations (incorporating weak curvature effects) permit similarity solutions (Savage and Hutter, 1989, Savage and Nohguchi, 1988, Nohguchi *et al*., 1989 and Hutter and Nohguchi, 1990). These are approximate solutions of the equations above because the centrifugal force term is ignored and the

variation of the slope angle ζ within the moving pile is replaced by a first-order Taylor series expansion about the centre of gravity. Savage and Nohguchi (1988) show that the motion of the centre of mass of the parabolic pile and its spread can be derived from a set of ordinary differential equations that must be solved numerically. The parabolic shape is preserved and the velocity distributions are simple.

Similarity solutions for granular flow down an inclined flat bed were previously found by Savage and Hutter (1989). They showed that the parabolic pile spreads linearly in time and its height decreases as t^{-1} when $t\rightarrow\infty$. They also found the solution for an M-wave, i.e. a pile with cliff-like edges and smaller depths towards the middle of the moving mass. Its spread grows as $t^{2/3}$ and its height decreases as $t^{-2/3}$ when $t\rightarrow\infty$. Stability analysis shows rigorously that both solutions are stable against small perturbations. A Eulerian scheme is able to reproduce the M-wave similarity solution quite well, while a Lagrangian scheme must be introduced for the parabolic pile shape.

Hutter and Koch (1991) present further laboratory experiments with various materials and bed linings. Angle of repose and bed friction angle are determined. The effect of chute walls is incorporated in an effective bed friction angle that showed a linear dependence on the pile depth. Both the general equation model and the similarity model are compared with the experimental results. Satisfactory agreement between the general equation model and the laboratory experiments is obtained if the internal angle of friction, ϕ, exceeds the total bed friction angle, δ (otherwise erosion might occur and a depth-averaged model is not appropriate), or is not close to it. Limited variations of δ along the bed do not seem to have a significant effect on the computational results. It is important to use dynamics values for ϕ and δ. For the similarity solution model no initial condition can be found that yields computational results for the position of the leading and trailing edges of the granular flow in sufficient agreement with the observations. However, when depth-to-length ratio of the initial pile geometry and the curvature of the bed are sufficiently small, this model may be used for diagnostic purposes.

3.25 The AVL quasi three-dimensional dense flow model

(P. Sampl)

Summary: A fluid mechanics model for dry dense flow snow avalanches is currently in development at AVL. Following Savage and Hutter (1989), the flowing snow is considered a cohesionless granular material. Shallowness of the flow is assumed. The model describes the two-dimensional movement of the avalanche continuum on a curved surface. A Lagrangian finite volume scheme is used for the calculation of the flow dynamics.

Physical Description: According to Savage and Hutter (1989) and, similarly, Norem (1993) the dry avalanche snow is assumed to be a cohesionless granular material, for which three different flow regimes can be distinguished:

(1) a quasistatic dense flow regime, where the snow particles are in permanent contact. Momentum transfer is due to contact and friction forces. The effect of the interstitial air is neglected. A Mohr-Coulomb yield criterion is used as constitutive relation for this regime;

(2) an inertial dense flow regime, when the dispersive pressure due to particle collisions is greater than the pressure due to gravitation. Savage and Hutter (1989) assume that only a thin layer near the bottom of the avalanche is in this state and the rest of the dense flow mass rides passively on top of this layer. This thin layer is collapsed to a boundary condition, a Coulomb-type bed friction law is assumed;

(3) a powder snow or aerosol regime, when snow particles at the upper surface of the dense flow mass get suspended in the air.

Within the dense flow avalanche regimes (1) and (2) are encountered.

Constitutive Equations: For the thin basal friction layer (regime 2) a Coulomb-type bed friction law is employed as a boundary condition, the bed friction angle δ being the parameter of this law. The parameter of the Mohr-Coulomb yield criterion for the dense flow mass above (regime 1) is the internal friction angle Φ. Together with the bed friction law active and passive states of stress must be distinguished (Koch *et al*., 1994).

Mathematical Description: The conservation laws for mass and momentum together with constitutive relations for the flowing material form the basis for dynamics calculations. Since dense snow avalanches are shallow, height-averaging is applied to the mass and momentum balances. The velocity height-profile above the basal friction layer is taken to be uniform. A local coordinate system with the first axis parallel to the velocity, the third axis normal to the avalanche bed surface and the second axis normal to the other two is used. Then

$$u_2 = u_3 = 0 \qquad (1)$$

is valid locally. The momentum balances in directions 1 and 2 averaged over a finite mass element then read

$$m_L \frac{D\overline{u_i}}{Dt} = m_L g_i - \sigma_{i3_B} A_B + \oint_{\delta V_{LAT}} \sigma_{ij} n_j dA \qquad (2)$$

where t denotes time, m_L the finite mass, u_i the velocity vector (overbar means averaging over the finite mass), g_i the vector of gravitational acceleration, σ_{ij} the stress tensor and A_B the contact area at the bottom. The surface integral sums all lateral stresses. The left hand side is the substantial derivative of the velocity. The stresses are assumed to vanish at the upper boundary of the dense flow avalanche. Together with the kinematic constraint at the surface and equation (1) one gets for the direction normal to the surface

$$m_L \frac{D\overline{u_3}}{Dt} \approx m_L \overline{u_1}^2 \frac{\partial^2 z_s}{\partial x_1^2} \approx m_L g_3 - \sigma_{33_B} A_B \qquad (3)$$

where z_s denotes the elevation of the surface in the local co-ordinate system. The lateral stresses in direction 3 are neglected. This equation gives the normal stress σ_{33B} at the bottom surface of the flow. With the bed friction angle δ the stress tensor at the bottom of the dense flow is given by

$$\sigma_{13_B} = -\sigma_{33_B} \tan\delta; \quad \sigma_{11_B} = k_{actpassX}\sigma_{33_B}; \quad \sigma_{22_B} = k_{actpassY}\sigma_{33_B}$$
$$\sigma_{12_B} = \sigma_{21_B} = \sigma_{23_B} = \sigma_{32_B} = 0 \qquad (4a\text{-}d)$$

where the active/passive earth pressure coefficients $k_{actpassX}$ and $k_{actpassY}$ are a function of the deformation rate, the bed friction angle δ and the internal friction angle Φ. For the calculation of the integral in equation (2), the stresses are assumed to vary linearly with flow hight.

Numerical Methods: A Lagrangian finite volume scheme is used for the solution of the two-dimensional dense flow equations. The flowing snow mass is decomposed into discrete elements. The Voronoi diagram (Watson, 1981) of the centre points of the elements defines the contact faces to the ground and between the elements. The body forces and the bottom shear stress can be calculated independently for each element. Lateral stresses couple the elements and are calculated at the contact faces. After all forces are summed up for each element, the element centre points are moved for one discrete timestep according to the flow equations and the procedure starts again. The advantage of the Lagrangian scheme is that the numerical reference points are always concentrated at the avalanche. With the alternative approach, a fixed Eulerian reference grid, the whole flow domain from release to runout has to be covered with grid points, which requires a much higher number of such points to obtain the same spatial resolution.

Advantages/Disadvantages of the Model:

+ model describes two dimensional movement of the deformable avalanche body on an arbitrary curved surface
+ Lagrangian grid that moves with the avalanche mass
+ model describes snow deposition
+ integrated tools for surface triangulation and definition of release area
+ graphical user interface, postscript files supported
+ supports most UNIX platforms
Ä only two-dimensional, no description of movements normal to surface
Ä no snow entrainment
Ä stability of Lagrangian scheme more difficult to achieve than that of Eulerian scheme
Ä only UNIX and LINUX version up to now

Practical Application: No practical application yet.

Verification of the Model: The model results were compared with observations of three recent major avalanche events in Austria. The predicted movement of the avalanche body looks plausible. Observed “avalanche fingers” in the runout are not predicted correctly. The front stops too early, subsequent avalanche mass seems to be deflected too much by the mass that already was deposited.

3.26 The Lang and Leo quasi three-dimensional granular deformable body model

(C.B. Harbitz)

Lang and Leo (1994) have developed a quasi three-dimensional deformable body model to describe the motion of dense avalanches, ice and rock slides. The slide masses are described as an incompressible cohesionless granular media obeying a Coulomb-type yield criterion moving down an open terrain of variable curvature in the longitudinal direction. The basal bed friction is described similarly by a Coulomb friction. An “earth pressure coefficient” is included. Lateral variations in topography and changes in volume fraction of granulate are

neglected. The mass is assumed to retain a lateral parabolic shape. This assumption is supported by experimental results reported by Lang *et al.* (1989). The model is an extension into three spatial dimensions of that by Hutter *et al*. described above. In addition a boundary drag term proportional to the velocity squared is included, as the analytical results indicate the existence of a flow transition regime analogous to a laminar to turbulent transition in a fluid.

A non-dimensional scheme is employed, choosing three characteristic length scales. The depth- and width-averaged three-dimensional balance equations including sidewise spreading of the mass are solved by a Lagrangian finite difference scheme (Savage and Hutter, 1989). With this method, the boundaries of the computational grid is convected with the depth- and width-averaged velocities. An artificial viscosity term $\mu \frac{\partial^2 u}{\partial x^2}$ is added to the equation of motion in order to smooth the solution.

According to the authors, kinematic theories predict quadratic dependence of stress on shear-rate, for rapidly shearing highly dispersed material, in good agreement with available laboratory data. The authors further state that this extreme case may be used to describe the behaviour of the dust cloud, which does not represent any type of snow avalanche activity that could be construed as destructive, and need not be considered.

This does not agree with the theory of Bagnold (1954), in which there is a linear dependence of stress on shear-rate at low solid concentrations (e.g. snow dust cloud) when energy dissipation is caused mainly by viscosity in the interstitial fluid (macro-viscous regime), while there is a quadratic dependence at high solid concentrations (e.g. dense snow avalanches) when energy dissipation is caused by particle interactions. The latter connection has proved to be important for the NIS-model described above. Besides dust clouds, or rather powder avalanches, might be severely destructive.

The numerical simulations are compared to experimental results by Lang *et al*. (1989), in plots of position and velocity versus time as well as width and height versus length. Contour or three-dimensional perspective plots are missing. The constant bed friction angle model is good for experiments with a starting zone angle of 35^o. For greater starting zone angles, the model greatly overestimates the runout distance, probably because a transition in flow regime occurs in the boundary layer where the boundary drag becomes non-negligible. When a linear combination of a constant bed friction and a boundary drag is applied, the model reflects well the general motion of the mass, and the authors state that the results justify the characterisation of the flow, and pursuance of averaged quantities. However, the maximum leading edge velocity is not attained by the model. Ideally, the boundary drag term should perhaps be included only when a critical velocity is attained.

The authors admit that some subjectivity is still required to determine constitutive parameters, and it is unknown if the models can represent naturally occurring events. Future work should include testing against natural events, determining the importance of topographical variations in the lateral direction, cohesion and particle size distribution.

3.27 The Takahashi and Yoshida/Hungr and McClung leading-edge run-up model

(C.B. Harbitz)

The traditional method of calculating avalanche run-up heights pioneered by Voellmy (1955) is based on the law of conservation of energy, including frictional energy losses, when modelling the flow as a point mass. According to McClung (1990), turbulent friction is not significant in most problems of interest with respect to run-up. Hence, including only a Coulomb-type basal resistance, the solution for the run-up height is

$$H_v = \frac{U_0^2 \sin\theta}{2g(\mu\cos\theta - \sin\theta)}$$

where U_0 is speed entering the run-up segment, θ is the inclination of the run-up barrier, g is the acceleration of gravity and μ is the dynamic Coulomb friction coefficient.

Perla *et al*. (1980) replaced U_0 by $U_0\cos(\theta_0-\theta)$ for conservation of linear momentum at the slope transition upstream of the run-up barrier, giving the corrected run-up height estimate

$$H_{vc} = \frac{U_0^2 \cos^2(\theta_0 - \theta)\sin\theta}{2g(\mu\cos\theta - \sin\theta)}$$

where θ_0 is the inclination above the slope transition.

Hungr and McClung's (1987) reformulation of the run-up equation by Takahashi and Yoshida (1979; see Takahashi (1991) for English version), allowed a calculation of the run-up of dry avalanches by considering the forces responsible for driving the front of the avalanche up the barrier with most of the mass remaining behind. Their one-dimensional expression for the time rate of change of the leading front momentum is given by

$$\frac{d(h\rho Ux)}{dt} = T_1 + T_2 + T_3 + T_4$$

where h is the flow height of the front, x is the avalanche length along the barrier at time t, U is the depth averaged speed of the avalanche front and ρ is the depth averaged avalanche density (assumed constant); $T_1 = \rho ghx\sin\theta$ is the gravity driving force, $T_2 = \rho h_0 U_0^2 \cos(\theta_0 - \theta)$ is the momentum flux between the body of the avalanche with height h_0 and its front, assuming both steady momentum supply at the toe of the barrier and supercritical flow so that the barrier does not influence the conditions upstream, $T_3 = \frac{1}{2}\rho g h_0^2 \cos\theta_0 \cos(\theta_0 - \theta)$ is the granular flow thrust force between the avalanche body and the front, analogous to depth averaged hydrostatic pressure, and $T_4 = \mu\rho ghx\cos\theta$ is the basal Coulomb friction force.

By also invoking the continuity equation

$$hx = h_0 U_0 t,$$

Takahashi (1991) and Hungr and McClung (1987) provide the following solution for the run-up height:

$$H = \frac{U^{*2} \cos^2(\theta_0 - \theta)\sin\theta}{g(\mu\cos\theta - \sin\theta)}$$

where

$$U^* = U_0\left(1 + \frac{gh_0\cos\theta_0}{2U_0^2}\right)$$

Note that the solution depends only on the incoming flow depth h_0, and not on the frontal depth h. If the fluid thrust force T_3 is neglected, then $U^* = U_0$ and the latter expression for H gives exactly twice the run-up height H_{vc} predicted by Perla *et al*. (1980) above. This is because the point mass model considers the entire mass to be lifted to height H_{vc}, and hence underestimates the run-up height compared to the leading front model, which requires only the front to be lifted to height H. Hungr and McClung (1987) showed that the comparison changes very little if turbulent drag proportional to U^2 is considered.

Experimental results by Chu *et al*. (1995) reveal that the fluid thrust force T_3 is negligible, and that the run-up height H_v based on Voellmy's (1955) approach without momentum loss at the slope transition is significantly overestimated (the opposite effect occurs if the approach angle θ_0 is close to zero). The Hungr-McClung theory (1987) provides excellent results in the intermediate range (θ=30^o) relevant for avalanche barriers constructed of earth materials. When the slope transition approaches 90^o, the maximum run-up height is determined by material that overrides that deposited previously at the bend. Neither model contains this "self-ramping" effect.

Leading-edge runout is reviewed by McClung and Mears (1995). They also compare their model to that in the Swiss Guidelines and to field examples. The results of these calculations clearly define model differences and the implications of different choices of friction coefficients.

4 SLUSH FLOW DYNAMICS MODELS

4.1 The Bozhinskiy - Nazarov quasi two-dimensional slush avalanche model

(A. Bozhinskiy)

Bozhinskiy - Nazarov`s model (1996) of slush avalanche dynamics is a quasi two-dimensional hydraulic type mathematical model which describes the unsteady motion of slush avalanches into a chute of given configuration. The model takes into account the variable density of slush avalanches and dependencies of friction and mass exchange coefficients on the degree of

water snow saturation. The model includes the incompressibility equation and the conservation mass and momentum equations

$$\frac{\partial \alpha_i}{\partial t} + \frac{\partial \alpha_i u}{\partial s} = \beta_i \qquad (1)$$

Here subscripts i = 1,2,3 relate accordingly to equations of incompressibility and conservation of mass and momentum: $\alpha_1 = F$, $\alpha_2 = \rho F$, $\alpha_3 = \rho u F$; ρ, u, F are the density, the averaged over cross section velocity and the area of cross section of slush avalanche respectively; $\beta_1 = Q$, $\beta_2 = M$, $\beta_3 = G - \partial P / \partial S - D - S$; Q, M are the volume and mass discharges of snow (and possibly rock material) that evolve into a slush avalanche; G is the moving force; $\partial P / \partial S$ is the gradient of the projection of the internal stresses in the direction of motion; D,S are respectively, the projections to the direction of motion of friction forces and drag forces connected with the change of chute form due to entrainment of snow along the chute; s is the coordinate along the slope; t is time.

The PC program was developed for the chute of rectangular cross section with given width B and depth H. Under assumption of hydrostatic distribution of pressure the entrainment terms in β_3 have the form

$$\begin{aligned} &G = \rho g h F \sin\psi, \quad P = \frac{1}{2}\rho g h F \cos\psi, \\ &D = (2h + B)\left(f_0 \rho g h \operatorname{sign} u \cos\psi + f_2 \rho u |u|\right), \\ &S = -\rho g h \cos\psi \left(h \frac{\partial B}{\partial s} + B \frac{\partial h}{\partial s} \right) \end{aligned} \qquad (2)$$

where $h = F / B$ is the depth of avalanche, ψ is the slope angle of chute; g is the acceleration of gravity; f_0, f_2 are the coefficients of dry and turbulent friction. The laws of mass exchange and friction for slush mass are formulated by analogy with the mudflows (Bozhinskiy and Nazarov 1995, 1996):

$$Q = m_e \kappa(\rho)(u - u_*)(\sin\psi - \sin\psi_*)B, \; M = \rho_s Q \qquad (3)$$

Here m_e is the non-dimensional empirical coefficient of snow entrainment, ψ_*, u_* are the critical values of slope and velocity when the entrainment takes place. The function

$$\kappa(\rho) = 1 - \exp\left[(\rho_s - \rho) / (\rho_w - \rho_s)\right] \qquad (4)$$

characterises the erosive behaviour of slush avalanche; ρ_s, ρ_w are the snow and water densities respectively. The yield coefficient for slush, $\eta = (\rho - \rho_s) / (\rho_w - \rho_s)$, is similar to that for mud mass. It is supposed that the friction coefficients are functions of the yield coefficient and consequently of the density of the slush mass, implying that $f_0 = k_0(1 - \eta)$, $f_2 = k_2 \eta$ where k_0, k_2 are constants. This means that the coefficient f_0 of dry friction is maximal for water unsaturated snow and equals to zero for water. On the other hand, the turbulent friction coefficient f_2 is maximal for water and equals to zero at $\rho = \rho_s$.

As the initial condition the snow starting mass is given, namely, we prescribe at $t = t_0$ the functions $F(s,t_0)$, $u(s,t_0)$, $h(s,t_0)$. The boundary conditions have the form

$$u(s_f,t) = w_f,\ F(s_f,t) = 0,\ \rho\,(s_f,t) = 0,$$
$$u(s_o,t) = Q(t) / \left[\rho_w F(s_o,t)\right],\ \rho\,(s_o,t) = \rho_w$$

where w_f is the front velocity. Thus the water discharge $Q(t)$ is given at the tail. The subscripts f,o correspond to the co-ordinates of the front and tail of the avalanche. The input data required for the model are the slope morphometry (the longitudinal profile, the width of chute), the point of slush avalanche origin, the discharge of water feeding the avalanche tail, the snow density, the snow depth, the initial volume of snow entrained into the motion, the coefficients of friction and entrainment. The output data are the co-ordinates of the front, the cross section area of avalanche (or the avalanche depth if the width of chute is given), the avalanche density and velocity. All output data are functions of the longitudinal co-ordinate and time. Thus, the co-ordinate of the front and the distributions of parameters mentioned above are known at each moment of time along the length of the chute. The pressure on the structures or obstacles can be calculated by the known values of density and velocity at the head of avalanche. The integral (over the length) characteristics besides the distributive ones are calculated. They are mass, volume and the average density of avalanche. The model was tested by using observed data from the right tributary of the Bear brook, the West Khybiny (Bozhinskiy *et al*., 1996) where a slush avalanche ran in 1977.

4.2 The Bozhinskiy and Nazarov two-layer quasi two-dimensional slush avalanche model

(C.B. Harbitz)

Bozhinskiy and Nazarov (1998) consider a two-layer hydraulic model with a pure water layer under a floating, water-saturated snow layer (slush). Interaction and mass exchange between the two layers and between the water or slush layer and the underlying snow cover is included. Snow entrainment, upper layer density variations, and rear end water feeding are considered in a channel of rectangular cross section. Parameters of the model are the coefficient of snow entrainment, the coefficients of dry and turbulent friction, the discharge of water feeding, the snow cover thickness and the slope angle. The dependency of depths, flow velocities and front co-ordinates of the upper and lower layers on these parameters are established. The structure and dynamics of slushflow are investigated, and an effect of water layer exhaustion due to fast absorption by entrained masses of snow is revealed.

5 POWDER SNOW AVALANCHE DYNAMICS MODELS

(Dieter Issler)

As soon as an avalanche reaches a certain threshold speed that strongly depends on the cohesion of the respective snow type (approx. 10 m/s for dry-snow avalanches), aerodynamic shear forces begin to tear off particles from the avalanche surface and to accelerate them relative to the avalanche. When they fall back on the main flow surface, the impacts may eject additional particles—a so-called *saltation layer* develops. No conclusive measurements exist,

but the density of the saltation layer is estimated to range from 10 to 50 kg/m³. At sufficiently high avalanche velocities, small saltating snow particles are suspended in the air at an increasing rate (i.e., their trajectories are no longer quasi-ballistic, but governed by the turbulence of the air), forming the characteristic "cloud" or *suspension layer* with densities in the range 1–10 kg/m³. (In the French literature on the subject, the term *aerosol* is often used for the term *suspension layer* preferred in this report). Suspension and shear stresses in avalanches are described in a general way by Norem (1995a).

The fraction of suspended material of an avalanche varies over a very broad range, depending on running distance, mass, velocity, snow granulometry, snow cover erodibility, surface topography, etc. In small or wet avalanches, the saltation layer is not strongly developed due to low velocities or large size and cohesion of the snow particles. For this reason, the suspension layer does not form or remains of very low density and tends to stay with or behind the dense flow, settling out as soon as the dense-flow part comes to rest; such powder snow clouds are irrelevant for practical purposes. However, in large dry-snow avalanches or when the avalanche falls over a cliff, a significant fraction of total avalanche mass (20–100%) may become suspended. The suspended material may move at higher velocity than the dense flow or separate from it when the latter comes to a stop, owing to large negative buoyancy and low friction. In the strict sense of the word, only in this stage would the flow be called a *powder-snow avalanche* (PSA), but commonly avalanches with a well developed suspension layer are mistakenly termed PSAs instead of *mixed avalanches*.

The models summarised in this chapter describe airborne turbulent particle flow by density current models or binary (solid-fluid) mixture models (cf. Savage and Hutter, 1990). They disregard the interaction with the dense flow and thus are not able to model the early stages of powder snow avalanche formation. For reviews, see Scheiwiller and Hutter (1982), Hopfinger (1983), Tesche (1986), Brørs (1991), Hermann and Hutter (1991), and Hutter (1996). Attempts to overcome this restriction will be examined in the subsequent chapter.

Density current models are based on local balances of total mass and linear momentum, often integrated over the current height. These models are restricted to the steep part of the track, where phase-separation and mass-change effects may be of minor importance under certain conditions. In a binary description, mass and momentum balances are formulated for each of the phases and their interaction is accounted for by the mutual interaction force. The interaction must be prescribed by a constitutive relation, which has to be adjusted by experiments because little is known about these processes. An intermediate approach—followed by many recent models—is to consider separate mass balances for snow and air, but only one momentum balance for the mixture. The justification given for this simplification is that the average relative velocity between snow particles and air is O(1 m/s)—the settling velocity of snow particles in air—and thus much smaller than the mixture velocity; snow particles have a small Stokes number and thus react rapidly to changes in air velocity. Extra diffusive and advective terms can be incorporated in the snow mass and mixture momentum balances to approximately describe the effects of relative motion.

Since powder-snow avalanches are highly turbulent, the equations have to be time averaged and the set must be closed by a turbulence closure model, e.g. a k-ε model (see Brørs, 1991). Layer averaging is often applied in order to obtain a more tractable system of differential equations. Ellison and Turner (1959), Chu *et al*. (1979), Fukushima *et al*. (1985) and Parker *et*

al. (1986) all assume steady flow conditions and derive a set of ordinary differential equations involving variations in the direction of the flow.

A set of equations for a three-dimensional turbulent model for powder snow avalanches has been developed by Scheiwiller (1986) and by Tesche (1986), and other three-dimensional powder snow avalanche models are now being developed into tools for avalanche hazard mapping in France, Switzerland and Austria. For the French and Swiss models the horizontal velocity components of the air and the particles are assumed to be equal, while the vertical velocity components of the two phases differ. This allows both entrainment and deposition of snow along the bed. The current Austrian and French developments aim at coupled dense flow/powder snow avalanche models; the powder-snow component of these models will be described in this chapter. Tab. 5.1 characterises the models described in this report with respect to their physical content, implementation and validation.

The following sections describing specific models are arranged roughly in the order of increasing physical complexity. Where a group of models share many features, one representative is described in some detail while only the key differences are emphasised for similar models. Numerical implementations are only briefly discussed because different numerical techniques may be applied to the same model and the development still goes on. As for dense-flow avalanche models, the term *block model* designates an approach treating the PSA as a mass point described by ordinary differential equations; since PSAs are extended objects, additional equations for the size change have to be specified. In such models, the centre-of-mass (or front) co-ordinate $\boldsymbol{x}(t)$ is the basic dynamical variable while the velocity $\boldsymbol{v}(t) \equiv d\boldsymbol{x}(t)/dt$ is a derived quantity, and they are considered zero-dimensional in Tab. 5.1. In models that describe the avalanche as a flow, the basic dynamical variable is the *field* $\boldsymbol{v}(\boldsymbol{x},t)$ where the co-ordinate $\boldsymbol{x}$ merely plays the role of a parameter like the time t. A model is termed one-, two- or three-dimensional if the fields depend on one (x), two (x, y), or all three components (x, y, z), respectively. As in hydraulics, many models simplify the equations by integrating the fields over the flow depth (*quasi two-dimensional* or *quasi three-dimensional* models).

At the present stage of development, reasonably sound mathematical models and efficient numerical techniques are available for density currents and binary mixtures. The methods are also well described in the literature. The remaining key problems—the modelling of the snow entrainment and deposition and the choice of the initial and boundary conditions for each application of the models—are directly connected to the scarcity of comprehensive, reliable experimental data and the concomitant lack of model validation. Nevertheless, for practical applications the recent numerical models for powder snow avalanches seem now to be able to reasonably simulate runout zones and stagnation pressure distributions. There are still major challenges to be faced before coupled models involving both the dense and turbid parts of avalanches can be developed, as will be seen in the following chapter.

Table 5.1: Summary of characteristic features of powder snow avalanche models described in this chapter. A dimension of 0 designates a (variable-size) block model; (0,1,2)+ stands for a model with 0, 1, or 2 explicit dimensions and averaging over height, (0,1)++ for height and width averaging, and 0+++ means that averaging over all avalanche dimensions has been performed (see introductory text).

Model name / Author(s)	*Dimensionality*	*Mass balances*	*Momentum balances*	*Turbulence*	*Transition layer*	*Air entrainment*	*Snow entrainment*	*Numerical scheme*	*Validation*
Voellmy	0+, stationary	0	1	no	no	no	no	none	?
AVAER (Beghin; Rapin)	0+++, non-stationary	2	1	no	no	empirical	user-prescribed	space marching	density current exp., observed PSAs
Kulikovskiy & Sveshnikova	0+++, non-stationary	2	1	no	no	boundary instability	yes	?	Russian experiments
Fukushima & Parker	0++, time-dependent	2	1	1-equation balance	no	empirical (thermal theory)	empirical (based on hydraulic exp.)	space marching	Maseguchi avalanche
Parker, Fukushima & Pantin	1+, mostly stationary	2	1	1-equation balance	no	empirical (hydraulic exp.)	empirical (based on hydraulic exp.)	space marching	Several hydraulic experiments
AVAL (Gauer)	0++ time-dep. / 1+ stationary	2	1	k-ε model depth-avg.	no	empirical (thermal theory)	empirical (based on hydraulic exp.)	Runge-Kutta in time / space	Hydraulic exp., Maseguchi aval.
AVL (Brandstätter & Sampl)	3, time-dependent	2	1 (2)	k-ε model	no	numerical simulation	no	finite-volume discretisation	density current exp., observed PSAs
SL-3D (Hermann, Issler & Gauer)	3, time-dependent	2	1 (2)	k-ε model	no	numerical simulation	empirical (based on hydraulic exp.)	finite-volume discretisation	density current exp., observed PSAs
CEMAGREF (Naaim)	3, time-dependent	2	1	modified k-ε model	no	numerical simulation	empirical (hydr. & wind tunnel exp.)	finite-volume discretisation	density current exp., observed PSAs
Tesche	3, time-dependent	2	2	extended k-ε model	no	numerical, free-surface flow	not specified	?	none
Scheiwiller	2 or 3, time-dep. or stationary	2	2	k-ε model	no	numerical, free-surface flow	no	finite diff./ weighted residuals	turbidity current experiments
SL-1D (Issler)	2×(1+), time-dep.	2+1	2×1	k-ε model depth-avg.	suspension / saltation	computed from turbulence	particle impacts	upwind finite differences	in progress

5.1 The Voellmy block model for powder snow avalanches

(D. Issler)

Voellmy's (1955) powder snow avalanche model was developed from his model for dense flow avalanches, with a few changes taking into account the nature of powder snow avalanches. It is essentially a one-dimensional block model for the calculation of asymptotic velocities, densities and pressures; only the momentum balance is considered.

Physical basis and assumptions: The density of the body is derived from the depth of the snow cover and the assumed flow height *since* no mass balance is solved. The momentum balance is derived for an endless fluid of height h; the gravitational force is assumed in equilibrium with a dry friction term and a turbulent drag proportional to v^2. The former is usually negligible, while the latter represents the turbulent entrainment of air at the avalanche-air interface. The terminal body velocity is given by

$$v_{term} = \sqrt{\xi h\left(1 - \frac{\rho_a}{\rho}\right)(\sin\varphi - \mu\cos\varphi)} \qquad (5.1.1)$$

where ξ is the coefficient of turbulent friction, φ is the slope inclination, ρ_a and ρ are the densities of flowing masses and ambient air respectively. For the calculation of dynamic pressure, two assumptions are made: (i) The velocity profile is parabolic. However, no statement is made about the density profile; (ii) At the front, a hydrostatic pressure distribution is assumed. The density at the front is determined from the equilibrium between stagnation pressure of the displaced air and hydrostatic pressure in the avalanche head. Using the above expression for the asymptotic velocity, the density in the head would have to be

$$\rho_f = \rho_a \frac{\xi}{2g}\sin\varphi \ . \qquad (5.1.2)$$

As in the dense flow avalanche model, the velocity is proportional to the flow height and asymptotically constant.

Numerical methods: Model application consists of a few simple formula evaluations.

Verification, practical applications and assessment: The model has been rarely used even before more realistic models were developed because its predictions are in open conflict with observations (e.g., no entrainment and deposition or growth of flow height with distance are contained in the model). A critical review has been given by Eglit (1984).

5.2 AVAER – a quasi three-dimensional variable-size block model by Beghin and Rapin

(F. Rapin and D. Issler)

Extensive laboratory experiments using water as the fluid and fine powders were carried out at CEMAGREF by Tochon-Danguy (Tochon-Danguy and Hopfinger, 1975; Hopfinger and Tochon-Danguy, 1977). Later on, again at CEMAGREF, Beghin extended these experiments, mostly using brine of variable salinity as a substitute for the air–snow mixture (Beghin *et al*.,

1981; Beghin and Brugnot, 1983; Beghin and Olagne, 1991). These measurements served to empirically specify the growth parameters and the shape factors of a variable-size block model that was developed by Beghin and later on by Rapin (1995) for use in consulting work at CEMAGREF.

Physical basis and model assumptions: The Beghin-Rapin model can be applied only when the powder snow avalanche flows independently of the dense-flow part. Gravity (driving force), air-entrainment effects (drag), and ground friction are the governing factors for the powder-snow part.

The PSA is assumed to be developed at the starting point of the calculation. It maintains a semi-ellipsoidal shape throughout its course, but height, length and width grow due to air entrainment. The growth coefficients are fitted from the laboratory measurements and depend on the slope angle and on the flow type (2- or 3-dimensional, with or without snow entrainment). A density dependence is acknowledged but not currently included in the model due to a lack of experimental validation. In this way, dynamics calculation of turbulent air entrainment is avoided. The mass balance takes into account the mass increase due to entrained air; snow entrainment can be specified by the user but again is not calculated dynamically (see Equation (5.2.2)).

The flow can be channelled (two-dimensional PSA) or spreading laterally on an open slope (three-dimensional PSA). Topographical situations intermediate between these two extremes (PSA with limited spreading) can be specified by the users. Sudden widening of a gully and gentle slopes (less than 15°) must be treated in a special way by the model while slope inclinations lower than 7.5° and higher than 60° are excluded in the model. The case of converging avalanche paths has not yet been studied.

From the initial and boundary data, the model calculates the PSA extensions, centre-of-mass velocity, front velocity, average density and average stagnation pressure as a function of the avalanche front co-ordinate. An empirical non-dimensionalised pressure profile is used to give information on the height dependence of the pressure.

Mathematical model: Input consists of the following variables:

φ_i : slope angles of path segments [°];
H_0, L_0, W_0 : initial height, length, and width of the PSA [m];
U_0 : initial velocity of the centre of mass [m/s];
ρ_0 : initial average avalanche density [kg/m^3]; ρ_s : density of entrained snow [kg/m^3];
h_s : height of entrainable snow cover [m]; λ : snow entrainment factor [–].

Output variables depend on the avalanche front (x_f) or centre-of-mass (x) position:

$H(x_f)$, $L(x_f)$, $W(x_f)$: height, length, and width of the PSA at front position x_f [m];
$S(x_f) = k'LW$: surface projected on the inclined plane [m^2], with $k' = \pi/4 \cong 0.75$;
$V(x_f) = kHLW$: volume [m^3] with $k = \pi/6 \approx 0.52$ for 3-dim. (open-slope) avalanches, and
$V(x_f) = kHL$ [m²] with $k = \pi/2 \cong 1.57$ for 2-dim. (confined) avalanches;
$U(x_f)$, $U_f(x_f)$: velocity of centre-of-mass and front, respectively [m/s];
$\rho(x_f)$: average avalanche density [kg/m^3]; $m(x_f) = \rho(x_f)V(x_f)$: avalanche mass [kg].

The geometry is specified by the three equations

$$\frac{dH}{dx_f} = \alpha_1(\varphi,\ldots)\,, \qquad \frac{dL}{dx_f} = \alpha_2(\varphi,\ldots)\,, \qquad \frac{dW}{dx_f} = \alpha_3(\varphi,\ldots)\,. \quad (5.2.1)$$

The values α_{1-3} for the growth rates depend on the slope angle, φ, and the track geometry (channelled two-dimensional avalanche vs. open-slope three-dimensional avalanche) and are listed in (Rapin, 1995). From this, the lower surface area, S_b, and the overall volume, V, can readily be calculated. The mass balance is expressed as

$$\frac{dm}{dx_f} = \rho_a \frac{dV}{dx_f} + \lambda h_s W \rho_s\,, \quad (5.2.2)$$

The momentum equation is expressed as

$$\frac{d}{dt}\left[\left(k_v\rho_a + \rho\right)VU\right] = \Delta\rho V g \sin\varphi - \tau_b S_b\,; \quad (5.2.3)$$

$\rho = m/V$ is the average mixture density, $k_v = (1.6 \div 2.0)H/L$ is the virtual mass coefficient. The bottom shear stress is taken as $\tau_b = C_D \rho U^2$, $C_D \cong 0.003$. $\Delta\rho \equiv \rho - \rho_a$ is the excess density of the mixture.

Numerical implementation: The avalanche *track* is discretised into segments of constant slope. The set of first-order ordinary differential equations (ODEs) in time is first converted to ODEs in space by virtue of the relation $\frac{d}{dt} = \frac{dx_f}{dt}\frac{d}{dx_f} = U_f \frac{d}{dx_f}$ and then transformed into difference equations that allow the solution to be marched down the track straightforwardly. The model is implemented as a Turbo Pascal program running on IBM-compatible PCs. A user interface allows interactive entry of topographical data, initial and boundary conditions, displays the results and keeps a log of the computations and their results.

Verification, practical applications and assessment: So far, verification has been possible against the laboratory measurements on density currents that were also used to construct and calibrate the model, and against observations of a real avalanche (Marie and Rapin, 1987). In consulting work, AVAER has been used many times as a decision aid for the experts (e. g., study of the Disputada avalanche in Chile in 1990; avalanche protection study for the Montenvers railway line near Chamonix, 1991), and it produces plausible results when used by an avalanche practitioner aware of the model's inherent limitations.

+ The lumped-mass formulation makes the numerical treatment relatively simple. Simulations can be carried out on personal computers in a short time. Even numerically inexperienced users can handle such a program.
+ The model makes very efficient use of (laboratory) experimental data in order to dispense with the need of calculating air entrainment and, as a prerequisite, turbulence.
– As in most other models, the interaction between the original dense-flow avalanche and the emerging powder snow avalanche is ignored, as is the saltation layer.
– Snow entrainment is not modelled but must be specified by the user.

- The effects of track curvature are not taken into account.
- The lumped-mass approach foregoes the possibility of obtaining vertical pressure distributions.
- The present implementation precludes model application to avalanche tracks with ascending or very steep slope segments.

5.3 The Kulikovskiy-Sveshnikova quasi two-dimensional variable-size block model

(M .E. Eglit)

Physical basis and assumptions: The KS model (Kulikovskiy and Sveshnikova, 1977) treats a powder snow avalanche as a cloud of *prescribed* geometrical form. It deals with the mass-centre velocity of the cloud, its mean density, its dimensions and form variation during the motion. The longitudinal cross-section is assumed to have a half-elliptic form with both diameters varying independently during motion.

The four basic equations of the model calculate the variation of the centre of mass velocity, length, height and mean density of the cloud. These four equations express that 1) an avalanche volume variation equals the air volume captured by the avalanche; 2) an avalanche mass variation is connected with the air and snow entrainment and also with snow sedimentation; 3) the avalanche momentum varies due to gravity, bottom friction, air drag and snow sedimentation; 4) the kinetic energy of the internal motion and deformation of the cloud is caused by gravity, the air pressure gradient on the top boundary of the cloud (due to air flow over the cloud) and turbulent diffusion.

Formulae for air and snow entrainment rates and for the other coefficients of the model are constructed on the basis of theories of turbulent jets and flows in open channels. For example, the air entrainment rate v_1 is assumed to be proportional to the avalanche velocity v and the square root of the ratio of the air density ρ_a and the cloud density ρ, i.e.

$$v_1 = kv\sqrt{\rho_a / \rho} \qquad (5.3.1)$$

This formula was used by Onufriev (1967) to calculate the motion of a circular vortex representing the front zone of a rising warm air jet and by Kalazhokov (1969) in the theory of motion of aerosol in a viscous fluid. It can be justified on the basis of the assumption that air entrainment occurs due to instability of the boundary between an avalanche and the ambient air. It is known (e.g. Landau and Lifshitz, 1983) that the rate of growth of disturbances on the boundary between two layers depends on the velocity difference of the layers and on the following combination of the fluid densities, ρ_1 and ρ_2:

$$\frac{\sqrt{\rho_1\rho_2}}{\rho_1 + \rho_2} \qquad (5.3.2)$$

If $\rho_1 = \rho_a$, $\rho_2 = \rho$ and $\rho_a << \rho$ then it can be approximated by $\sqrt{\rho_a / \rho}$ to obtain (5.3.1).

It should be specially highlighted that the crucial difference between the model of A. G. Kulikovskiy and E. I. Sveshnikova and many other models of the snow cloud is that the growth rate of an avalanche is not prescribed, but is found by solving the basic system of equations. Another difference is that the ratio of length and height of a cloud need not be

prescribed. Its variation can be calculated because the system includes the equation for kinetic energy of internal motion.

Verification and practical applications: Many computations were made with this model. The dependence of results on the initial conditions and on the values of the model coefficients was studied. The character of the motion for a variety of conditions was investigated. For example, it was found that for given slope and model coefficients all possible initial conditions could be separated into two domains: a cloud on a constant slope *grows* if its initial velocity and height are high enough and die out in the opposite case. It was also found that avalanche velocity on a constant slope at first increased with a constant acceleration dependent on the slope angle. There existed a certain limit velocity that depended mainly on the initial mass of the avalanche and the amount of snow involved from the slope. After reaching this limit velocity, the avalanche decelerated. The details can be found in (Kulikovskiy and Sveshnikova, 1977) and (Eglit and Sveshnikova, 1980).

5.4 The Fukushima-Parker quasi two-dimensional block model

(K. Nishimura and D. Issler)

This model was proposed by Fukushima and Parker (1990) and is based on the Parker-Fukushima-Pantin model (Parker *et al*., 1986) described in Sec. 5.5. It is summarised at this point because it is a block model similar in approach to the Kulikovskiy-Sveshnikova model (see Sec. 5.3).

Physical basis and model assumptions: The suspension layer of a powder snow avalanche is modelled as an elliptic half cylinder with its axis on the ground in the spanwise direction of the flow. In this way, the two-dimensional phenomenon is reduced to the motion of the centre-of-mass. Following the work of Beghin *et al.* (1981) based on laboratory experiments, the ratio of the principal axes of the ellipse, i.e., the length L over twice the height H, is assumed to depend on the slope angle φ (in degrees) as

$$\frac{L}{2H} = 4.24 \cdot \varphi^{-1/3}. \qquad (5.4.1)$$

Furthermore, the height, the length and thus the volume grow as air is entrained.

Fukushima and Parker (1990) derived the basic equations of powder-snow avalanches based on thermal theory. In this model, the following effects are also taken into account: (a) The total buoyancy of the avalanche varies freely via erosion and deposition of snow; (b) a treatment of conservation of kinetic energy of turbulence is included; (c) the angle of the slope varies in the flow direction. The model consists of four ordinary differential equations in time, i.e. the conservation equations of fluid mass, snow particle mass, momentum of the cloud, and the kinetic energy of the turbulence:

$$\frac{dA}{dt} = E_a U P_i \ , \qquad (5.4.2)$$

$$\frac{d(CA)}{dt} = v_s (E_s - r_0 C \cos\varphi)\ P_b \ , \qquad (5.4.3)$$

$$\frac{d}{dt}\left[\left(\rho + k_v \rho_a\right) UA\right] = (\rho - \rho_a) Ag \sin\varphi - \tau_i P_i - \tau_b P_b \ , \qquad (5.4.4)$$

$$\begin{aligned}\frac{d}{dt}\left[\left(\rho + k_v \rho_a\right) KA\right] &= U\left(\tau_i P_i + \tau_b P_b\right) - \rho_a RgCv_s A - \rho_a \varepsilon_0 A \\ &+ \tfrac{1}{2}\rho_a\left[\left(1 + k_v\right) E_a U P_i + Rv_s\left(E_s - r_0 C\cos\varphi\right) P_b\right] U^2 \\ &- \xi_p \rho Rg\cos\varphi\ h\left[\tfrac{1}{2} C E_a U P_i + v_s\left(E_s - r_0 C\cos\varphi\right) P_b\right].\end{aligned} \qquad (5.4.5)$$

Here A is the area of the avalanche, with P_i and P_b the perimeters of the upper and lower boundaries, respectively. E_a is a coefficient of entrainment of ambient air into the avalanche and U is the velocity at the mass centre of the avalanche. C is the mean volume concentration of snow particles, c_b is the near-bed concentration, v_s is the fall velocity of snow particles in still air. τ_i and τ_b are shear stresses acting on the upper and the lower boundaries, respectively. ρ and ρ_b denote the average density of the avalanche and the near-bed density; ξ_p is a coefficient related to the potential energy of suspended snow particles and K denotes the average kinetic energy in an avalanche. k_v is the coefficient of virtual mass, i.e., the mass of the surrounding air that needs to be accelerated or decelerated when the avalanche velocity changes. A discussion of the physical meaning of various terms can be found in Sec. 5.5.

It should be noted that the effects of track curvature are not taken into account in the formulation presented in Fukushima and Parker (1990), even though the test case exhibits some rather abrupt slope changes.

Constitutive assumptions: The closure assumptions closely follow those of Parker *et al*. (1986), except for the shape evolution and the top shear stress:

(i) The shape of the avalanche is given by Eqns. (5.4.1) and (5.4.2); the coefficient of air entrainment at the upper surface (dimensionless) is assumed to be

$$E_a = 0.1 \cdot \frac{\varphi\,[\text{degrees}]}{90°} \ . \qquad (5.4.6)$$

(ii) The ratio of bottom particle concentration to average concentration is a decreasing function of the turbulent shear stress (see Parker (1982), García (1985)),

$$r_0 = c_b / C = 1 + 31.5\mu^{-1.46} \ , \qquad (5.4.7)$$

with $\mu \equiv u_* / v_s \equiv \sqrt{\tau_b / \rho_b}\,/ v_{s_s}$ and v_s the settling velocity of the particles. (r_0 = 1.6 would also be a reasonable fit to the available data, though.)

(iii) The top and bottom shear stresses, τ_i and τ_b, are related to the average turbulence K:

$$\tau_i / \rho_a \cong \tau_b / \rho_b \cong \alpha K \quad \text{with} \quad \alpha \cong 0.1 \ . \qquad (5.4.8)$$

(iv) The sediment entrainment rate, E_s, is fitted from laboratory flume experiments (Akiyama and Fukushima, 1985; García, 1985); it depends on the shear stress velocity through μ and on the particle Reynolds number $\text{Re}_p \equiv \left(Rgd_p^{\,3}\right)^{1/2} / \nu$:

$$Z = \text{Re}_p^{\frac{1}{2}} \mu \ , \qquad (5.4.9)$$

where d_p is particle diameter, and ν the kinematic viscosity of the fluid. Then the authors set

$$E_s = \begin{cases} 0.3\,, & Z > Z_m = 13.2\,, \\ 3\cdot 10^{-12} Z^{10}\left(1-\dfrac{Z_c}{Z}\right), & Z_c < Z < Z_m\,, \\ 0\,, & Z < Z_c \cong 5\,, \end{cases} \qquad (5.4.10)$$

where Z_c and Z_m are threshold and saturation values of Z, respectively.

(v) The viscous dissipation rate, ε_0, is taken to grow more rapidly than the turbulence itself:

$$\varepsilon_0 = \frac{\beta K^{3/2}}{h}\ . \qquad (5.4.11)$$

β is taken from the equilibrium condition to this set of equations in the case of a pure density current and is a rather complicated expression not reproduced here.

Numerical methods: Nothing precise is known about the numerical methods used by the authors. For comparison purposes, Gauer (1994) implemented the model with a fourth-order Runge-Kutta scheme. It appears that the model has not been developed further for routine use (user interface, etc.).

Assessment: The advantages and drawbacks of this model may be assessed as follows:

+ The processes in the suspension layer are treated in a physically reasonable way (balance equations for all important field variables).
+ Attention is paid to snow and air entrainment and to their interdependence with turbulence in the avalanche.
+ The lumped-mass formulation makes the numerical treatment relatively simple. Simulations can be carried out on personal computers in a short time. Even numerically inexperienced users can handle such a program.
– As in most other models, the interaction between the original dense-flow avalanche and the emerging powder snow avalanche is ignored, as is the saltation layer.
– No genuine theory of the entrainment processes is given, so the parameters have to be calibrated from hydraulic data in the absence of measurements in real powder snow avalanches.
– The effects of track curvature and lateral spreading are not taken into account.
– The lumped-mass approach foregoes the possibility of obtaining vertical pressure distributions.
– Some constitutive assumptions preclude model application to avalanche tracks with nearly horizontal or even ascending slope segments.

Verification and practical applications: The authors present an application of the model to the Maseguchi (Japan) avalanche event of 1986. The simulations impressively demonstrate that the depth of the layer of fresh loose snow available for *entrainment* is an important parameter. Their numerical results were confirmed by Gauer's (1994) implementation. The study case does not appear to be very well chosen, however, because not very much detailed information is available on that event. In particular, there seems to be disagreement among experts as to whether the destruction and deaths in the village were caused by a powder snow avalanche or a dense flow (McClung *et al.*, 1993).

5.5 The Parker-Fukushima-Pantin quasi two-dimensional model for turbidity currents

(D. Issler)

The model was developed by Parker *et al*. (1986) in order to study the importance of sediment entrainment and turbulence in submarine turbidity currents. Due to the physical similarity of turbidity currents and powder snow avalanches, it can be applied to powder snow avalanches with small modifications, mainly in the entrainment functions (see (Fukushima and Parker, (1990) and Gauer (1994)).

Physical basis and assumptions: The model describes the dynamics of a so-called long turbidity current, i.e., the body of the avalanche rather than its head. The turbidity current is considered as a dilute suspension of fine particles in water. The model is quasi two-dimensional: The two-dimensional equations in *x, z* are integrated over *z*. It can deal with smooth slope changes in an approximate way.

The set of basic field equations comprises the balances of total mass, suspended sediment, mixture momentum, and mixture turbulent kinetic energy. In the latter, the authors consider the turbulence expenditure of keeping the particles in suspension against their settling velocity, entraining fluid at the upper surface and particles at the bottom surface of the flow.

$$\frac{\partial h}{\partial t} + \frac{\partial (Uh)}{\partial x} = E_a U \ , \tag{5.5.1}$$

$$\frac{\partial (Ch)}{\partial t} + \frac{\partial (UCh)}{\partial x} = v_s \left(E_s - r_0 C \right) \ , \tag{5.5.2}$$

$$\frac{\partial (Uh)}{\partial t} + \frac{\partial (U^2 h)}{\partial x} = -\frac{1}{2} Rg \frac{\partial (Ch^2)}{\partial x} + RgCh \sin\varphi - u_*^{\ 2} \ , \tag{5.5.3}$$

$$\begin{aligned} \frac{\partial (Kh)}{\partial t} + \frac{\partial (UKh)}{\partial x} = {} & u_*^{\ 2} U + \frac{1}{2} U^3 E_a \\ & - Rgv_s Ch - \frac{1}{2} RgChUE_a - \frac{1}{2} Rghv_s \left(E_s - r_0 C \right) - \varepsilon_0 h \ . \end{aligned} \tag{5.5.4}$$

h is the flow height, U the depth-averaged velocity, $0 \le C \le 1$ the depth-averaged volumetric particle concentration, and K the depth-averaged turbulent kinetic energy per unit mass. Here, the usual assumptions of shallow-water theory have been made. In order to simplify the model, the profile functions have been assumed constant from bottom to upper flow surface. Note that in the applications only the stationary case is treated, resulting in ordinary differential equations instead of the PDEs given above.

In the equation for the turbulence level, (5.5.4), the first term on the right-hand side is the production of turbulence due to shear stress at the bottom. On accelerating a volume UE_a of air per unit time and unit surface area to velocity U, an amount $U^3E_a/2$ of mean-flow kinetic energy is transferred to turbulent kinetic energy; this is captured by the second term. The third term describes the expenditure of turbulence to maintain the suspension against gravitational settling (a factor cos φ ought to be added for steeper slopes), while the fourth and the fifth

term describe the turbulent energy spent on mixing the entrained air and snow throughout the avalanche. Finally, ε_0 is the viscous dissipation of turbulent energy.

Constitutive assumptions: The closure assumptions differ from those described in Sec. 5.4 in the following respects:

- The dimensionless coefficient of water entrainment at the upper surface, E_a (or e_w in their notation) is taken to be a function of the (global) Richardson number Ri characterising the stratification of the flow,

  $$\mathrm{Ri} = \frac{RgCh}{U^2} \ , \qquad (5.5.5)$$

  with $R \equiv \left(\rho_{mix} - \rho_{fluid}\right) \Big/ \rho_{fluid}$. The authors use

  $$E_a(\mathrm{Ri}) = \frac{0.00153}{0.0204 \ + \ \mathrm{Ri}} \ , \qquad (5.5.6)$$

  giving typical values $E_a = (0.5 \div 5) \times 10^{-3}$; at the transition from critical to sub-critical flows, $E_a = 1.5 \times 10^{-3}$.

- As in the later block model by Fukushima and Parker (1990) described in Sec. 5.4, the (bottom) shear stress velocity, u_*, is related to the average turbulence K:

  $$u_*^{\,2} = \alpha K \quad \text{with} \quad \alpha \cong 0.1 \, . \qquad (5.5.7)$$

  Shear stresses at the top of the flow are neglected, however.

Numerical methods: The authors implemented the model for *stationary* flows only. The equations are hyperbolic, so a simple step method computing downstream values from upstream values was used. In his re-implementation, Gauer (1994) used a fourth-order Runge-Kutta method. No efforts have been made to turn this model into a tool for practical use in avalanche problems (see, however, the section on the Fukushima-Parker model). An implementation for transient problems is possible with moderate effort.

Verification and practical applications: This model was used to study whether sediment entrainment in submarine turbidity currents can lead to ever-growing flows. It was found that this is indeed the case under certain conditions; the phase-space trajectories of the system were mapped and revealed three different regions: Sub-critical flows are of no interest here; if the initial sediment transport rate and/or velocity is too small, the flow dies out, but if they are beyond a certain line in phase space, they grow indefinitely. A critical line was found that connects two fixed points, "0" (no flow) and "infinity" (infinite sediment transport rate, a runaway situation), and is approached by all phase space trajectories in one or the other direction.

Detailed experimental verification of the model for real submarine turbidity currents has not been possible because no data is available. Good agreement was found in tests against laboratory data on plane wall jets.

5.6 AVAL — Gauer's quasi two-dimensional models with *k-ε* turbulence closure

(D. Issler)

In his diploma thesis, Gauer (1994) replaced the turbulent kinetic energy balance and the heuristic expression for viscous dissipation of turbulence in the models of Parker *et al*. (1986) and of Fukushima and Parker (1990) by the depth-integrated *k-ε* model. He also fitted the experimental entrainment data by a more gradual function of bottom shear stress.

Physical basis and assumptions: The motivation for the development of this model was to understand more clearly the role played by the turbulence model in the numerical simulation of powder snow avalanches. The models by Parker *et al*. (1986) and by Fukushima and Parker (1990) were taken as a starting point because they clearly recognise the paramount importance of turbulence both for air entrainment at the upper avalanche surface and particle entrainment at the bottom. Both models employ a first-order turbulence model, i.e., a balance equation for the mean turbulence level K and a heuristic, algebraic expression for the mean viscous dissipation of turbulence, ε_0. It is well known that second-order turbulence models are often clearly superior to first-order models; for this reason, the well-known *k-ε* model was implemented and tested.

The depth-averaged but non-stationary *k-ε* equations have a rather complicated appearance and are not reproduced here. The *k*-equation describes the physical processes in a qualitatively similar way to Eqns. (5.4.5) and (5.5.4). The dissipation rate, however, depends not only on the local turbulence level as in Eqn. (5.5.11), but also on advection by the flow, particle settling and the dissipation itself; a partial differential equation is solved for ε_0. The "canonical" values obtained from experimental data on many different types of flows were chosen for the various parameters of the turbulence model.

Constitutive assumptions: As in Parker *et al*. (1986), uniform profile functions from bottom to avalanche height are assumed for all field variables. Notwithstanding this, the ratio of bottom to average concentration, r_0, is assumed to be the following function of the shear velocity:

$$r_0 = 1.97 - 0.0091\mu \qquad (5.6.1)$$

on the basis of the same data used by Parker *et al*. (1986) and Fukushima and Parker (1990). Further constitutive equations are needed for the entrainment rates of air and snow. For air, Gauer follows Fukushima and Parker (1990), cf. Eqn. (5.4.6). The basic formulation of the snow entrainment rate is taken from (Parker *et al.*, 1986), but the threshold value and the functional dependence on Z are specified differently (cf. Eqns. (5.4.9), (5.4.10)):

$$Z_c = \sqrt{\mathrm{Re}_p} \cdot \frac{u_{*,c}}{v_s} , \qquad (5.6.2)$$

where the critical shear velocity, $u_{*,c} = \sqrt{\tau_c(\varphi, F_k)/\rho}$, is inferred from mechanical considerations of the aerodynamic force needed to extract snow grains from the snow cover and can vary greatly with, e.g., temperature and slope angle. Eqn. (5.5.10) is replaced by the much more gradual, but unbounded function

$$E_s = \begin{cases} 0\,, & Z < Z_c\,, \\ 5.2 \cdot 10^{-5} Z^{1.74}\,, & Z > Z_c\,. \end{cases} \qquad (5.6.3)$$

The k-ε model expresses the effective viscosity of the turbulent flow as

$$\nu_{eff.} = c_\mu \cdot \frac{K^2}{\varepsilon}\,. \qquad (5.6.4)$$

Gauer modifies an extension of the standard k-ε model that takes buoyant forces and the near wall damping of turbulence better into account by departing from the usual value $c_\mu \cong 0.09$. In the quasi two-dimensional stationary model (corresponding to the Parker-Fukushima-Pantin model), the bottom shear stress is related to the mean turbulence through a standard wall function. In the transient lumped-mass model, density weighting is used instead.

Numerical methods: A fourth-order Runge-Kutta scheme is implemented as a TurboC program. The model runs on a PC, porting to *other* platforms would be possible. No effort was made to create a user-friendly interface since the model was created in a research project.

Assessment: Essentially the same remarks apply as for the Parker-Fukushima-Pantin and Fukushima-Parker models, respectively. The treatment of turbulence with an extra differential equation for the dissipation appears to improve model behaviour in some situations, especially in the runout. The more gradually growing *entrainment* function may be more realistic, but conclusive data is missing. Despite Gauer's attempts to deduce the constitutive assumptions from mechanical considerations, several empirical relations from hydraulic experiments had to be introduced.

Verification and applications: The computational examples presented in Parker *et al*. (1986) and Fukushima and Parker (1990) were used to investigate the differences between the models. In Gauer (1995), application to the Albristhorn powder snow avalanche event of early 1995 (Issler *et al*., 1996) gave results in good agreement with the pressure distribution inferred from the observed damages.

5.7 The AVL three-dimensional powder-snow avalanche model

(P. Sampl)

Summary: The powder snow avalanche is considered as a mixture of air and suspended snow particles of varying density. The flow of this snow-in-air suspension is calculated following the single-phase "heavy gas" approach (Tesche, 1986; Hermann *et al*., 1994). The "heavy gas" equations are solved using the programme package FIRE of AVL, a simulation software for turbulent three-dimensional flows based on an Eulerian finite volume scheme. It was developed for automotive applications (gas/liquid flows in engines, car aerodynamics, etc.).

Physical Description: According to Savage and Hutter (1989) and, similarly, Norem (1993) the dry avalanche snow is assumed to be a cohesionless granular material, such that three different flow regimes can be distinguished:

(1) a quasi-static dense flow regime, where the snow particles are in permanent contact. Momentum transfer is due to contact and friction forces. The effect of the interstitial air is neglected.

(2) an inertial dense flow regime, when the dispersive pressure due to particle collisions is greater than the pressure due to gravitation. The effect of the interstitial air is neglected here also.

(3) a powder snow or aerosol regime, when snow particles at the upper surface of the dense flowing mass are suspended in the air above due to shear stresses that are caused by the velocity difference between the dense flowing mass and the air. This aerosol is treated as a mixture of air and a variable amount of snow particles. As the density of the mixture is higher than that of the surrounding air, it is accelerated by gravity.

The slip velocity between particles and air in the mixture is neglected. Thus, the mixture is treated as a single-phase "heavy gas". Sedimentation of the snow particles has also been neglected up to now, but could be taken into account by applying a "sedimentation velocity" to the snow particles. Entrainment of snow from the ground is also not accounted for yet, while entrainment of ambient air is.
Constitutive Equations: As mentioned above, the aerosol phase of the avalanche is modelled as a heavy gas. The density of this gas depends on the local snow volume fraction, which is computed by the model. Thus, the constitutive properties are given by the density and viscosity of the air and the density of the snow particles together with the local snow volume fraction. Since the snow volume fraction is assumed to be very small (of the order of 10^{-2}), the viscosity of the air determines the laminar stresses. In other words, the snow-air mixture is treated as a Newtonian fluid of variable density. However, the laminar stresses are very small compared to the turbulent stresses (which are calculated using a turbulence model).

Mathematical Description: The powder snow avalanche is treated as a single-phased Newtonian "heavy gas". Furthermore, the powder snow avalanche is assumed to be a turbulent flow, thus Reynolds averaging is applied (indicated by overbars). The bulk density ρ is a function of the volumetric snow concentration c:

$$\overline{\rho} = (1-\overline{c})\rho_1 + \overline{c}\rho_2 \qquad (5.7.1)$$

with ρ_1 and ρ_2 the material densities of air and snow particles, respectively. The mass balance for the snow-air mixture is given by

$$\frac{\partial \overline{\rho}}{\partial t} + \frac{\partial\left(\overline{\rho}_a\ \overline{u}_j\right)}{\partial x_j} = 0 \qquad (5.7.2)$$

(time t, co-ordinates x_i and velocity vector u_i). A separate mass balance for the snow alone is required and reads

$$\frac{\partial \overline{c}}{\partial t} + \frac{\partial\left(\overline{c}\,\overline{u}_j\right)}{\partial x_j} = -\frac{\partial\left(\overline{c'u'_j}\right)}{\partial x_j} \qquad (5.7.3)$$

where primed quantities denote the turbulent fluctuation parts. The momentum balance for the mixture is given by

$$\frac{\partial\left(\overline{\rho}\,\overline{u}_i\right)}{\partial t}+\frac{\partial}{\partial x_j}\left(\overline{\rho}\,\overline{u}_i\overline{u}_j\right)=-\frac{\partial\overline{p}}{\partial x_i}+\frac{\partial}{\partial x_j}\left(\overline{\tau_{ij}}-\overline{\rho}\,\overline{u'_i\,u'_j}\right)+\overline{\rho}g_i \qquad (5.7.4)$$

with the pressure p and the gravitational acceleration g_i. The shear stresses are taken to be caused by the air. The viscous stresses for a Newtonian fluid can be written

$$\overline{\tau_{ij}}=\eta\left(\frac{\partial\overline{u_i}}{\partial x_j}+\frac{\partial\overline{u_j}}{\partial x_i}\right)-\frac{2}{3}\eta\frac{\partial\overline{u_k}}{\partial x_k}\delta_{ij} \qquad (5.7.5)$$

with the viscosity of air η and the Kronecker-Delta δ_{ij}. The turbulent stresses arising from fluctuation velocities are modelled as

$$-\overline{\rho}\overline{u_i'u_j'}=\eta_t\left(\frac{\partial\overline{u_i}}{\partial x_j}+\frac{\partial\overline{u_j}}{\partial x_i}\right)-\frac{2}{3}\left(\overline{\rho}k+\eta_t\frac{\partial\overline{u_k}}{\partial x_k}\right)\delta_{ij} \qquad (5.7.6)$$

where η_t is a turbulent viscosity that is calculated using a standard turbulence model (k-ε model; Rodi, 1980). In this model k is the energy of the turbulent fluctuations and ε is the dissipation rate of this energy. The transport equations for both both of these quantities must be solved. The turbulent mixing of the snow particles in the air is modelled as

$$-\overline{c'u_i'}=\frac{1}{\rho}\frac{\eta_t}{\sigma_t}\frac{\partial\overline{c}}{\partial x_i} \qquad (5.7.7)$$

where σ_t is the turbulent Schmidt number.

Numerical Methods: The three-dimensional “heavy gas” equations for the suspension layer are solved on the basis of a finite-volume scheme and a spatially fixed Eulerian grid. This grid is generated automatically above the prescribed terrain topology and covers also the ambient air to capture its entrainment in the mixture. An algorithm similar to the SIMPLE algorithm is used for the numerical integration process. At the start of the calculation, the mixture containing the prescribed snow mass is at rest in the bottom grid-cell layer above the release area.

Advantages/disadvantages of the Model:

+ three dimensional model
+ arbitrary terrain topology, arbitrary shape of release areas
+ turbulent stresses and mixing / two-equation turbulence model
+ entrainment of ambient air
+ integrated tools for surface triangulation and specification of release area
+ automatic generation of the Eulerian grid
+ graphical user interface, post-processing tools
+ supports most UNIX platforms
– high computational effort (> 50 000 grid points needed)
– mixture treated as a single phase
– no sedimentation
– no snow entrainment from the ground
– supports only UNIX platforms

Practical Application: The model has already been applied to a number of recent avalanche events in Austria. This work has largely been performed by the Institute for Avalanche

Research in Innsbruck. The model is, of course, only applicable to the powder snow part of avalanches.

Verification of the Model: Verification is very difficult, as high-quality measurement data are very rare. Comparisons of the model predictions with observations yielded plausible results (Brandstätter *et al.,* 1996).

5.8 SL-3D — the Swiss three-dimensional powder snow avalanche model

(D. Issler)

Physical basis and assumptions: This model was developed simultaneously but independently of the AVL model (Sec. 5.7) and Naaim's three-dimensional model (Sec. 5.9). As in those models, two separate mass conservation equations are solved for the mixture and snow but only one momentum balance for the mixture. The SL-3D model further parallels Naaim's and Tesche's models (see Sec. 5.10) in that it allows for particle settling in the direction of gravity, approximating the relative velocity between phases by the single-particle settling velocity. In contrast to Tesche's model but in line with the AVL model, the powder snow avalanche is not treated as a free-surface flow but re-circulation of displaced air around and over the avalanche is computed explicitly. Again, the k-ε model is the turbulence closure of choice at the present stage of development, due to its relative economy and robustness.

The main difference between Tesche's model and the SL-3D model (Hermann *et al.*, 1994) concerns the specification of an entrainment model in the latter. Gauer's (1994) ansatz with the local entrainment rate a function of the bed shear stress (see the section on AVAL above) was adopted. In addition, snow entrainment is limited in this model by the erodible snow cover, which is allowed to vary locally.

Numerical implementation: The model is implemented as a set of modules to the general flow solver CFX 4 from AEA Technology plc (Great Britain). CFX 4 is a finite-volume code based on a structured body-fitted grid; thus a fixed Eulerian grid is used as default. It is possible to take into account the changes in snow cover depth by using a so-called transient grid whose bottom adapts itself to the snow surface as it is constantly modified by entrainment or deposition.

Several versions of the powder snow modules exist: The snow may be treated as a passive scalar field in an essentially one-phase approach, or as a second phase with essentially the same velocity as the carrier phase, the air. CFX 4 also offers the option of solving a full two-phase problem with several choices of inter-phase forces, but this option has rarely been used.

Validation and applications: The front velocities of saline solutions measured by Beghin and Olagne were reproduced within the limits of experimental uncertainty. The model was later on applied to a large powder snow avalanche that occurred in Switzerland in 1995 (Issler *et al*., 1996) and for which the release and runout zones had been mapped, estimates of released and deposited masses were available, and forest damage delineated the high-pressure areas. Using the entrainment model as in Gauer (1994), very good agreement was found between the simulated maximum pressure distribution and the field data.

More effort is required to explore issues such as optimum size and shape of the computational domain, optimum distribution of grid cells, optimisation of time step length vs. number of iterations per time step, advantages and drawbacks of fully compressible computations, etc.

Meanwhile, the model has been used in consulting with good success. However, simulation results may depend very sensitively on the amount of erodible snow along the track. Specifying reasonable initial and boundary conditions is of paramount importance and requires a specialist.

Advantages/disadvantages of the model:

+ three-dimensional model
+ arbitrary terrain topology, arbitrary shape of release areas
+ turbulent stresses and mixing / two-equation turbulence model
+ entrainment of ambient air, entrainment and sedimentation of snow
+ integrated tools for user-assisted grid generation
+ graphical user interface, post-processing tools
+ supports most UNIX platforms and several supercomputers
– high computational effort (> 50 000 grid points needed)
– mixture treated as a single phase
– specialist required for meaningful application in consulting etc.
– supports only UNIX platforms and certain supercomputers

5.9 Naaim's three-dimensional pure powder-snow avalanche model

(D. Issler)

At CEMAGREF in France, the development of a three-dimensional powder-snow avalanche model was undertaken around the same time as in Austria and Switzerland, the goals as well as the approach being very similar. In parallel, flume and wind tunnel (Naaim and Martinez, 1995) studies were conducted in order to obtain empirical input for the snow entrainment function from the analogies of powder snow avalanches with turbidity currents in water and snow drift. In the following, only the main features that differ from the AVL and SL-3D models will be summarised on the basis of (Naaim, 1995).

Note that the model has been developed further since: Separate mass and momentum balances for snow and air have been introduced, turbulent closure is now by means of a k-ε model modified for the effect of particles, and the erosion and deposition flux have been formulated differently, using the most recent results from flume and wind tunnel studies. Moreover, the model has been coupled with a two-dimensional depth-averaged model for the dense-flow avalanche that generates the powder-snow cloud. For this reason, the new model is described in Chapter 6.

Physical basis and assumptions: Reynolds averaged balance equations are written for the air-snow mixture, where the air is considered an ideal gas. As in SL-3D and Tesche's models, particles settle at constant relative velocity under the influence of gravity and undergo turbulent diffusion. Turbulence is modelled by means of a transport equation for k and a characteristic length scale, L, of energetic turbulent structures in the flow (whose precise

choice is not detailed, however). The turbulent viscosity, ν_t, and dissipation, ε, are given by, respectively,

$$\nu_t = C_1 L k^{1/2} \quad \text{with} \quad C_1 = 0.43 \quad , \quad \text{and} \quad \varepsilon = C_\varepsilon \frac{k^{3/2}}{L} \quad \text{with} \quad C_\varepsilon = 0.078 \qquad (5.9.1)$$

Snow erosion from the ground is supposed to occur due to turbulent friction on the ground, which is defined with reference to a *mixture* density $\tau_f = \rho_m u_*^2$, where u_* is the friction velocity. It is supposed that a threshold shear stress, $\tau_s = \rho u_{*,s}^2$, must be exceeded for erosion to take place. If this is the case, the erosive mass flux is taken to be proportional to u_* and some near-ground concentration that depends on the snow properties. If the threshold is not exceeded, deposition occurs at a rate proportional to the particle settling velocity and the near-ground concentration.

Numerical methods: The code for numerical solution of the powder snow model appears to have been written explicitly for this application, in contrast to the general-purpose codes adapted by AVL and in SL-3D. The equations are put in conservative, finite-volume form as in FIRE and CFX. The discretisation is second order in space and first order in time, an explicit scheme being used. Field gradients are approximated by minimising a certain functional that involves the nearest neighbours of each cell. Advective fluxes on cell faces are computed using a one-dimensional approximate Riemann solver. For the diffusive fluxes, the gradients on cell faces are obtained by interpolation between two cells.

Validation and applications: Good agreement with experimental data (front velocity, flow height) on density currents (obtained by Beghin) was achieved. Further validation using flume data on turbidity currents (with particle erosion and sedimentation) was recently reported; without the erosion/sedimentation model, the experimental data could not have been reproduced.

The model has been applied to several powder snow avalanche events in France, Andorra and Turkey. Good agreement of calculated maximum pressures with observed damage extent has been claimed, but as experienced with the other models, strong dependence of stagnation pressure on initial and boundary conditions makes it difficult to unambiguously assess the success of the numerical simulations.

5.10 Tesche's three-dimensional powder-snow avalanche model

(D. Issler)

Tesche (1986) gave a review of existing avalanche models, discussed the formation, structure and basic processes of powder snow avalanches, and set forth a set of three-dimensional equations for powder snow avalanches. He also discussed a large number of aspects relevant to numerical solution of these equations, but no report on an actual implementation of these schemes seems to have appeared since. It is nevertheless of interest to point out the mathematical model's main differences from the three models developed some five to ten years later.

Starting out from the set of two-phase equations, the relative motion of the phases is approximated by the settling velocity of the particles. This analysis reveals certain extra terms

in the snow mass balance and the mixture momentum balance due to volume averaging and particle settling. The current models (AVL, Naaim, SL-3D) neglect some or all of these corrections due to a lack of well-founded turbulence models for binary mixtures.

Tesche describes powder snow avalanches as free surface flows. The boundary conditions at the upper avalanche surface are to express the opposing effects of particle settling and turbulent diffusion (there appear to be certain errors in Tesche's formulation, though); the upper surface is defined as the minimum (moving) surface through which there is no particle flux. At the bottom surface, the net mass flux is determined by settling, partial re-suspension of settled particles, and the erosion of particles from the original snow pack. No momentum boundary conditions are given, but symmetry-plane conditions are postulated for k and ε at the free surface, and the law-of-the-wall at the bottom surface. No explicit expression is given for the erosion rate at the snow surface.

5.11 The Scheiwiller-Hutter two-component model for powder snow avalanches

(D. Issler)

The development of this model was part of a joint research project between the Laboratory of Hydraulics, Hydrology and Glaciology (VAW) of ETH Zurich and the Swiss Federal Institute for Snow and Avalanche Research (SFISAR), with a goal of obtaining simple formulae for practical applications in avalanche hazard mapping. Due to the lack of experimental data, laboratory measurements at a scale of roughly 1/1000 were performed with polystyrene particles in a water tank in order to test the numerical model (Scheiwiller, 1986); these investigations were continued later, see (Hermann and Hutter, 1991; Keller, 1995).

The original approach aimed at a full two-component model for air and snow particles (Scheiwiller and Hutter, 1982; Scheiwiller, 1986), to be described in this section. The inadequacy of then available multi-phase solvers led later to a simplified approach in terms of an extended one-component model that was discussed in Sec. 5.8. For simple geometries, a one-dimensional model—albeit with a more sophisticated treatment of snow entrainment and deposition—was derived (see the following section).

Physical basis and assumptions: Scheiwiller and Hutter (1982) and Scheiwiller (1986) set up the equations for a two-component flow in which the particles are treated as a fluid perfectly mixed with the ambient air. Both "gases" are assumed incompressible; density variations are solely due to particle concentration differences.

From the particle Reynolds number, $\mathrm{Re}_p = d_p v_{rel} / \nu_{air} = O(10^2)$ with d_p particle diameter, v_{rel} the relative velocity between particles and air, and ν_{air} the kinematic viscosity of air, it is deduced that particles interact through their wakes. Scheiwiller proposes the following expression for the inter-phase friction **m** (momentum transfer from particles to the air):

$$\mathbf{m}_{p\to f} = C_f \frac{\sqrt{\hat{\rho}_p \hat{\rho}_{air}}}{\tau} \cdot (1 - c_p) c_p (\mathbf{u}_p - \mathbf{u}_{air}) \ ; \qquad (5.11.1)$$

$\hat{\rho}_{p,air}$ and $\mathbf{u}_{p,air}$ are the intrinsic densities (velocities) of snow grains and air, respectively; c_p is the volumetric particle concentration. The value of the friction coefficient, C_f, is considered

constant. Finally, τ is a reaction time of the particles to a change in air velocity; in certain numerical simulations, Scheiwiller (1986) set $C_f / \tau = 3$ (no units specified!).

Boundary conditions and constitutive assumptions: The boundary conditions are formulated in terms of jump conditions at the free surface and at the bottom of the powder snow avalanche. The avalanche surface is defined as the line where particle concentration drops to zero. Outside the avalanche, laminar flow is assumed—disregarding the re-circulation flow over the avalanche. The ansatz for the air entrainment rate is

$$E_{air} = E_1 \cdot (p - p_{air}) + E_2 \cdot u_{|\,|air} + E_3 u_{\perp air} \ , \qquad (5.11.2)$$

allowing for pressure effects as well as separate dependencies on longitudinal and cross-stream air velocity (no values are suggested for $E_{1,2,3}$). Turbulence is treated in terms of Reynolds averaging; Scheiwiller (1986) proposes the k-ε model as closure, without specifying in detail how the turbulent motion of the particles should best be taken into account.

Numerical methods: The model was implemented first in an early version of the general-purpose code PHOENICS and applied to the quasi-stationary, quasi two-dimensional laboratory experiments. The results being unsatisfactory, the Kantorovich technique (method of weighted residuals) was subsequently used to reduce the problem to one dimension: Any field $\Phi(x,z,t)$ is decomposed according to

$$\Phi(x,z,t) = \sum_{k=1}^{\infty} f_k^{(\Phi)}(x,z)\varphi_k(x,t) \ ; \qquad (5.11.3)$$

in practice, the infinite series is truncated after a small number of terms (2 in this case). The success of the approximation depends on the choice of the shape functions $f_k^{(\Phi)}(x,z)$. Note that truncation after the first term corresponds to depth averaging in the context of the shallow-water approach. A Pascal program was specifically written for solving the simplified system of equations.

Verification, practical applications and assessment: The model has only been applied to the laboratory measurements described by Scheiwiller (1986). With the Kantorovich technique, reasonable correspondence between measured and computed velocity and density profiles could be obtained, yet at the expense of choosing k-ε model coefficients far from their usual values. Despite its scientific appeal, the Scheiwiller-Hutter model has been superseded by the more practical approach described in Sec. 5.8.

5.12 SL-1D — a quasi two-dimensional two-layer model

(D. Issler)

In Issler (1998), powder snow avalanches are treated as a two-layered flow with a denser saltation layer underneath the suspension layer. The balance equations for the suspension layer resemble those of AVAL (Gauer, 1994) with the k-ε turbulence model, except for being fully time and space-dependent. Balance equations for snow mass and momentum are used to describe the saltation layer.

Physical basis and assumptions: The model takes into account pressure measurements and field observations on powder snow avalanches that are *best* interpreted in terms of a multi-layered structure with a rather dense so-called saltation layer underneath the cloud of suspended snow grains (Norem, 1995a). Mass exchange with the snow cover or—eventually—the dense-flow avalanche is mediated by the saltation layer in which particles from fine grains to football-sized blocks jump through the air and land again if they are not suspended by a turbulent eddy.

The suspension layer is treated in a very similar way as in AVAL by Gauer (1994), i.e., balance equations for air mass, snow mass, total momentum, turbulent kinetic energy and dissipation are formulated and integrated over the flow height. The layer grows due to air entrainment; its mass changes due to particles settling into the saltation layer or being lifted into suspension by turbulent eddies.

In the saltation layer, the air mass and momentum can be neglected. Depth-averaged balance equations are solved for the snow mass and the snow momentum, neglecting variation of hydrostatic pressure from the suspension layer. The height of the saltation layer is assumed proportional to the impact energy of landing particles that eject others or rebound, and thus to the average layer velocity squared. Momentum exchange between the layers is due to the aerodynamic shear stress computed from turbulence in the suspension layer, and to mass exchange. The effects of slope changes are partially taken into account by incorporating the local centrifugal acceleration in the effective gravitational constant and by adjusting the particle settling velocity.

Boundary conditions and constitutive assumptions:

(i) The velocity and density profiles in the suspension layer are assumed to be the same as in Keller's (1995) water-tank experiments, i.e.,

$$f_\rho(\zeta) \cong 1.3 - 0.6 \cdot \zeta \qquad \text{and} \qquad f_U(\zeta) \cong 1.4 \cdot (1 - \zeta^2) \qquad (5.12.1)$$

in terms of the non-dimensional variable $\zeta \equiv z / h(x,t)$. (These profile functions are expected to be improved on the basis of three-dimensional simulations.)

(ii) Following Owen's reasoning in aeolian sediment transport, the aerodynamic component of the bottom shear stress in the saltation layer is neglected compared to the effect of particle impacts. – At the interface of the saltation and suspension layer, the aerodynamic shear stress is determined from the suspension-layer turbulence using wall functions and an approximate expression for the effective roughness height that depends on the concentration and depth of the saltation layer. – At the upper surface of the suspension layer, turbulent momentum exchange with the surrounding air induces the entrainment of air into the avalanche. Thus most of the air that receives momentum from the flow through shear becomes part of the avalanche in the process; this explains why along the upper surface the shear stress exerted from *outside* the system is considered negligible compared to the other effects. In contrast to many depth-averaged models like AVAER (Sec. 5.2) or the Fukushima-Parker model (Sec. 5.4), the entrainment rate is computed from the turbulent kinetic energy of the suspension layer; the ratio of turbulence at the boundary to average turbulence is a free parameter but can be inferred from three-dimensional simulations.

(iii) The settling rate from the suspension layer to the saltation layer is expressed as in the Parker-Fukushima-Pantin (1986) model with a coefficient describing the ratio of bottom and depth-averaged concentrations. — The suspension rate is given by the product of the concentration difference between the layers with the mean vertical velocity fluctuation, expressed in terms of the turbulent kinetic energy. — The non-aerodynamic part of the inter-layer shear stress is computed from these mass exchange rates, with two coefficients describing the ratios of boundary and depth-averaged velocities in the two layers.

(iv) The particle landing rate is given by the saltating mass per unit area divided by the average saltation time; the latter is proportional to the average saltation velocity. — The particle ejection rate in turn is proportional to the landing rate and is expected to vary slowly with particle kinetic energy. The corresponding factor is modelled as the first-order Taylor expansion around an equilibrium value; the typical formation distance of powder snow avalanches serves for estimating the corresponding expansion coefficient. — The bottom friction in the saltation layer is approximated by the momentum loss of impacting particles minus the momentum imparted to ejected particles.

Numerical methods: The resulting array of conservative PDEs is solved by means of a simple explicit upwind finite-difference scheme, with small modifications at the front and rear. Implementation of the MacCormack (1969) scheme (relatively simple explicit two-step time discretisation scheme with most advantages of an implicit scheme), achieving second-order precision in both time and space, is planned. The equation solver can be simply extended to accommodate additional equations (dense-flow avalanche, e.g.) and is efficient, but the time steps and the grid cells must be relatively small for good stability; artificial viscosity may be advantageous. Tests with a physically simpler density-current model (Hermann, 1992, unpublished) showed good results.

The scheme is being implemented in a platform-independent way as an ANSI C program. A user-friendly graphical interface based on the data analysis and graphics package IDL (available for most platforms used today) has been completed by Mullins; it allows problem definition (topography, initial conditions, boundary conditions), monitoring of the runs, and rapid yet flexible visualisation and documentation of simulation results. An interface to the one-dimensional transient Voellmy-Salm model for dense-flow avalanches is also provided.

Verification, practical applications and assessment: This will become possible only after full numerical implementation of the model in the course of 1998. General aspects are:

+ Explicit modelling of the processes affecting the mass balance allows rough *a priori* estimates of the model parameters.
+ More accurate parameter values can be found by means of detailed simulation of the basic processes in the saltation layer and of saltation trajectories.
+ The model can easily be coupled to a dense-flow avalanche model.
+ The computational effort is moderate by today's standards.
– A one-dimensional model is not able to deal with complicated topographies.
– Model validation requires more comprehensive field measurements.
– Additional model equations increase the computational load.

Distribution of the code, interface and guidelines on powder snow avalanche computation to avalanche practitioners in Switzerland (and abroad) is planned.

6 COUPLED AVALANCHE DYNAMICS MODELS

(P. Sampl)

Coupled models try to describe all aspects of snow avalanches: the dense flow as well as the formation and movement of the powder snow part of avalanches, together with the coupled flow of both parts. In principle, the complete avalanche could be described by an universal two-phase model for air and snow particles that is valid over the encountered range of particle volume fractions: from the high values of the dense layer to the very low values of the powder layer. Unfortunately, such two-phase models are very complex and still affected with uncertainties, especially at high particle volume fractions (see e.g. the contributions in Roco, 1993). In practice, separate models for the dense flow and the powder flow, as described in the preceding chapters, are applied.

If a coupled model is built upon separate sub-models for the dense and the powder layer, the need for an additional sub-model to describe the exchange of mass and momentum between these layers arises. This exchange happens across some “transition layer”. Across this layer the particle concentrations decrease from the high values of the dense layer to the low values of the powder layer. Similar exchange processes take place between the powder layer and the snow cover, when they are in direct contact. The latter are modeled in some of the powder snow models described in chapter 5. Gravitation, air-particle interaction and particle-particle interaction are assumed to govern particle entrainment in the powder layer:

- fluid-particle interaction: air drag lifts snow particles from the dense layer or snow cover; the air drag is induced by velocity differences between the dense and the powder layer; threshold and saturation conditions are considered; (see e.g. the Parker-Fukushima-Pantin-Model or the AVAL-Model in chapter 5 or Naaim’s coupled model in this chapter),
- turbulent eddies in the transition and powder layer disperse lifted particles and yield diffusive flux of the particle phase; this in turn can enhance or damp turbulence (cf. the models cited above);
- particles settle due to gravitation;
- particle-particle interaction: settling particles hit the dense layer and rebound or eject other particles (“saltation” Norem, 1995a; see the SL-1D-Model; the transition-layer is specified more precisely as a “saltation layer” in this context);
- instability of the “boundary” between the dense and the powder layer caused by velocity difference, analogous to the Kelvin-Helmholtz instability; subsequent “tangling” of the boundary causes mixing and hence mass transfer (see the Kulikovskiy-Svesnikova-Model in chapter 5);

Only a few coupled models for snow avalanches have been formulated up to the present. The SL-1D-Model describes mass and momentum transfer within the saltation- and powder-layers and the interaction between these layers and with the underlying snow cover. The model can easily be coupled to a model for the dense layer to give a complete coupled model. In the Russian coupled model mass transfer between the layers is modeled based on the boundary instability theory. The transition layer is collapsed to an interface between dense and powder

layer. In both models averaging over the height of the considered layers is applied. Naaim's coupled model comprises a depth-averaged, two-dimensional dense flow model and a three-dimensional two-phase (air and particles) model for the powder layer, also with the transition layer collapsed to an interface. Mass transfer between the layers is determined by the friction velocity at the layer-interface and by a settling velocity that depends on turbulence in the powder layer. However, some points remain open with this model and have not yet been clarified with the author: the kind of turbulence-averaging applied to the two phases, the density which is used in the turbulence equations, the turbulent shear stresses for both phases, etc.

It was already mentioned in the preceding chapters that verification and validation of avalanche models are far from being complete. This statement is even more valid for coupled models. A lot of experimental and theoretical work remains to be done especially to clarify the important exchange processes between different avalanche layers.

6.1 SL-1D - a quasi two-dimensional two-layer model

See Sec. 5.12.

6.2 The Russian quasi two-dimensional coupled model

(M.E. Eglit)

Summary: The two-layer model (Eglit 1983; Eglit and Vel'tishchev 1985; Nazarov 1991, 1992, 1993) is intended to describe an avalanche consisting of two layers: a lower dense layer and an upper powder layer that interact with each other. An hydraulic approach is applied to both layers. It means that only the values of velocity and density averaged over the thickness of the layer (or over the cross-section of the layer) are studied.

Physical Description: The model takes into account snow sedimentation in the powder layer, friction and mass exchange at the boundary of the layers as well as mixing with the ambient air and entrainment of the snow from the snow cover.

The transformation of a dense avalanche into a powder one and also the motion of a single-layer powder avalanche can be described by this model.

The basic assumptions concerning friction and mass exchange are similar to those made in the MSU model of dense avalanches and the Kulikovskiy-Sveshnikova model for powder snow avalanches.

Mathematical Description: One of the simplest variants of the governing equations for the two-layer model is written below (Eglit, 1983). These equations describe a one-dimensional motion down a wide slope. Equations for channeled avalanches can be found in (Nazarov 1991, 1992, 1993).

Let ρ_1, v_1, h_1 and ρ_2, v_2, h_2 be the density, velocity and thickness of the dense layer and the powder layer respectively; ρ_{01}, h_0 the density and thickness of the underlying snow cover; ρ_a the air density and ψ the slope angle.

The equations for a powder layer are

$$\begin{aligned}
&\frac{\partial h_2}{\partial t}+\frac{\partial h_2 v_2}{\partial x}=V_{2a}+V_{21}-V_s,\\
&\frac{\partial \rho_2 h_2}{\partial t}+\frac{\partial \rho_2 h_2 v_2}{\partial x}=\rho_a V_{2a}+\rho_1 V_{21}-(\rho_2-\rho_a)V_s,\\
&\frac{\partial \rho_2 h_2 v_2}{\partial t}+\frac{\partial \rho_2 h_2 v_2^2}{\partial x}=g(\rho_2-\rho_a)h_2\sin\psi-\frac{\partial}{\partial x}\left[(\rho_2-\rho_a)h_2^2 g\cos\psi/2\right]-\\
&.\tau_{2a}-\tau_{21}-(\rho_2-\rho_a)V_s v_2+\rho_1 V_{21}v_1-gh_2(\rho_2-\rho_a)\cos\psi\frac{\partial(h_0+h_1)}{\partial x}.
\end{aligned}\qquad (1)$$

Here V_{2a}, V_{21}, V_s are the rates of change in thickness due to the entrainment of air and snow and sedimentation; τ_{2a}, τ_{21} are friction forces at the snow powder - air boundary and snow powder - dense layer boundary respectively.

The equations for a dense layer are (the density is assumed to be constant in this layer)

$$\begin{aligned}
&\frac{\partial h_1}{\partial t}+\frac{\partial h_1 v_1}{\partial x}=-V_{21}+V_{10}+V_s,\\
&\frac{\partial \rho_1 h_1 v_1}{\partial t}+\frac{\partial \rho_1 h_1 v_1^2}{\partial x}=\rho_1 h_1 g\sin\psi-\frac{\partial \rho_2 h_2 g\cos\psi}{\partial x}h_1-\tau_{12}-\tau_{10}-\\
&\frac{1}{2}\frac{\partial \rho_1 h_1^2 g\cos\psi}{\partial x}-\rho_1 h_1 g\cos\psi\frac{\partial h_0}{\partial x}-\rho_1 V_{21}v_1+(\rho_2-\rho_a)V_s v_2
\end{aligned}\qquad (2)$$

Here V_{10}, τ_{12} and τ_{10} are the rate of thickness variation and the friction forces connected with an interaction between the powder layer and the snow cover upon which the avalanche moves.

The equation describing variation of snow cover thickness h_0 is $\frac{\partial h_0}{\partial t}=-V_{10}$.

Formulae for the mass exchange between layers are

$$V_{2a} = m_a v_2 \frac{\sqrt{\rho_2 \rho_a}}{\rho_2 + \rho_a}$$

$$V_{21} = \begin{cases} m_{12}|v_2 - v_1| \dfrac{\rho_2 \rho_1}{\rho_2 + \rho_1} & \left(h_1 > 0 \text{ and } x < x_f\right) \\ m_{01}|v_2| \sqrt{\dfrac{\rho_2 \rho_0}{\rho_2 + \rho_0}} & \left(h_1 = 0 \text{ or } x > x_f\right) \end{cases} \qquad (3)$$

$$V_{10} = \begin{cases} m_{01}|v_1| \sqrt{\dfrac{\rho_1 \rho_0}{\rho_1 + \rho_a}} & \left(h_0 > 0\right) \\ 0 & \left(h = 0\right) \end{cases}$$

Here m_a, m_{12}, m_{01} are empirical coefficients while x_f is a coordinate of the leading front of a dense layer of the avalanche.

The bottom friction for a dense layer is assumed to consist of two terms $\tau_{10} = f_1 + f_2$.

Dry friction f_1 is defined by different formulae in moving ($v \neq 0$) and stopped ($v = 0$) parts of an avalanche:

$$f_1 = \begin{cases} 0 & \left(f_{11} < 0\right), \\ f_{11}\text{sign}v & \left(0 \le f_{11} \le f_{12}\right), \\ f_{12}\text{sign}v & \left(f_{11} > f_{12}\right), \end{cases} \qquad \text{at } v \neq 0;$$

$$f_1 = \begin{cases} f_{13} & \left(|f_{13}| < \min\left(|f_{11}|, |f_{12}|\right)\right), \\ f_{11}\text{sign}f_{13} & \left(|f_{13}| \ge f_{11},\ f_{11} < f_{12}\right), \\ f_{12}\text{sign}f_{13} & \left(|f_{13}| \ge f_{12},\ f_{12} < f_{11}\right), \end{cases} \qquad \text{at } v = 0;$$

where $f_{11} \equiv \mu\left(\rho_1 h_1 + \rho_2 h_2\right) g \cos\psi$, $f_{12} = \tau_*$ and

$$f_{13} = \rho_1 h_1 g \sin\psi - h_1 \frac{\partial \rho_2 h_2 g \cos\psi}{\partial x} - \frac{1}{2} \frac{\partial \rho_1 h_1^2 g \cos\psi}{\partial x} - \rho_1 h_1 g \cos\psi \frac{\partial h_0}{\partial x} - \tau_{12} + \left(\rho_2 - \rho_a\right) V_s v_2$$

Hydraulic friction is defined by $f_2 = k_{10} \rho_1 v_1^2 \text{sign} v_1$. In these relations μ and k_{10} are the dimensionless coefficients of dry and hydraulic bottom friction, respectively, while τ_* is the upper limit of shear stress in the snow cover (Grigoryan, 1979).

Application and Verification: Numerical investigation of the single-layer and two-layer models has been performed. The contributions of different terms and coefficients of the equations as well as the initial conditions were studied. The ranges of possible values of coefficients were obtained by comparison of calculated and observed data (Eglit and Vel'tishchev, 1985; Blagoveshchenskiy and Eglit, 1985; Nazarov 1991, 1992, 1993).

Calculation of some natural avalanches in the Caucasus, the Khibiny mountains and the Pamir mountains (at Fortambek Glacier) as well as a comparison of calculated and measured parameters have been made with the use of the single-layer and two-layer models by A.N. Nazarov (Nazarov, 1992, 1993).

The values of the friction, mass-exchange and other coefficients for two Fortambek avalanches and for a Khybiny one, used by A.N. Nazarov, are given in Tab. 6.1. They were chosen to fit the measured data for these particular avalanches and to be in accordance with the range of values fitting the other known data about avalanches and similar phenomena.

Table 6.1 Values of friction, mass-exchange and other coefficients

Avalanche	m_{01}	m_{02}	m_{12}	m_a	v_s (m/s)	k_{10}	k_{20}	μ	τ_* / ρ_1 (m^2/s^2)
Fortambek 1	0.01	0.01	0.05	0.04	0.07	0.02	0.03	0.30	5
Fortambek 2	0.01	0.01	0.05	0.16	0.07	0.02	0.03	0.30	5
Khibiny	0.01	0.00	0.01	0.04	0.20	0.02	0.03	0.25	10

Here m_a is the coefficient of air entrainment, m_{12} and m_{02} are coefficients of snow entrainment into the powder layer from the snow cover and the dense layer, respectively, m_{01} determines the amount of snow entrained from the snow cover; v_s is the vertical velocity of particle sedimentation ($v_s = V_s / \cos\psi$) and k_{20} is the friction coefficient for the powder layer.

6.3 Naaim's quasi three-dimensional coupled avalanche model

(M. Naaim, minor updates by D. Issler, P. Sampl, and C.B. Harbitz)

Dense flow avalanche model

Physical basis and assumptions: Naaim and Ancey (1992) assume that the avalanche in the first phase is a granular dense flow that is simulated using a two-dimensional model based on the shallow water equations. We adopt the following formulation for the friction term:

$$\tau = \tau_0 + \rho_d g h \cos\theta \tan\varphi + a\left\|\vec{u}_d\right\| + b\left\|\vec{u}_d\right\|^2$$

With this general formula several kinds of rheological behaviour can be described: a Bingham-fluid (parameters τ_0 and a; for wet avalanches), granular fluid with Coulombian friction (bed friction angle φ), Voellmy-fluid (parameters φ and b), etc. The non-linear and depth-integrated equations of balance of mass and momentum for the dense flow then read:

$$\frac{\partial}{\partial t}\begin{pmatrix} h \\ hu \\ hv \end{pmatrix} + \frac{\partial}{\partial x}\begin{pmatrix} hu \\ hu^2 \\ huv \end{pmatrix} + \frac{\partial}{\partial y}\begin{pmatrix} hv \\ huv \\ hv^2 \end{pmatrix} + \begin{pmatrix} 0 \\ \partial_x \\ \partial_y \end{pmatrix}\left(\frac{1}{2} kg\cos\theta \cdot h^2\right) = -gh\begin{pmatrix} 0 \\ \cos\theta_x \\ \cos\theta_y \end{pmatrix} - \frac{1}{\left\|\vec{u}_d\right\|}\begin{pmatrix} 0 \\ u \\ v \end{pmatrix}\frac{\tau}{\rho_d}$$

where h is the flow depth, $\vec{u}_d = (u,v)^t$ the dense flow velocity, θ_x and θ_y are the terrain slope angles in the x and y directions respectively and k the active or passive earth pressure coefficient relating normal stresses in x and y directions to bottom pressure.

Numerical methods: The above system of equations is solved using a finite element method on a mesh consisting of quadrilateral elements that are put on the digitised terrain model, Fig. 6.1-6.2. The elevation of the nodes of this irregular mesh is determined and the mean slope and the orientation of each element are computed.

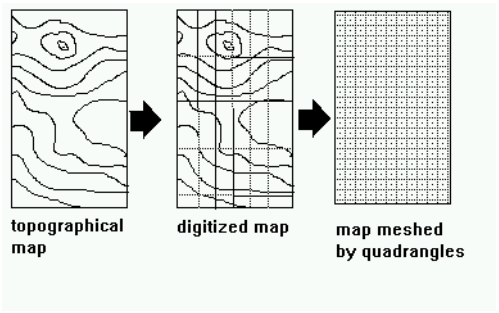

Figure 6.1: Terrain model and irregular grid of quadrilateral elements for finite element method.

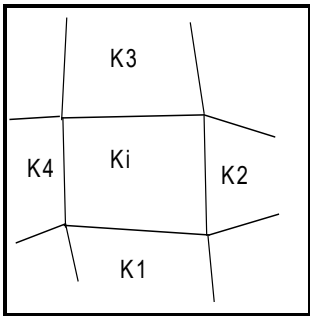

Figure 6.2: Picture segment from Fig. 6.1, showing example of quadrilateral elements.

The numerical solution procedure begins by defining a spatial average of U = (h,hu,hv) on each element K_i in time t^n and t^{n+1} by the projection:

$$U_{ki}^{n} = \frac{1}{V_{ki}} \int_{ki} U(\vec{x}, t^{n}) dv \text{ and } U_{ki}^{n+1} = \frac{1}{V_{ki}} \int_{ki} U(\vec{x}, t^{n+1}) dv$$

The numerical solution is then made by integration of the system of equations system on $[K_i]$ x $[t^n, t^{n+1}]$. The following system of difference equations is obtained:

$$U_{ki}^{n+1} = U_{ki}^{n} - \frac{\Delta t}{S_{ki}} \sum_{1}^{na} \begin{bmatrix} E \\ F \end{bmatrix}^{\rightarrow} n \, l_a + \Delta t . G\left(\frac{U_{ki}^{n} + U_{ki}^{n+1}}{2}\right)$$

where G is the contribution of the right hand side of the mass and momentum equations above and na is the number of neighboring edges of K_i. The numerical flux through each edge is determined using a simplified Riemann solver (Naaim, 1991). The gradients are calculated by minimizing the function F:

$$F = \sum_{j=1}^{nev} \left(\left[U_{kj} - U_{ki} - \begin{bmatrix} \partial U / \partial x \\ \partial U / \partial y \end{bmatrix} (\vec{x}_{kj} - \vec{x}_{ki}) \right]^2 \right)$$

where nev is the number of neighbors of K_i. These gradients are then limited in order to avoid the creation of new extremes. The Riemann problem is written as:

$$\frac{\partial U}{\partial t}+\frac{\partial}{\partial x_n}\begin{bmatrix}E\\F\end{bmatrix}=0/\begin{cases}U=U_{kg}+\begin{bmatrix}Ux_{kg}\\Uy_{kg}\end{bmatrix}(\vec{x}_a-\vec{x}_{kg}) \text{ if } x_n<0\\ U=U_{kd}+\begin{bmatrix}Ux_{kd}\\Uy_{kd}\end{bmatrix}(\vec{x}_a-\vec{x}_{kd}) \text{ if } x_n>0\end{cases}$$

where a indicates a neighbouring facet of the element. After the numerical flux calculation, the contribution of source terms (second member terms) is explicitly calculated and added to the final solution.

In order to validate the numerical model, a reduced scale physical model was built and several experiments allowed validation (Naaim, 1998).

Powder snow avalanche model and coupling

Physical basis and assumptions: In the powder avalanche model by Naaim and Gurer (1997) the avalanche is considered as a two-phase flow formed by air and snow particles in suspension. The gravity effect applied to the suspension produces the flow. We assume that air is a Newtonian perfect gas. The equations are written in a Cartesian co-ordinate system formed by three axes: the x- and y-axis in a horizontal plane and the vertical z-axis. The gravity vector is given by $\vec{g}=(0,0,-g)^t$. The other variables are: ρ_a the density of the air, ρ_s the density of the snow, $\vec{u}_a=(u_a,v_a,w_a)^t$ the velocity vector of the gaseous phase, $\vec{u}_s=(u_s,v_s,w_s)^t$ the velocity vector of the dispersed solid phase, p the pressure of the gaseous phase, c the particulate volumetric concentration. In a powder avalanche, c is very small, hence the interaction between the particles is assumed to be negligible. The equations governing the flow are the mass and momentum balances of fluid mechanics. Mass and momentum conservation is considered separately for each phase.

Air mass conservation :

$$\frac{\partial \rho_a}{\partial t}+\frac{\partial}{\partial x_i}(\rho_a u_{ai})=0$$

Particle mass conservation :

$$\frac{\partial (c)}{\partial t}+\frac{\partial}{\partial x_i}(c u_{si})=0$$

Air momentum conservation :

$$\frac{\partial(\rho_a u_{ai})}{\partial t}+\frac{\partial}{\partial x_j}(\rho_a u_{ai}.u_{aj})+\frac{\partial p}{\partial x_i}=\frac{\partial}{\partial x_j}(\upsilon\frac{\partial}{\partial x_j}(\rho_a u_{ai}))+\rho_a g_i+F_i.$$

(Since c is very small, the local air density $(1-c)\rho_a$ is approximated by ρ_a in all the equations.) Particle momentum conservation :

$$\frac{\partial(c u_{si})}{\partial t}+\frac{\partial}{\partial x_j}(c u_{si}.u_{sj})+\frac{1}{\rho_s}\frac{\partial p}{\partial x_i}=+c g_i-\frac{F_i}{\rho_s}$$

where $F_i=\frac{18\mu}{d^2}c(1-c)(1+\mathrm{Re}_p^{2/3})(u_{si}-u_{ai})$, $\mathrm{Re}_p=\frac{\|\vec{u}_{si}-\vec{u}_{ai}\|d}{\upsilon}$, the particle diameter d, the viscosity of the air $\mu=\rho_a\upsilon$, and the pressure p defined by equation of state for ideal gases. The introduction of the Reynold's decomposition followed by a statistical processing allows

the determination of the averaged equations for the mean movement. In these equations second order correlations resulting from the non-linearity of the original equations appear. They are modelled using the Boussinesq approximation and the turbulent viscosity concept. Equations of mass and momentum are written as follows (for convenience the usual overbar indicating averaged quantities is omitted):

Air mass conservation:

$$\frac{\partial \rho_a}{\partial t} + \frac{\partial}{\partial x_i}(\rho_a u_{ai}) = 0$$

Particle mass conservation:

$$\frac{\partial (c)}{\partial t} + \frac{\partial}{\partial x_i}(c u_{si}) = 0$$

Air momentum conservation:

$$\frac{\partial (\rho_a u_{ai})}{\partial t} + \frac{\partial}{\partial x_j}(\rho_a u_{ai}.u_{aj}) + \frac{\partial p}{\partial x_i} = \frac{\partial}{\partial x_j}(\upsilon_t \frac{\partial}{\partial x_j}(\rho_a u_{ai})) + \rho_a g_i + F_i$$

Particle momentum conservation:

$$\frac{\partial (c u_{si})}{\partial t} + \frac{\partial}{\partial x_j}(c u_{si}.u_{sj}) + \frac{1}{\rho_s}\frac{\partial p}{\partial x_i} = \frac{\partial}{\partial x_j}(\frac{\upsilon_t}{\sigma_c}\frac{\partial}{\partial x_j}(u_{si})) + c g_i - \frac{F_i}{\rho_s}$$

The turbulence model proposed by Chen and Wood (1985) was chosen, as it takes into account the back reaction of the particles on the turbulence characteristics. This model is based on the classical k-ε model, with new terms introduced in order to model the reduction of the turbulence induced by the particles. The model is presented as follows:

Turbulent kinetic energy conservation:

$$\frac{\partial (k)}{\partial t} + u_{ai}\frac{\partial k}{\partial x_i} = \frac{\partial}{\partial x_i}(\frac{\upsilon_t}{\sigma_k}\frac{\partial k}{\partial x_i}) - \overline{u'_{ai}u'_{aj}}\frac{\partial u_{ai}}{\partial x_j} - \varepsilon + S_k$$

Turbulent kinetic energy dissipation rate:

$$\frac{\partial (\varepsilon)}{\partial t} + u_{ai}\frac{\partial \varepsilon}{\partial x_i} = \frac{\partial}{\partial x_i}(\frac{\upsilon_t}{\sigma_\varepsilon}\frac{\partial \varepsilon}{\partial x_i}) - C_{1\varepsilon}\frac{\varepsilon}{k}\overline{u'_{ai}u'_{aj}}\frac{\partial u_{ai}}{\partial x_j} - C_{2\varepsilon}\frac{\varepsilon^2}{k} + S_\varepsilon$$

with

$$S_k = -\frac{2k}{t^*}(1 - \exp(-\frac{t^*\varepsilon}{2k}))c\ ,\ S_\varepsilon = -\frac{2\varepsilon}{t^*}c \text{ and } t^* = \frac{d^2\rho_s}{18\mu}.$$

The turbulent viscosity is linked to the kinetic turbulent energy k and the turbulent kinetic energy dissipation ε by

$$\mu_t = \rho\upsilon_t = \rho C_\mu \frac{k^2}{\varepsilon}.$$

The turbulent stresses are modelled according to the Boussinesq approximation:

$$-\rho\overline{u'_{ai}u'_{aj}} = \mu_t\left(\frac{\partial \bar{u}_{aj}}{\partial x_i} + \frac{\partial \bar{u}_{ai}}{\partial x_j}\right).$$

The values of the constants used in this model are:

$$C_\mu = 0.09, \sigma_k = 1, \sigma_\varepsilon = 1.22, C_{1\varepsilon} = 1.44, C_{2\varepsilon} = 1.92.$$

The powder avalanche model needs a set of boundary conditions at its interface with the dense flow or the ground, depending on whether it interacts or not with a dense flow. Concerning the velocity at the interface, the flow is considered to be a turbulent boundary layer defined by friction velocity and roughness:

$$\vec{u}_p - \vec{u}_d = \frac{\vec{u}_*}{K}\log(\frac{z - z_d}{z_o})$$

where $\vec{u}_p$ is the mean velocity in the first cell of the powder flow and $\vec{u}_d$ is the velocity in the dense flow. When the powder avalanche flows without a dense part, the ground velocity is chosen to be zero. The turbulence parameters near the ground are linked to the module of the friction velocity u_* by:

$$k = \frac{\sigma_{\varepsilon(C_{\varepsilon 2} - C_{\varepsilon 1})}}{K^2} u_*^2 \text{ and } \varepsilon = \frac{\sigma_{\varepsilon(C_{\varepsilon 2} - C_{\varepsilon 1})}}{K^2} \frac{u_*^3}{Kz}$$

where K is the von Kármán constant.

Erosion flux: First it is assumed that snow particles are mainly driven by direct aerodynamic forces. The number N of eroded grains per bed unit area per unit time is proportional to the excess shear stress:

$$N = \xi(\rho_a u_*^2 - \rho_a u_{*_t}^2)$$

Where u_{*_t} is the snow threshold friction velocity and ξ is a constant. u_{*_t} depends on the snow cohesion, density and granulometry. The erosion occurs only when $u_* > u_{*_t}$. Its flux per unit area, φ_e, is given by:

$$\varphi_e = A\rho_a(u_*^2 - u_{*_t}^2)$$

The coefficient A varies with the degree of inter-granular bindings in the dense flow surface layer. The turbulent friction is modified by snow particles, but few experimental data are available on changes in shear velocity as a function of particle concentration. We assume that the effective friction velocity near the ground u_{r*}, responsible for erosion, is linked to the computed friction velocity by the following formula:

$$u_{r*} = u_* + (u_{*_t} - u_*)(\frac{c}{c_{\max}})^2$$

The friction velocity u_* is replaced by u_{r*} in the flux equation. When the particle concentration is zero, the effective friction velocity is equal to the computed one. When the particle concentration reaches its highest value, the effective friction velocity is equal to the threshold friction velocity. We assume a maximum volumetric concentration $c_{\max}$ of 0.05.

Deposition flux: The deposition flux, which occurs when $u_* < u_{*_t}$, is proportional to the particle settling velocity u_f. It is modified by the turbulence of the flow. At $u_* = u_{*_t}$, the deposition is equal to zero. At $u_* = 0$ the deposition occurs with its maximum value. The force exerted by the flow on the particle is proportional to u_*^2, therefore we suggest that the deposition flux can be estimated by the following model:

$$\varphi_d = cu_f(\frac{u_{*_t}^2 - u_*^2}{u_{*_t}^2}).$$

This deposition model was proposed and validated in the case of drift sand formation in a wind tunnel (Naaim *et al*., in press), and also validated by experiments with suspension flows in a water tank.

Verification and applications: For a practical application of the model the following input is required: a digital terrain model, the release area, determined by field observations, the snow

height, density, cohesion and friction angle, estimated from meteorological data. At the start the avalanche is assumed to be a dense flow simulated by the two-dimensional model based on shallow water equations described before. The (dry) snow is assumed to be a granular material represented by a Mohr-Coulomb model. At the interface between the air and the dense flow, the erosion occurs and the powder avalanche can appear and develop. The powder avalanche model has been successfully applied to reproduce many observed powder avalanches in France (Bourgeat, Vaujany and Meribel) and in Andorra (Arinsal). In each case, the meteorological data were analysed and a field inquiry concerning damages caused by these avalanches was performed. The pressures necessary to cause the damages were reconstructed and compared to simulation results.

7 SUBAQUEOUS GRAVITY MASS FLOWS

(C.B. Harbitz)

Several similarities between subaqueous gravity mass flows and snow avalanches indicate that experimental and theoretical experience from subaqueous mass flows can be transferred into the study of snow avalanches. The most important similarities are (Norem *et al*., 1990):

- They are the very few natural gravity mass flows that are pure two-phase phenomena. Other natural subaerial flows mostly consist of water-saturated materials or have a high water content.
- Both kinds of masses flow over an erosive bed consisting of the same material as in the flow.
- In both cases there is a dense flow close to the bed and a turbidity current consisting of suspended particles above.

An important difference is that the density of the interstitial fluid, compared to the density of the particles, is higher for subaqueous flows than for snow avalanches. This makes the pore pressure an important parameter in modelling subaqueous flows. Other differences are presented below.

7.1 Flow mechanisms

Subaqueous flows may originate from an instant perturbation of the affected sediments (e.g. seismic activity), from long-term deposition of sediments on an inclined slope accompanied by excess pore pressures, from sea-level changes, from ice-loading, from erosive currents or from a combination of these factors that make the masses unstable. After triggering, the masses move as a turbidity current, a debris flow or a combination of these. Once in motion, the flowing masses may increase due to mass entrainment from the underlying sediments.

7.1.1 Turbidity currents

Turbidity currents are one of the fundamental processes in subaqueous mass transport. A subaqueous turbidity current (or suspension flow) consists of a muddy or cloudy mixture of sediment stirred up in a fluid.

A plain turbidity current is triggered by the mechanisms described above, while a turbidity current associated with a debris flow is a result of the shear forces at the debris flow head/ambient water interface, which tear particles off the debris flow, primarily above the thicker front or head of the flow, and bring them into suspension. Such a turbidity current will not surpass the debris flow until the latter is resisted by topography or decreasing slope inclination. A (surpassing) turbidity current is distinguished by thin deposits.

One obvious difference between powder snow avalanches and subaqueous turbidity currents is the density ratio between the dense flow and the turbidity current, which is approximately 1.5 for subaqueous turbidity currents and 100 for powder snow avalanches. The shear stresses at the upper boundary of the dense flow are thus more important for subaqueous flows (Norem *et al*., 1990).

A turbidity current might travel hundreds of kilometres, even along an almost horizontal abyssal plain before depositing a «graded bed» turbidite in a stream-like topography. This can be seen from seismic recordings, core samples of deposited materials or numerous submarine cable breaks.

Long travel distances on very gentle slopes are explained by Bagnold (1962) as a result of auto-suspension, in which the power provided by the tangential gravity component on the excess weight of the entrained sediment is sufficient not only to maintain the suspension, but also to contribute towards the power needed to maintain the flow of the fluid against the fluid drag exerted at the bed boundary.

7.1.2 Debris Flows

Debris flows, in which the masses move with a strong solid/fluid interaction as a more or less concentrated fluid, are triggered by the mechanisms described for subaqueous flows in general. Edgers and Karlsrud (1982) point out that geological evidences of subaqueous debris flows have been found in a number of areas. Turbidity currents were previously emphasised as the predominant mechanism in very large and rapid subaqueous flows. However, it is difficult to see how the main body of a flowing mass will become sufficiently dilute to turn into a low density current (Edgers and Karlsrud, 1982; Mohrig, 1997). The viscous flow analysis of run-out velocity by Edgers (1981), provides good agreement with field observations. For the back-calculated debris flow viscosities, the Reynolds number indicates laminar conditions at the debris/water interface. This precludes the large amount of turbulent mixing necessary to maintain the flow primarily as a turbidity current. The debris flow viscosities also agree remarkably with viscosities of clearly viscous subaerial quick clay slides.

Subaqueous debris flows are considered either as a saturated mass of cohesionless material, or as a visco-plastic material where no deformation takes place until a specified stress is applied to the material, after which deformation is driven by the excess of the stress beyond the yield stress. An example is the frequently used Bingham fluid model, describing a viscous Newtonian fluid combined with a yield stress. Such a fluid moves as a plug flow riding on top of a deformation zone along the bed. Recent investigations indicate that material properties, including clay rheology, are of great importance to the flow dynamics and travel distance for the majority of events. The material properties also affect the rate of erosion and channelisation. Absence of erosion is no evidence of a pure turbidity current, since

subaqueous debris flows might also be non-erosive due to hydroplaning as demonstrated by recent laboratory experiments (Mohrig *et al.*, 1998).

Field observations reveal that the travel distance decreases when the slope angle increases. The reason is probably that gentle slopes accumulate larger volumes of masses than the steeper ones before flow initiation, implying low frequent events with longer travel distances. This is again in agreement with the observations of dense snow avalanches. Further similarities arise from the fact that both kinds of mass flow over an erosive bed consisting of the same material as in the flow. However, as stated above, the shear stresses at the upper boundary of the dense flow are more important for subaqueous flows and the density of the interstitial fluid, compared to the density of particles, is higher for subaqueous debris flows than for avalanches. This increases the significance of the pore pressure. Furthermore, the starting conditions of the two kinds of flow are different. The majority of dense flow avalanches are released when there is a catastrophic failure (fracture) of a hard slab overlying a weak layer, whereas a subaqueous flows start as a homogeneous material that is perhaps instantaneously liquefied, and thus starts as a retrogressive flow (Norem *et al*., 1990).

The debris flows come to rest because of decreasing slope inclination, the termination of hydroplaning due to reduced front velocity (see below) and reduced excess pore pressure.

7.1.3 Liquefaction, lubrication and hydroplaning

Instantaneous liquefaction is closely linked to the triggering mechanism, which is often associated with an increase in pore water pressure due to a failure in the sediment matrix. It is also possible that rapid migration of methane gas or liberation of gas and water from layers of gas hydrate occur and result in further excess pore water pressure. In the subsequent motion, the sediments probably flow upon liquefied layers where excess pore pressures generated by the additional weight allow the layers to act as lubricants. Released pore water may also penetrate into the sliding masses and enhance the liquefaction.

Hydroplaning on thin layers of water might also occur in the front of subaqueous debris flows. This effect dramatically reduces the basal friction, thus increasing the head velocity. These high velocities promote sediment suspension and turbidity current formation. Hydroplaning also provides a mechanism for head surging. The presence of a basal layer of water offers an additional explanation for the long travel distances of many subaqueous flows on very gentle slopes (Mohrig *et al.*, in press), and the experiments show a remarkable visual resemblance to powder snow avalanches, where aeroplaning may occur. A theoretical description of hydroplaning with applications is provided by Harbitz *et al*. (in preparation).

7.2 Computational models

7.2.1 Turbidity currents

Turbidity currents are described by density current models or binary (two-phase solid/fluid) mixture models. These models are restricted to the steep part of the track, where phase-separation effects are of minor importance. Some of the powder snow avalanche models described in Sec. 5 were originally developed for subaqueous turbidity currents.

Shear stresses on the dense flow/turbidity current interface of subaqueous flows are described by Norem *et al*. (1990) and Norem and Schieldrop (1991).

Today's existing mathematical and numerical models for density currents and binary mixtures are well-founded and verified. The methods are also well described in the literature. The problems are to a large extent connected to the correctness of the input parameters of the models.

7.2.2 Debris flows

Empirical procedures for debris flows provide either statistical information on the run-out distance or pure limiting criteria. The studies by Edgers and Karlsrud (1982) fall within the second group. The authors describe the mechanisms of subaqueous mass flow runout based on an investigation of case studies detected by geophysical surveys of flow remnants. Lacasse and Boisard (1996) added information to these studies.

Statistical models for run-out length of subaqueous debris flows are probably not very convenient, as the variations in material properties seem to be considerable. A better way is probably to present empirical limiting criteria for flow behaviour, as performed by Fannin and Rollerson (1993) for subaerial debris flows.

Among continuum models for subaqueous flows, the Bingham fluid model by Jiang and LeBlond (1992, 1993), which also treats the interaction with the surface waves generated by the subaqueous mass flow, and the Bagnoldian model by Norem *et al*. (1990) should be mentioned. Huang and García (in press) present an analytical model obtained by a matched-asymptotic method, which can predict the asymptotic runout characteristics of subaqueous and subaerial non-hydroplaning mudflows. A critical condition for hydroplaning to occur is found with the help of the model. Mangeney *et al*. (in press) present an analytical and numerical solution for one-dimensional dam-break type problems, also applicable to debris flows and dense snow avalanches. The model is based on the depth-averaged long wave equations, including a Coulomb-type friction at the flow base. The analytical solution is obtained by the method of characteristics and is able to describe the flow over a constant slope. Comparison between analytical and numerical results shows the remarkable stability and precision of the numerical method as well as its ability to deal with strong discontinuities. The present model can be useful in practice for fluid flows where nonlinear effects are important or where strong changes (hydraulic jumps) are to be expected. The analytical solution may be very useful for testing similar models for dam-break type problems, such as water floods, landslides, and debris or dense snow avalanches.

The main parameter for modelling the flow of saturated materials is the excess pore pressure build-up. Most models assume the excess pore pressure to be constant, but Hutchinson (1986) presents a geotechnical rigid body model where dissipation of excess pore pressure is controlled according to the consolidation theory.

The main problems associated with debris flows are related to the understanding and description of material properties. These properties are very different for flowing and deposited material. In addition the accessibility of the materials is relatively restricted, and the materials have probably changed considerably during the long period of time since many of the recorded mass flows occurred.

7.2.3 Interaction with surface waves and coupled models

The interaction with surface waves was until recently only described in models with relatively simple descriptions of the mass flow, though this might be a substantial reason for dissipation of mass flow energy (Harbitz, 1992; Jiang and LeBlond, 1992, 1993). Assier Rzadkiewicz *et al*. (1997) have now presented a two-dimensional model to study water waves generated by subaqueous flows that separate into a dense flow and a turbidity current. The numerical model is validated against analytical solutions and experiments. The simulations show that the Bingham model associated with diffusion is not the most appropriate model for the study of granular flows. However, it reproduces the experiments with an acceptable accuracy when the parameters have been adjusted to match the observed shape of the flow.

Back-analysis of tsunamis in combination with tide gauge records can provide valuable information regarding the initial location, extent (volume), shape and motion of the tsunami source. Otherwise these aspects are only anticipated and prescribed input functions to a subaqueous mass flow model until the seabed conditions both before and after the event is carefully recorded. Anyhow, the dynamics of a subaqueous mass flows can not be determined purely from studies of the flow remnants. However, the flow dynamics are closely related to the temporal and spatial distribution of generated tsunami heights.

8 PRACTICAL NEEDS IN AVALANCHE MODELLING

(Urs Gruber)

The aim of avalanche modelling in practice is to determine the hazard at a given location in order that protective measures against this danger can be undertaken. The modelling requirements of the practitioners depend basically on the defence strategies they want or can apply. The simplest strategy is to avoid the presence of any human being or building in an endangered area. In this case, the only need of the practitioners is the maximum reach of an avalanche. However, it is often not possible to keep houses and traffic roads out of endangered areas. Then the main requirement in practice is the impact pressure of an avalanche event at a given location. Due to economic and risk management considerations, the impact pressure must be related to a frequency. For the reliable dimensioning of protective measures also more detailed information about the duration of the impact pressure, the shear forces and the run-up height are required.

All the needs mentioned above are difficult to reach completely by the current avalanche models. It has to be noted, that today there is not — and probably never will be — a single model that is able to answer all questions. Therefore some “intermediate” needs for practical avalanche hazard and risk management should also be mentioned. The mapping and the registration of the important characteristics of historical events are very useful in practice. They help to judge the frequency of an avalanche in a certain area as well as to verify and subsequently to improve the reliability of avalanche models. Another requirement in practice is to have rules for the specification of release areas, which are based mainly on the local precipitation rate, the terrain configuration, the expected snow type and the snow transport by wind. Concerning the application of deterministic avalanche models in practice, rules for the

specification of the friction parameters are required. For the application of the statistical models a significant statistical size of comparable avalanches is needed.

9 FUTURE MODEL DEVELOPMENT

(C.B. Harbitz, D. Issler, and C.J. Keylock)

To meet the practical needs in hazard mapping and the theoretical needs for better understanding of the underlying physics in avalanche dynamics, a substantial effort in computational model development is desirable. The cruder the knowledge of initial and boundary conditions, the more one should favour relatively simple and robust models at the expense of detail in the predictions. Nevertheless, very often great detail is required and thus rather sophisticated models are needed, too.

Determination of realistic initial conditions is a serious problem in practical applications that has not received sufficient attention in the past. Typically, both the initial avalanche mass (fracture area and depth) and the flow behaviour (friction coefficients, snow entrainment and deposition rates, fraction of suspended snow) are non-linearly dependent upon the return period. On the one hand, very simple models do not adequately reflect this non-linearity and may give strongly distorted results; on the other hand, determination of the effect of uncertainties in the initial conditions on the results requires a large number of simulations that are not presently possible with the more demanding advanced models. We suggest that combining simple models allowing rapid scanning of the relevant parameter space with more advanced models for detailed simulations of selected scenarios could help bridge this gap. The simple models will not disappear but acquire new meaning when combined with the more sophisticated ones.

For such combined analyses to yield meaningful results, the simple and advanced models must be properly matched. The following are among the relevant criteria:

- The input and output parameters of the simple model must be among those of the advanced model.
- The physical processes described by the simple model should also be contained in the matching advanced model so that parameter dependencies found with the simple model will also be reflected by the advanced one. E.g., a one-dimensional model with a simple snow entrainment mechanism explores dimensions of the parameter space that are inaccessible to two- or three-dimensional models without snow entrainment.
- Before practical applications are considered, the two models should be compared in situations that can reasonably be described with the simple model. In this way, a set of parameter values for one model can be approximately related to a set of values for the other model (e.g., friction or entrainment coefficients).

In order to account for the extraordinary variability of avalanche motion in response to initial and boundary conditions, flow-regime transitions and snow mass balance should be properly described. The vast majority of models in use today completely neglect these phenomena.

In simple models, flow-regime transitions may be captured “manually” by choosing different sets of parameter values in different sections of the path. Indeed, investigations by Gubler

(1987) showed that velocity and flow-depth measurements of several avalanches could only be satisfactorily reproduced by the Voellmy-Salm model if turbulent friction in the track was set significantly below the "canonical" values of the Swiss guidelines (Salm et al., 1990) whereas a higher dry friction coefficient had to be used in the runout. It is obvious that only very few experts will be able to correct for model deficiencies in this way, and a high degree of subjectivity is thereby introduced.

So far, these effects have been qualitatively incorporated in only a few models. The Russian models take up a suggestion by Grigoryan (1979) that shear stresses cannot exceed a material-dependent maximum value—an observation that helps explain the abnormally long runout distances of very large rock and snow avalanches. The Norwegian NIS model (Norem, Irgens and Schieldrop , 1987, 1989) goes a step further by combining visco-elasticity and cohesion; depending on the choice of exponent in the shear dependence of the stresses, the inertial or macro-viscous flow regimes of a granular material (Bagnold, 1954, 1956) can be described.

What appears to be missing at present, however, is a dynamical determination of the effective constitutive law of avalanching snow in response to the local flow parameters. It is the authors' opinion that the discrete element method (or particle dynamics approach), modelling the flow in terms of a large number of (inelastically) colliding particles of varying size, holds the promise of eliciting some main features of avalanche flow regimes and their transitions. Future models could allow for variation in elemental mass and size, material properties, spin, etc. However, it remains to be seen whether or not such an approach (even one that includes all the additional sophistications mentioned) is directly applicable to snow, which exhibits visco-plastic-like behaviour. In fact, it is possible that these approaches are of most use for determining the properties of the saltation layer (McElwaine, pers. comm., 1998). The results could then be used to construct constitutive relations for practically useful models. Systematic laboratory experiments and theoretical investigations have been conducted by several groups (Hutter and Koch, 1991; Hutter *et al*., 1995; Keller *et al*., 1998; Koch *et al*., 1994), but much more work will be required before this approach bears fruit in practical applications. To quote Perla *et al*. (1984): "Ultimately, one could hope for a model that somehow blends continuum and particle simulation since this is, after all, a way in which an avalanche behaves".

The importance of entrainment-deposition is emphasised in the continuum models of Hopfinger (1983) and Beghin and Brugnot (1983) who assume that the growth rates of an avalanche cloud are linear functions of slope angle. The centre-of-mass model of Maeno and Nishimura (Sec. 3.9) applies a velocity dependent rate of entrainment. Ostroumov (1972) extended entrainment to the whole flow of the Russian dense snow avalanche models (Sec. 3.14). In the Russian powder snow avalanche model (Sec. 5.3), the growth rate of the avalanche is not prescribed, but is found by solving the basic system of equations. Some other powder snow avalanche models apply empirical approaches based on hydraulic experiments (cf. Tab. 5.1) for the snow entrainment, while the SL-1D model (Sec. 5.12) focuses on particle impacts. Their functions are found empirically from watertank experiments using density currents.

The importance of snow entrainment has been illustrated by contrasting two maps of maximum stagnation pressures for the runout zone of a large PSA path in the Swiss Alps, both produced with the code SL-3D (Hermann *et al.,* 1994). In the first run, a large initial mass corresponding to an event with a return period of about 300 years was specified, but snow entrainment and deposition were disabled. In contrast, the second run started with a

much smaller initial mass (roughly corresponding to a return period of 30 years), but Gauer's shear-stress dependent entrainment model (Gauer, 1994) was enabled and initial erodible snow depth varied from 0.2 to 0.8 m, depending on altitude and slope angle. Comparisons of the temporal evolution of total avalanche mass show that the mass of the PSA may grow enormously if sufficient erodible snow is available in the track. While the avalanche without entrainment already begins to decelerate in the track, in the presence of entrainment, maximum speed is reached only at the beginning of the runout zone. It is highly probable that such a result is also valid for dense snow avalanches. On long avalanche paths, initial avalanche mass appears to be much less important than snow entrainment for a wide range of initial conditions.

10 CO-ORDINATED EXPERIMENTS

(C.B. Harbitz, D. Issler, and C.J. Keylock)

Model development and verification require comprehensive measurements on real avalanches for improved understanding of the underlying physics, validation of the modelling approach, and calibration of the parameters. The remaining key problems—modelling of snow entrainment and deposition, and choice of the initial and boundary conditions for each application of the models—are directly connected to the scarcity of comprehensive, reliable experimental data and the concomitant lack of model validation.

The SAME Work Package 3 has described the directions for future experimentation (cf. the proposal for a co-ordinated European full-scale avalanche experiment), detailing the parameters, measurement techniques, required precision, site requirements, feasibility, and priorities.

11 CONCLUDING REMARKS

(C.B. Harbitz, D. Issler, and C.J. Keylock)

Various models for computation of avalanche motion are presented. The models include empirical procedures for runout distance computations, in addition to dynamics models describing the physics of dense and powder snow avalanches, the coupled combination of these, and slush flows. A few (quasi) three-dimensional models already exist, and effort is now being made to expand more of the one- and two-dimensional models into three dimensions. However, it is the impression of the authors that it is of equal importance to improve the two-dimensional models further.

The model report and the SAME work package 3 meetings suggest that future model development will be in the directions of flow-regime transitions and snow mass balance. Density variations are represented in very few models, and then simply, while the resultant effects on other physical parameter values such as viscosity, are not represented in any of the dynamics models. Other aspects of the moving media (e.g. particle size distributions, particle concentration and rotation, temperature changes, and energy dissipation) are not adequately described in any of the dynamics models. There is a conspicuous lack of any description of stability and accuracy of the applied numerical methods.

Significant improvements in the quality of avalanche hazard mapping require parallel progress along three complementary paths:

- *Improved knowledge of initial conditions:* Combining an extensive survey of the parameter space with detailed simulations of selected scenarios for each practical problem, as advocated in the section on future model development, should contribute towards a more comprehensive assessment of avalanche hazard, taking into account the uncertainty of our estimates and computations. Beyond this, research into the quasi-stochastic (climate, probability distribution of key weather elements) as well as causal factors (topography) determining release areas and volumes in function of avalanche frequency needs to be intensified.
- *Modelling of the basic physical processes of avalanche dynamics:* Higher accuracy and reliability of the dynamics models can only be achieved if snow entrainment or deposition and changes in the flow regime are correctly captured. Particle-dynamics models hold promise as a tool for studying the basic processes, interpreting measurements, and for developing practically useful continuum approximations. Detailed analysis of theoretical approaches successful in other gravitational mass movements should stimulate future development in avalanche dynamics. As an example, Kanatani (1979) models the flow of granular materials by a polar continuum, where the rotation of particles mentioned above is described as an additional tensor field. For fast flows in which particle collision play an important role, the particle fluctuations are regarded as macroscopic “heat”, and a thermodynamic analogy is developed (Kanatani, 1980). The “thermal dilatation” of the flow is analysed to see the normal stress effects, i.e. the pressure caused by the velocity gradient of the flow. Finally, an entropy formulation is obtained, which is an extension of classical continuum thermodynamics.
- *Comprehensive measurements on real avalanches:* For guiding model development and allowing full verification of sophisticated models, a new generation of experiments is required in which the processes in the interior of avalanches are studied in detail. According to the findings from a working group of SAME, these objectives can be reached by combining existing experimental techniques in one small and one large experimental site, but only at substantial cost. A corresponding proposal is being elaborated.

All points listed above underline the substantial benefits, and even necessity, of international collaboration in the field of avalanche dynamics. The need is felt most urgently for experimentation due to the high costs of the required equipment. However, measurements of flow height, density and vertical velocity gradients, front velocity, distribution of deposits, etc. along the slide path would increase the understanding of the mechanisms involved and would be helpful in evaluating the dynamics models. At present, several models with different descriptions of the dynamics and the material properties can all replicate the deficient recorded observations from one specific event through the tuning of parameter values. Thus, all predictions of runout distance, impact pressure, etc. for a possible event are based on a high degree of subjective judgement and experience, and hence are encumbered with uncertainty.

If progress in modelling is to keep pace with experiment, parallel development of nearly identical models should be abandoned in favour of co-ordinated investigations at different

levels, from basic studies of granular dynamics to the elaboration of practical procedures for hazard mapping.

12 REFERENCES

Akiyama, J. and Fukushima, Y. 1985. Entrainment of non-cohesive bed sediment into suspension. External Memorandum **195**, St. Anthony Falls Hydraulic Laboratory, University of Minnesota, Minneapolis, U.S.A.

Alean, J. 1984. Untersuchungen über Entstehungsbedingungen und Reichweiten von Eislawinen. Mitteilung No. **74** der *Versuchsanstalt für Wasserbau, Hydrologie und Glaziologie an der Eidgenößischen Technischen Hochschule (Zürich).*

Alean, J. 1985. Ice avalanches: Some empirical information about their formation and reach. *Journal of Glaciology* Vol. **31**, No. **109**.

Assier Rzadkiewicz, S., Mariotti, C., and Heinrich, Ph. 1997. Numerical simulation of submarine landslides and their hydraulic effects. *J. Waterway, Port, Coastal and Ocean Engrg, ASCE*, **123**, 149-157.

Bagnold, R.A. 1954. Experiments on a gravity free dispersion of large solid spheres in a Newtonian fluid under shear. *Proceedings of the Royal Society of London*, Ser. A**225**, 49-63.

Bagnold, R.A. 1956. The flow of cohesionless grains in fluids. *Phil. Transaction of the Royal Society of London*, **249**, 235-297.

Bagnold, R.A. 1962. Auto-suspension of transported sediment; turbidity currents. *Proceedings of the Royal Society of London*, **A 265**, 315-319.

Bakhvalov, N.S. and Eglit, M.E. 1970. Study of the solutions of equations of motion of snow avalanches. *Materialy Glyatsiologicheskikh Issledovaniy (Data of Glaciological studies)* **16**, 7-14. English transl. in *Glaciological Data Report* **GD-16**, 117-128, 1984.

Bakhvalov, N.S. and Eglit, M.E. 1973. Investigation of the one-dimensional motion of a snow avalanche along a flat slope. *Izv. Akad. Nauk SSSR Mekh. Zhidk. Gaza* **5**, 7-14. English transl. in *Fluid Dynamics* **8** 1973.

Bakkehøi, S., Cheng, T., Domaas, U., Lied, K., Perla, R.I. and Schieldrop, B. 1981. On the computation of parameters that model snow avalanche motion. *Canadian Geotechnical Journal* **18**(**1**), 121-130.

Bakkehøi, S., Domaas, U. and Lied, K. 1983. Calculation of Snow Avalanche Run-out Distance. Annals of Glaciology, Vol. 4, 24-29. Also in: *Norwegian Geotechnical Institute*, publication no. **151**, 1984.

Bakkehøi, S. and Norem, H. 1993. Comparing topographical and dynamical run-out models by ideas of "Nearest Neighbour Method". *Proceedings, 2nd Avalanche-Dynamics-Workshop in Innsbruck, 1993. Wildbach und Lawinenverbau, Vol. 63, no. 138, 1999.*

Bakkehøi, S. and Norem, H. 1994. Sammenlikning av metoder for beregning av maksimal utløpsdistanse for snøskred (Comparison of methods for calculation of maximum avalanche runout distance). *Norwegian Geotechnical Institute*, report **581200-30** (in Norwegian).

Barbolini, M. 1996. Sulla simulazione delle valanghe di neve densa (On modeling of dense snow avalanches) *Tesi di Laurea, Politecnico di Milano* (In Italian).

Barbolini, M. and Nettuno, L. 1996. La modellazione matematica delle valanghe di neve densa: un approccio modellistico di tipo integrale. *SVI-Notizie* No. **1**, November 1996 (In Italian).

Bartelt, P.A and Gruber, U. 1997. Development and calibration of a Voellmy-fluid dense snow avalanche model based on a Finite Element Method. *Swiss Federal Institute for Snow and Avalanche Research, Internal Report* No. **714**, Davos.

Bartelt, P.A, Gruber, U. and Salm, B. 1997a. Numerical Modeling of Dense Snow Avalanches using a Voellmy-fluid flow law solved by a Finite Difference Method. *Swiss Federal Institute for Snow and Avalanche Research, Internal Report* No. **716**, Davos.

Bartelt, P.A, Salm, B. and Gruber, U., 1997b. Modelling dense snow avalanche flow as a Criminale-Ericksen-Filby fluid without cohesion. *Swiss Federal Institute for Snow and Avalanche Research, Internal Report* No. **717**, Davos.

Bartelt, P.A. and Salm, B. 1996. A comparison between steady and transient dense snow avalanche models. *Presented at the symposium "Snow as a physical, ecological and economical factor", Davos (CH),* November 1996, 20-23.

Beghin, P., Hopfinger, E.J., and Britter, R.E. 1981. Gravitational convection from instantaneous sources on inclined boundaries. *J. Fluid Mech.* **107**, 407–422.

Beghin, P. and Brugnot, G. 1983. Contribution of experimental and theoretical results to powder snow avalanche dynamics. *CRREL* Rev. **8**, 67–73.

Beghin, P. and Olagne, X. 1991. Experimental and theoretical study of the dynamics of powder snow avalanches. *Cold Regions Sci. Technol.* **19**, 317–326.

Benda, L.E. and Cundy, T.W. 1990. Predicting deposition of debris flows in mountain channels. *Canadian Geotechnical Journal,* **(27)** pp 409-417.

Blagoveshchenskiy, V.P. 1991. The determination of snow avalanche parameters. *Alma-Ata* (in Russian). 116 pp.

Blagoveshchenskiy, V.P., and Eglit, M.E. 1985. Matematicheskoe modelirovanie vlijanija parametrov lavinnih ochagov i fizicheskih svoistv snega na dvizhenije lavin (Mathematical modelling of the effect of the parameters of avalanche sources and physical properties of the snow on the dynamics of avalanches). *Materialy Glyatsiologicheskikh Issledovaniy (Data of Glaciological Studies)* **53**, 108-112 (In Russian with English summary).

Blagoveshchenskiy, V.P., Mironova, E.M., and Eglit, M.E. 1995. Calculation of avalanche parameters in little-studied mountain areas. *Materialy Glyatsiologicheskikh Issledovaniy (Data of Glaciological Studies)* **79**, 36-40 (Russian with English summary).

Bozhinskiy, A.N. and Nazarov, A.N. 1995. The mathematical model of mudflow dynamics. *Data of Glaciological Studies* **79**, 55 - 58 (In Russian).

Bozhinskiy, A.N. and Nazarov, A.N. 1996. On the wave nature of mudflows. *Proceedings of the Russian Academy of Sciences*, **347** No. **3**, 408 - 410 (In Russian with English translation in the USA).

Bozhinskiy, A.N. and Nazarov, A.N. 1998. Dynamics of two-layer slushflows. *NGI Publications* **203**. *(25 Years of Snow Avalanche Research at NGI, Anniversary Conference, Voss, Norway, 12–16 May, 1998, Proceedings). Norwegian Geotechnical Institute, Oslo.*

Bozhinskiy, A.N., Nazarov, A.N., Sapunov, V.N., and Chernouss, P.A. 1996. The mathematical model of slushflow dynamics. *Proceedings of the International Conference "Avalanches and Related Subjects", 2 - 6 September, "Apatit" Kirovsk, Russia,* 44 - 49.

Brandstätter, W., Hagen, G., Hufnagel, H., Schaffhauser, H.1996. Ein gasdynamisches Lawinensimulationsmodell. *Proceedings INTER-PRAEVENT 96, Garmisch Partenkirchen.*

Breitfuss, G. and Scheidegger, A.E. 1974. On a possible mechanism of Alpine debris flows. *Annali di Geofisica*, **XXVII**, Nr. **1-2**, 47-57.

Brugnot, G. and Pochat, R. 1981. Numerical simulation study of avalanches. *Journal of Glaciology* Vol. **27**, No. **95**, 77-88.

Brørs, B. 1991. Turbidity current modelling. *Division of Structural Engineering, Norwegian University of Science and Technology,* Dr.Ing.-thesis 1991:**38**.

Buser, O. 1983. Avalanche Forecast with the Method of Nearest Neighbours. An Interactive Approach. *Cold Regions Science and Technology,* Vol. **8**, No. **2**, 155-163.

Buser, O., Bütter, M. and Good, W. 1987. Avalanche forecast by the nearest neighbour method. *IAHS*, publ. no. **162**.

Buser, O. and Frutiger, H. 1980. Observed maximum run-out distance of snow avalanches and the determination of the friction coefficients μ and ξ. *Journal of Glaciology* Vol. **26**, No. **94**, 121-130.

Butler, D.R. and Malanson, G.P. 1992. Effects of terrain on excessive travel distance by snow avalanches. *Northwest Science* vol. **66** no.**2**, 77-85.

Cannon, S.H 1993. An empirical model for the volume change behaviour of debris flows. *Hydraulic Engineering '93, San Francisco,* pp. 1768-1777.

Chen, C. P. and Wood, P. E. 1985. A turbulence closure model for dilute gas particle flows. *Canadian J. Chem. Engng.* **63**(3), 349-360.

Chu, T., Hill, G., McClung, D.M., Ngun, R., and Sherkat, R. 1995. Experiments on granular flows to predict avalanche runup. *Canadian Geotechnical Journal* **32**, 285-295 (1995).

Chu, F.H., Pilkey, W.D. and Pilkey, O.H. 1979. An analytical study of turbidity current steady flow. *Marine Geology* **33**, 205-220.

Criminale, W.O.jr., Ericksen and Filby,G.L. 1958. Steady Shear Flow of Non-Newtonian Fluids. *Archive Rat. Mech. Anal* **1**, 410-417.

Dade, W.B. and Huppert, H.E. (in press). *Accepted for publication in Geology.*

Danilova, E.M and Eglit, M.E. 1977a. The motion of chute avalanches. *Materialy Glyatsiologicheskikh Issledovaniy (Data of Glaciological Studies)* **31**, 65-74 (In Russian with English summary).

Danilova, E.M. and Eglit, M.E. 1977b. The motion of snow avalanches under conditions of limiting friction. *Izv. Akad. Nauk SSSR Mekh. Zhidk. Gaza* **5**, 30-37. English transl. in *Fluid Dynamics* **12** 1977.

Dent, J. 1982. A biviscous modified bingham model for snow avalanche motion. *PhD. Thesis Montana State University.*

Dent, J.D. and Lang, T.E. 1983. A biviscous modified bingham model of snow avalanche motion. *Annals of Glaciology* **4**, 42-46.

Domaas, U. and Harbitz, C.B. 1998. Avalanche run-up heights on deflecting dams: Centre-of-mass computations compared to observations. *NGI Publications* **203**. *(25 Years of Snow Avalanche Research at NGI, Anniversary Conference, Voss, Norway, 12–16 May, 1998, Proceedings). Norwegian Geotechnical Institute, Oslo.*

Edgers, L. 1981. Viscous analysis of submarine flows. *Norwegian Geotechnical Institute, Oslo Norway.* Rep. **52207-3**, 15 pp.

Edgers, L. and Karlsrud, K. 1982. Soil flows generated by submarine slides - Case studies and consequences. *Norwegian Geotechnical Institute*, publ. **143**.

Eglit, M.E. 1968. Theoretical approaches to the calculation of the motion of snow avalanches. In: *Itogi Nauki, Moscow, VINITI*, 60-97. English translation *in Glaciological Data Report* GD-**16**, 63-118 (1974).

Eglit, M.E. 1982. Calculation of the parameters of avalanches in the region of braking and halting, *Materialy Glyatsiologicheskikh Issledovaniy (Data of Glaciological Studies)* **53**, 35-39 (In Russian with English summary).

Eglit, M.E. 1983. Some mathematical models of snow avalanches. In: *Advances in the Mechanics and the Flow of Granular Materials* Vol. **2**, 577-588 (Shahinpoor, M., ed.), Trans Tech. Publ., Clausthal - Zellerfeld, and Gulf Publ. Co., Houston, Texas.

Eglit, M.E. 1984. Theoretical approaches to avalanche dynamics. Teoreticheskie pdkhody k raschetu dvizheniia snezhnikh lavin. In*: Itogi Nauki, Moscow, VINITI, Gidrologiia Sushi. Glatsiologiia* (1967), 69–97. English transl. in: *Glaciological Data Report* **GD-16** 1984, Soviet Avalanche Research—Avalanche Bibliography Update: 1977–1983. World Data Center A for Glaciology [Snow and Ice], University of Colorado, Boulder CO, U.S.A., 63–116.

Eglit, M.E. 1998a. Mathematical and physical modelling of powder-snow avalanches in Russia. *Annals of Glaciology* **26**, 281-284.

Eglit, M.E. 1998b. Mathematical modeling of dense avalanches. *NGI Publications* **203**. *(25 Years of Snow Avalanche Research at NGI, Anniversary Conference, Voss, Norway, 12–16 May, 1998, Proceedings). Norwegian Geotechnical Institute, Oslo.*

Eglit, M.E. and Sveshnikova, E.I. 1980. Matematicheskoe modelirovanie snezhnih lavin (Mathematical modeling of snow avalanches). *Materialy Glyatsiologicheskikh Issledovaniy (Data of Glaciological Studies)* **38**, 79-84 (In Russian with English summary).

Eglit, M.E. and Vel'tishchev, N.N. 1985. Issledovanije matematicheskih modelei snezhno-pilevoi lavini (Investigation of mathematical models of powder-snow avalanche*). Materialy Glyatsiologicheskikh Issledovaniy (Data of Glaciological Studies)* **53**, 116-120 (In Russian with English summary).

Ellison, T.H. and Turner, J.S. 1959. Turbulent entrainment in stratified flows. *J. Fluid Mech.* **6**, 432-448.

Fannin, R.J. and Rollerson, T.P. 1993. Debris flows: some physical characteristics and behaviour. *Canadian Geotechnical Journal* **30**, 71-81.

Fannin, R.J. and Wise, M.P. 1995. A method for calculation of debris flow travel distance. *Proceedings of the 48th Canadian Geotechnical Conference, Vancouver, B.C., 25-27 September 1995*.

Fukushima, Y. and Parker, G. 1990. Numerical simulation of powder snow avalanches. *Journal of Glaciology* Vol. **36** No. **123**, 229-237.

Fukushima, Y., Parker, G. and Pantim, H.M. 1985. Prediction of ignitive turbidity currents in Scripps Submarine Canyon. *Marine Geology* **67**, 55-81.

Föhn, P. and Meister, R. 1982. Determination of avalanche magnitude and frequency by direct observations and/or with the aid of indirect snowcover data. *IUFRO/FAO collegium on research on small torrential watersheds (inc. avalanches),* June 1981, Grenoble, France.

Galbiati, G.L. and Savi, F. 1996. Simulazione matematica del ruscellamento e dell'infiltrazione; applicazione alla scala della particella. *In: Scritti dedicati a Giovannni Tournon, presented at the Workshop: I problemi dei grandi comprensori irrigui,* Novara **I,** Giugno 1996, 6-7 (In Italian).

García, M.H. 1985. Experimental study of turbidity currents. *M.Sc. thesis, University of Minnesota, Minneapolis, U.S.A.*

Gauer, P. 1994. Bewegung einer Staublawine längs eines Berghangs. *Diploma thesis, Fachbereich Mechanik* (III), *Technische Hochschule Darmstadt, Germany,* April 1994.

Gauer, P. 1995. A model of powder snow avalanches. In: *F.Sivardière (editor), Proc. of the Colloquium on the contribution of scientific research to safety with snow, ice and avalanches, Chamonix, France,* May 30–June 3, 1995. *ANENA / Editions du CEMAGREF. Antony, France.*

Grigoryan, S.S. 1979. Novii zakon trenija i mehanizm krupnomasshtabnih gornih obvalov i opolznei (A new law of friction and mechanism for large - scale slag heaps and landslides). *Dokl. Akad. Nauk SSSR* **244(4)**, 846-849; English transl. in *Soviet Phys. Dokl*. **24** (1979).

Grigoryan, S.S., Eglit, M.E., and Yakimov, Yu.L. 1967. A new formulation and solution of the problem of the motion of a snow avalanche. *Trudy Vycokogornogo Geofizicheskogo Instituta* **12**, 104-113 (In Russian).

Grigoryan, S.S. and Ostroumov, A.V. 1975a. On the mechanics of the formation and collapse of mountainous slag heaps. Report No. **1724**, *Inst. Mekh. Moskov. Gos. Univ., Moscow* (In Russian).

Grigoryan, S.S. and Ostroumov, A.V. 1975b. Calculation of the parameters of the motion and the force action on an avalanche dike "Tubri" (Nizhnyaya Svanetiya). Report No. **1695**, *Inst. Mekh. Moskov. Gos. Univ., Moscow* (In Russian).

Grigoryan, S.S. and Ostroumov, A.V. 1977. Mathematical simulation of the process of motion of a snow avalanche (summary only). *Journal of Glaciology* Vol. **19**, 664-665.

Gruber, U. 1998. Der Einsatz numerischer Simulationsmethoden in der Lawinengefahrenkartierung: Möglichkeiten und Grenzen. Dissertation, Geographischen Institut der Universität Zürich (in preparation).

Gubler, H.U. 1987. Measurements and modelling of snow avalanche speeds. *International Association of Hydrological Sciences Publication* **162** (Symposium at Davos 1986 - *Avalanche Formation, Movement and Effects),* 405-420.

Gubler, H.U. 1993. Swiss Avalanche-Dynamics Procedures for Dense Flow Avalanches. *AlpuG, Dr. H. Gubler, Richtstattweg 2, CH-7270 Davos Platz.*

Harbitz, C.B. 1992. Model simulations of tsunamis generated by the Storegga Slides. *Marine Geology* **105**, 1-21.

Harbitz, C.B. 1995. Flateyri, Island; Etterberegning av skredet 26 oktober 1995 (Back-calculation of the Oct. 26 1995 avalanche). *Norwegian Geotechnical Institute*, report **581250-1** (in Norwegian).

Harbitz, C.B. 1996. Computational models for rock slide and debris flow motion. *Norwegian Geotechnical Institute*, report **585910-6**.

Harbitz, C.B., Elverhøi, A., Mohrig, D., and Parker, G. (in preparation). Hydroplaning of muddy debris flows on high latitude glacigenic deep-sea fans: Theoretical descriptions and applications. *To be submitted to Journal of Geophysical Research*.

Heim, A. 1932. *Bergsturz und Menschenleben.* Zürich, Verlag Fretz und Wasmuth.

Hermann, F. and Hutter, K. 1991. Laboratory experiments on the dynamics of powder-snow avalanches in the run-out zone. *Journal of Glaciology* Vol. **37**, No. **126**.

Hermann, F., Issler, D., and Keller, S. 1994. Towards a numerical model of powder snow avalanches. *In: Proc. 2nd Europ. Comp. Fluid Dynamics Conf., Stuttgart, 1994,* 948-955, (S. Wagner et al., eds.), J. Wiley & Sons, Ltd., Chichester, UK.

Hopfinger, E.J. 1983. Snow avalanche motion and related phenomena. *Ann. rev. Fluid Mech*. 1983, **15**, 47-76.

Hopfinger, E.J. and Tochon-Danguy, J.C. 1977. A model study of powder snow avalanches. J. Glaciol. **19**, 343–356.

Hsü, K.J. 1975. Catastrophic debris streams (sturzstroms) generated by rockfalls. *Geological Society of America Bulletin* vol **86**, 129-140.

Huang, X. And García, M.H. (in press). Modeling of non-hydroplaning mudflows on continental slopes. *Accepted for publication in Marine Geology*

Hungr, O. 1995. A model for the runout analysis of rapid flow slides, debris flows, and avalanches. *Canadian Geotechnical Journal* **32**, 610-623.

Hungr, O. and McClung, D.M. 1987. An equation for calculating snow avalanche run-up against barriers in avalanche formation, movement and effects. *Proceedings, Davos Symposium, 1986. International Association of Hydrological Sciences,* Publication **162,** 605-612.

Hutchinson, J.N. 1986. A sliding-consolidation model for flow slides. *Canadian Geotechnical Journal* **23**, 115-126.

Hutter, K. 1991. On flow of granular materials. *Lecture notes. Techn. Hochschule Darmstadt.*

Hutter, K. 1996. Avalanche Dynamics. *In: Hydrology of Disasters,* 317-394, (V. P. Singh, ed.). Kluwer Academic Publishers, Dordrecht/Boston/London, 1996.

Hutter, K. and Koch, T. 1991. Motion of a granular avalanche in an exponentially curved chute: experiments and theoretical predictions. *Phil. Trans. R. Soc. Lond. A* (1991) **334**, 93-138.

Hutter, K., Koch, T., Plüss, C., and Savage, S. 1995. The dynamics of avalanches of granular materials from initiation to runout, Part II:Experiments. *Acta Mechanica*, **109**, 127-165.

Hutter, K. and Nohguchi, Y. 1990. Similarity solutions for a Voellmy model of snow avalanches with finite mass. *Acta Mechanica* **82**, 99-127.

Irgens, F., Schieldrop, B., Harbitz, C.B., Domaas, U. and Opsahl, R. 1998. Simulations of dense snow avalanches on deflecting dams. *Annals of Glaciology* Vol. **26**.

Issler, D. 1998. Modelling of snow entrainment and deposition in powder snow avalanches. *Annals Glaciol.* **26**, 253–258.

Issler, D., Gauer, P., Schaer, M., and Keller, S. 1996. Staublawinenereignisse im Winter 1995: Seewis (GR), Adelboden (BE) und Col du Pillon (VD). *Internal Report* **694**, Swiss Fed. Inst. for Snow and Avalanche Res., Davos, Switzerland.

Jiang, L. and LeBlond, P.H. 1992. The coupling of a submarine slide and the surface waves which it generates. *Journal of Geophysical Research*, vol. **97**, no. **C8**, 12 731-12 744, aug. 15, 1992.

Jiang, L. and LeBlond, P.H. 1993. Numerical modeling of an underwater Bingham plastic mudslide and the waves which it generates. *Journal of Geophysical Research*, vol. **98**, no. **C6**, 10 303-10 317, jun. 15, 1993.

Jóhannesson, T. 1998a. Icelandic avalanche runout models compared with topographical models used in other countries. *NGI Publications* **203**. *(25 Years of Snow Avalanche Research at NGI, Anniversary Conference, Voss, Norway, 12–16 May, 1998, Proceedings). Norwegian Geotechnical Institute, Oslo.*

Jóhannesson, T. 1998b. A “flexible box” model for avalanche flow. *Icelandic Meteorological Office, Draft Report.*

Kalazhokov, H.H. 1969. K poluempiricheskoy teorii dvizhenija sistemy chastits grubodispersnih aerozoley v vjazkoy zhidkosty (Semi-empirical theory for motion of aerosols in a viscous fluid). *Trudy Vysokogornogo Geofizicheskogo Instituta* **13**, 101-113.

Kanatani, K. 1979. A Continuum Theory for the Flow of Granular Materials. *Theoretical and Applied Mechanics. Japanese National Committee on Theoretical and Applied Mechanics*. Vol. **27**, 571-578.

Kanatani, K. 1980. A Continuum Theory for the Flow of Granular Materials (II). *Theoretical and Applied Mechanics. Japanese National Committee on Theoretical and Applied Mechanics*. Vol. **28**, 485-492.

Keller, S. 1995. Physikalische Simulation von Staublawinen - Experimente zur Dynamik im dreidimensionalen Auslauf. *Ph.D. thesis, Swiss Federal Institute of Technology, Zurich, Switzerland,* October, 1995. Available as: *Mittlg. Versuchsanstalt für Wasserbau,*

Hydrologie und Glaziologie, Swiss Federal Institute of Technology Zurich, Nr. **141**, 249 pp.

Keller, S., Youichi, I., and Nishimura, K. 1998. Measurements of the vertical distribution in ping-pong-ball avalanches. *Annals of Glaciology* Vol. **26**.

Kent, A. and Hungr, O. 1995. Runout characteristics of debris from mine waste dump failures in mountainous terrain. *Canada center for Mineral and Energy Technology, Edmonton, Coal Research Laboratories*.

Keylock, C.J. 1997. Snow avalanches. *Progress in Physical geography* **21**, **4**, 481-500.

Keylock, C.J., McClung, D.M., and Magnusson, M.M. (in press). Avalanche risk mapping by simulation. *Accepted for publication in Journal of Glaciology*.

Kleemayr, K. 1996. Review of avalanche run-out calculation models and evaluation for the application in hazard-zone mapping. *Internationales Symposion INTERPRAEVENT 1996 — Garmish Partenkirchen. Tagungspublikation,* Band **2**, 3-18.

Knopoff, L. 1958. Energy release in earthquakes. *Geophysical Journal* vol.**1**, 44-52.

Koch, T., Greve, R., and Hutter, K. 1994. Unconfined flow of granular avalanches along a partly curved surface. II: Experiments and numerical calculations. Proc.R.Soc.London A, 445, 415-435.

Kozik, S.M. 1962. The calculation of snow avalanche motion. *Leningrad* (in Russian). 76 pp.

Kulikovskiy, A.G. and Eglit, M.E. 1973. A two-dimensional problem on the motion of a snow avalanche along a slope with smoothly changing properties. Prikl. Mat. Mekh. 37, 837-848. English transl. in J. Appl. Math. Mech. 37 , 792-803, 1973.

Kulikovskiy, A.G and Sveshnikova, E.I. 1977. Model dlja rascheta¨dvizhenija pilevoi snezhnoi lavini (A model for calculation of motion of powder snow avalanche. Materialy Glyatsiologicheskikh Issledovaniy (Data of Glaciological Studies) 31, 74-80 (In Russian with English summary).

Kumar, A. 1994. Continuum approach to avalanche dynamics. Extended abstracts, Int. symp. on snow and related manifestations, Snow & Avalanche Study Establishment, Manali (HP), India, Sep. 1994.

Körner, H.J. 1976. Reichweite und Gescwindigkeit von Bergsturzen und Fließschneelawinen. Rock Mechanics Vol. 8, No. 4, 225-256.

Körner, H.J. 1980. The energy line method in the mechanics of avalanches. Journal of Glaciology Vol. 26, No. 94, 501-505.

Lacasse, S. and Boisard, P. 1996. Recurrent sliding of underwater slope on Cap Lopez in Gabon. *Norwegian Geotechnical Institute*, report **522070-12**.

Landau, L.D. and Lifshitz, E.M. 1983. Fluid mechanics, Pergamon Press, Oxford; New York. 3rd edition.

Lang, R.M. and Leo, R. 1994. Model for avalanches in three spatial dimensions - Comparison of theory to experiments. *Cold regions research and engineering laboratory* report **94-5**.

Lang, R.M., Leo, R., and Hutter, K. 1989. Flow characteristics of an unconstrained non-cohesive granular medium down an inclined, curved surface: Preliminary experimental results. *Annals of Glaciology* Vol. **13**, 146-153.

Lied, K. and Bakkehøi, S. 1980. Empirical Calculations of Snow-Avalanche Run-Out Distance Based on Topographic Parametres. Journal of Glaciology, Vol. 26, No. 94, 165-177. Also in: *Norwegian Geotechnical Institute*, publication no. **133**, 1981.

Lied, K. and Toppe, R. 1988. Calculation of maximum snow-avalanche run-out distance by use of digital terrain models. Annals of Glaciology, Vol. **13**, 1989, 164-169. Also in: *Norwegian Geotechnical Institute*, publication no. **183**, 1992.

Lied, K., Weiler, C., Bakkehøi, S. and Hopf, J. 1995. Calculation methods for avalanche run-out distance for the Austrian Alps. *Norwegian Geotechnical Institute*, report **581240-1**.

Locat, J., Norem, H. and Therrien, P. 1992. An approach to rock avalanche dynamics. *Norwegian Geotechnical Institute*, report **585000-10**.

MacCormack, 1969. The effect of viscosity in hypervelocity impact cratering. *AIAA Paper*, 69-354.

Maeno, N. and Nishimura, K. 1987. Numerical Computation of Snow Avalanche Motion in a Three-Dimensional Topography. *Low Temperature Science*, Ser. **A**, **46**, 99-110.

Mangeney, A., Heinrich, Ph., and Roche, R. (in press). Analytical and numerical solution of the dam-break problem for application to water floods, debris and dense snow avalanches. PAGEOPH 1999.

Marie, R. and Rapin, F. 1987. L'avalanche du Hount Nègre du 31 janvier 1986 à Barèges et Sers. *Neige et avalanches (ANENA review)* **47**, 25-35.

Martinelli, M. jr. 1986. A test of the avalanche runout equations developed by the Norwegian Geotechnical Institute. *Cold Reg. Sci. Technol.* **13** (**1**), 19-33.

Martinelli, M.jr., Lang, T.E., and Mears, A.I. 1980. Calculations of avalanche friction coefficients from field data. *Journal of Glaciology* Vol. **26**, No. **94**, 109-119.

McClung, D.M. 1990. A model for scaling avalanche speeds, *Journal of Glaciology* Vol. **36**, No. **123**, 188-198.

McClung, D.M., Kobayashi, S., and Izumi, K. 1993. Simulation of a destructive avalanche at Maseguchi, Japan. *Annals of Glaciology* **18**, 17-21.

McClung, D.M. and Lied, K. 1987. Statistical and geometrical definition of snow avalanche runout. *Cold Reg. Sci. Technol.,* **13** (**2**), 107-119.

McClung, D.M. and Mears, A. 1995. Dry-flowing avalanche run-up and run-out. *Journal of Glaciology*, Vol. **41**, No. **138**, 359- 372.

McClung, D.M., Mears, A.I. and Schaerer, P. 1989. Extreme avalanche run-out: Data from four mountain ranges. *Annals of Glaciology* Vol. **13**, 180-184.

McClung, D.M., Nettuno, L. and Savi, F. 1994. One dimensional modelling for flowing avalanche runout and runup. *In: International symposium on snow and related manifestation, Snow & Avalanche Study Establishment, Manali (HP), India,* Sep. 1994.

McClung, D.M. and Schaerer, P.A. 1993. *The Avalanche Handbook*. The Mountaineers. Seattle. 265 pp.

McClung, D.M. and Tweedy, J. 1994. Numerical avalanche prediction: Kootenay Pass, British Columbia, Canada. *Journal of Glaciology* **40** No. **135**, 351-358.

Mellor, M. 1978. Dynamics of snow avalanches. *In: Rockslides and avalanches* Vol **1**, 753-792, (Voight, B., ed.), Elsevier.

Melosh, H.J. 1979. Acoustic fluidization: a new geological process? *Journal of Geophysical Research* **84**, 7513-7520.

Middleton, G.V. and Southard, J.B. 1984. Mechanics of Sediment Transport. *Short Course No.* **3***, Society of Economic Paleontologists and Mineralogists. Tulsa, Oklahoma.* 411 pp.

Mironova, E.M. 1985. Computation of avalanche flows based on a two-dimensional hydraulic model. *Materialy Glyatsiologicheskikh Issledovaniy (Data of Glaciological Studies)* **53**, 113-115 (In Russian with English summary).

Mironova, E.M.1987. Mathematical modelling of the motion of water flows, snow avalanches, and floods. *Candidate's dissertation, Moscow* (In Russian).

Mironova, E.M. an Eglit, M.E.1988. The set of software for numerical modelling of snow avalanches, mudflows and water flows. *Materialy Glyatsiologicheskikh Issledovaniy (Data of Glaciological Studies)* **63**, 161-165 (In Russian with English summary).

Mohrig, D. 1997. Exchange of sediment between experimental subaqueous debris flows and turbidity currents. *EOS, Transactions, AGU Fall Meeting*, **78**, p. 278.

Mohrig, D., Elverhøi, A., and Parker, G. (in press). Experiments on the relative mobility of muddy subaqueous and subareial debris flows, and their capacity to remobilize antecedent deposits. *Mar. Geol.*

Mohrig, D., Whipple, K.X., Hondzo, M., Ellis, C., and Parker, G. 1998. Hydroplaning of subaqueous debris flows. *Geol. Soc. Am. Bull.*,**110**, 387-394.

Moskalev, J.D. 1977. The dynamics of snow avalanches and avalanche calculations. *Leningrad* (in Russian). 232 pp.

Murty, B.S. and Eswaran, V. 1994a. A shock-capturing scheme for avalanche modelling. *Extended abstracts, Int. symp. on snow and related manifestations, Snow & Avalanche Study Establishment, Manali (HP), India,* Sep. 1994.

Murty, B.S. and Eswaran, V. 1994b. Numerical Modelling of Avalanches. *Report submitted to Snow & Avalanche Study Establishment, Manali (HP), India,* May 1994.

Naaim, M. 1991. Modélisation numérique des effets hydrodynamiques produit par un glissement solide dans une retenue de barrage. *Ph.D. thesis, Joseph* Fourier University, Grenoble, 180pp.

Naaim, M. 1995. Modélisation numérique des avalanches aérosols. *La Houille Blanche* Nr. **5/6**–1995, 56–62.

Naaim, M. 1998. Dense avalanche numerical modeling: Interaction between avalanche and structures. *NGI Publications* **203**. *(25 Years of Snow Avalanche Research at NGI, Anniversary Conference, Voss, Norway, 12–16 May, 1998, Proceedings)*. *Norwegian Geotechnical Institute, Oslo.*

Naaim, M. and Ancey, C. 1992. Dense avalanche model. *European Summer University, Chamonix, Cemagref Publications*, 173-181.

Naaim, M., Bouvet, F. and Hugo, M. (in press). Numerical simulation of drifting snow: erosion and deposition models. Accepted for publication in *Annals of Glaciology, vol***. 26**.

Naaim, M. and Gurer, I. 1997. Two-phase numerical model of powder avalanche. Theory and application. *Journal of Natural Hazards*, Volume **16**, 18 pp.

Naaim, M. and Martinez, H. 1995. Experimental and theoretical determination of concentration profiles and influence of particle characteristics in blowing snow. *Surveys Geophys*. **16**, 695–710.

Natale, L. and Savi, F. 1992 Propagazione di un'onda di sommersione in un canale vuoto. Jornadas de enquentro trilateral para el estudio de la hidraulica de las ondas de submersion. Zaragoza, 10-12 September 1992 (In Italian).

Natale, L., Nettuno, L., and Savi, F. 1994. Numerical simulation of snow dense avalanche: an hydraulic approach. *Proceedings of the 24th Annual Pittsburg International Conference on modelling and simulations, Pittsburg* (IASTED 1994).

Natale, L., Nettuno, L., and Savi, F. 1996. Comparison among finite difference schemes for the integration of shallow water equation. *Proceedings of the 26th Annual Pittsburg International Conference on modelling and simulations, Pittsburg* (IASTED 1996).

Nazarov, A.N. 1991. Matematicheskoe modelirovanie snezhno-pilevoi lavini v ramkah uravnenii dvuhsloinoi melkoi vodi (Mathematical modeling of a snow-powder avalanche in the framework of the equations of two-layer shallow water. *Izv. Akad. Nauk SSSR Mekh. Zhidk. Gaza* **1**, 84-90. English transl. in *Fluid Dynamics* **12** (1991), 70-75.

Nazarov, A.N. 1992. Opit primenenija dvuhsloinoi modeli dlja rascheta dvizhenija pilevih lavin (Use of two-layer model for calculating of motion of powder snow avalanches). *Materialy Glyatsiologicheskikh Issledovaniy (Data of Glaciological Studies)* **73**, 73-79 (In Russian with English summary).

Nazarov, A.N. 1993. Matematicheskoe modelirovanie nestacionarnogo dvizhenija snezhno-pilevyh lavin (Mathematical modelling of non-stationary motion of powder-snow avalanches). *Thesis, Moscow,* 170pp. (In Russian).

Nettuno, L. 1996. La modellazione delle valanghe di neve densa: aspetti modellistici e sperimentali (On modeling of flowing avalanches: modelisation and experimentation). *Ph.D. Thesis, University of Pavia.*

Nishimura, K. 1991. Studies on the dynamics of fluidised snow. *Contributions from the Institute of Low Temperature Science, Hokkaido University*, Ser. **A-37**, 55 pp.

Nobles, L.H. 1966. Slush avalanches in Northern Greenland and the classification of rapid mass movements. *I.A.H.S. Publication* **69**, 267-272.

Nohguchi, Y. 1989. Three-dimensional equations for mass centre motion of an avalanche of arbitrary configuration. *Annals of Glaciology* Vol. **13**, 215-217.

Nohguchi, Y., Hutter, K. and Savage, S.B. 1989. Similarity solutions for a finite mass granular avalanche with variable friction. *Continuum Mech. Thermodyn.* **1**, 239-265.

Norem, H. 1992a. A general discussion on avalanche dynamics. *Norwegian Geotechnical Institute*, report **581200-25**.

Norem, H. 1992b. Simulation of snow-avalanche flow by a continuum granular model. *Norwegian Geotechnical Institute*, report **581200-26**.

Norem, H., 1993. Ideas on a phase diagram for granular materials. *Proceedings of the Pierre Beghin International Workshop on Rapid Gravitational Mass Movements*, 237-243.

Norem, H. 1995a. Shear stresses and boundary layers in snow avalanches. *Dr. Ing. Harald Norem A/S*, report **A951-1**. Also in: *Norwegian Geotechnical Institute*, report **581240-3.**

Norem, H. 1995b. The Ryggfonn project, summary report 1981-1995. *Dr. Ing. Harald Norem A/S*, report **A952-1**.

Norem, H., Irgens, F. and Schieldrop, B. 1987. A continuum model for calculating snow avalanche velocities. *Proceedings of Avalanche Formation, Movements and Effects, Davos 1986,* IAHS publication **162**, 363-378. Also in: *Norwegian Geotechnical Institute*, report **58120-9.**

Norem, H., Irgens, F. and Schieldrop, B. 1989. Simulation of Snow-Avalanche Flow in Run-Out Zones. *Annals of Glaciology* Vol. **13**, 218-225.

Norem, H., Locat, J. and Schieldrop, B. 1989. An approach to the physics and the modelling of submarine flowslides. *Norwegian Geotechnical Institute*, report **522090-2**.

Norem, H., Locat, J., and Schieldrop, B. 1990. An approach to the physics and the modelling of submarine flowslides. *Mar. Geotechnol.,* **9***:* 93-11.

Norem, H., Nishimura, K. and Maeno, N. 1992. Comparing model and full-scale experiments on snow avalanche dynamics. *Norwegian Geotechnical Institute*, report **581200-28**.

Norem, H. and Schieldrop, B. 1991. Stress analyses for numerical modelling of submarine flowslides. *Norwegian Geotechnical Institute*, report **522090-10**.

Nujic, G.L. 1994. Efficient implementation of non-oscillatory schemes for the computation of free surface flows. *IAHR Journal.*

Onufriev, A.T. 1967. Teorija dvizhenija vihrevogo koltsa pod deistviem cily tjazhesty (Theory of motion of circular vortex under gravity). *Prikladnaja mehanika i tehnicheskaja fizika* **2**, 3-15 (In Russian).

Ostroumov, A.V.1972. A model of the motion of snow avalanches of chute type. *Candidate's dissertation, Moscow* (In Russian).

Parker, G. 1982. Conditions for the ignition of catastrophically erosive turbidity currents. *Mar. Geol.* **46**, 307–327.

Parker, G., Fukushima, Y., and Pantin, H.M. 1986. Self-accelerating turbidity currents. *J. Fluid Mech.* **171**, 145-181.

Perla, R.I. 1980. Avalanche Release, Motion and Impact. *Dynamics of Snow and Ice Masses,* Academic Press, Inc.

Perla, R.I., Cheng, T.T. and McClung, D.M. 1980. A Two-Parameter Model of Snow-Avalanche Motion. *Journal of Glaciology* Vol. **26**, No. **94**, 197-207.

Perla R., Lied K., and Kristensen, K. 1984. Particle simulation of snow avalanche motion. *Cold Regions Science and Technology* **9**, 191-202.

Pope, S.B. 1985. Pdf methods for turbulent reactive flows. *Prog. Energy Combust. Sci.* **11**, 119-192.

Rapin, F. 1995. French theory for the snow avalanches with aerosol. In: G. Brugnot (ed.), Université européenne sur les risques naturels. Session 1992: Neige et avalanches. Editions du CEMAGREF, 163–172.

Roco, M.C. (ed.) 1993. Particulate two-phase flow. *Butterworth-Heinemann, Boston/London/Oxford/Singapore/Sydney/Toronto/Wellington*.

Rodi, W., 1980. Turbulence Models and their application in Hydraulics. *Int.Assoc.Hydr.Res. (IAHR),* Delft.

Salm, B. 1993. Flow, Flow Transition and Runout Distances of Flowing Avalanches. *Annals of Glaciology* Vol. **18**, 221-226.

Salm, B., Burkard, A., and Gubler, H.U. 1990. Berechnung von Fliesslawinen; eine Anleitung für Praktiker mit Beispielen. *Mitteilungen des Eidgenössischen Institutes für Schnee und Lawinenforschung*, Nr. **47**, Davos.

Sartoris, G. and Bartelt, P.A. 1997. Upwinded finite difference schemes for dense snow avalanche modeling. *Swiss Federal Institute for Snow and Avalanche Research, Internal Report* No. **715**, Davos.

Sassa, K. 1988. Geotechnical model for the motion of landslides. In: Bonard, C. (ed.): Landslides. *Proceedings, 5th International Symposium on Landslides, 10-15 July 1988, Lausanne, Switzerland*. Vol. **1**. Rotterdam, A.A. Balkema, 1153-1158.

Savage, S.B. and Hutter, K. 1989. The motion of a finite mass of granular material down a rough incline. *J. Fluid Mech*. Vol. **199**, 177-215.

Savage, S.B. and Hutter, K. 1990. The dynamics of avalanches of granular materials from initiation to runout, Part I: Analysis. *Acta Mech.* **86**, 201-223 (1991).

Savage, S.B. and Nohguchi, Y. 1988. Similarity solutions for avalanches of granular materials down curved beds. *Acta Mech.* **75**, 153-174.

Scheiwiller, T. 1986. Dynamics of Powder Snow Avalanches. Ph.D. thesis. Available as: Mittlg. Versuchsanstalt für Wasserbau, *Hydrologie und Glaziologie, Swiss Federal Institute of Technology Zurich,* Nr. **81**, 115 p.

Scheiwiller, T. and Hutter, K. 1982. Lawinendynamik, Übersicht über Experimente und theoretische Modelle von Fließ- und Staublawinen. Mitteilung No. **58** der *Versuchsanstalt für Wasserbau, Hydrologie und Glaziologie an der Eidgenößischen Technischen Hochschule (Zürich),* 166 pp.

Sholtz, Bretz, and Nori, 1997. *Contemporary Physics.* Vol. **38** No. **5**, 338-341.

Takahashi, T. 1991. Debris flow. *International Association of Hydraulic Research.* A.A. Balkema, Rotterdam, The Netherlands.

Takahashi, T. and Yoshida, H. 1979. Study on the deposition of debris flows, Part I - Deposition due to abrupt change of bedslope. *Annals, Disaster Prevention Research Institute, Kyoto University, Japan,* **22 B-2** (In Japanese with English abstract).

Tesche, T.W. 1986. A three dimensional dynamic model of turbulent avalanche flow. *Proc. Int. Snow Science Workshop, Lake Tahoe California,* 1-27.

Tochon-Danguy, J.C. and Hopfinger, E.J. 1975. Simulation of the dynamics of powder avalanches. In*: Mécanique de la neige; Actes du Colloque de Grindelwald, avril 1974. IAHS Publication* No. **114**, 369–380.

Voellmy, A. 1955. Über die Zerstörungskraft von Lawinen. *Schweiz. Bauzeitung* **73**, 159-165, 212-217, 246-249, 280-285.

Volodicheva, N.A., Mironova, E.M., Oleinikov, A.D., and Eglit, M.E. 1986. The use of mathematical modelling to determine the boundaries of propagation of avalanches. *Materialy Glyatsiologicheskikh Issledovaniy (Data of Glaciological Studies)* **56**, 78-81 (In Russian with English summary).

Watson, D. F., 1981. Computing the n-dimensional Delaunay tesselation with application to Voronoi polytopes. *The Computer Journal,* Vol. **24**, no. **2**, 167-172.

Yoshimatsu, H. 1991. Study of the mechanics of debris flow and its simulation model. *Journal of Japan Landslide Society* **28-2**.

Zenke, B. and Hildebrandt, M. 1983. Vorschlag eines statistisch-graphischen Verfahrens zur Lawinenreichweiten-bestimmung auf unstetigen Strichen, Wildbach- und Lawinenverbau. *Wildbach- und Lawinenverbau,* **47** Jg, Heft **2**, Nov. 1983 (in German).

Kontroll- og referanseside/
Review and reference page

Oppdragsgiver/*Client* **EU Program SAME** **Kontraktsreferanse/** **Contract reference**	**Dokument nr/*Document No.*** 581220-1 **Dato/*Date*** 11 December 1998
Dokumenttittel/*Document title* A survey of computational models for snow avalanche motion **Prosjektleder/*Project Manager*** Karstein Lied **Utarbeidet av/*Prepared by*** Carl B. Harbitz	**Distribusjon/*Distribution*** ☐ **Fri/*Unlimited*** ☒ **Begrenset/*Limited*** ☐ **Ingen/*None***
Emneord/*Keywords* Snow avalanche, runout distance, computation, dynamic motion	
Land, fylke/*Country, County* **Kommune/*Municipality*** **Sted/*Location*** **Kartblad/*Map*** **UTM-koordinater/*UTM-coordinates***	**Havområde/*Offshore area*** **Feltnavn/*Field name*** **Sted/*Location*** **Felt, blokknr./*Field, Block No.***

Kvalitetssikring i henhold til/*Quality assurance according to*
NS-EN ISO9001

Kontrollert av/ *Reviewed by*	**Kontrolltype/ *Type of review***	**Dokument/*Document***		**Revisjon 1/*Revision 1***		**Revisjon 2/*Revision 2***	
		Kontrollert/*Reviewed*		**Kontrollert/*Reviewed***		**Kontrollert/*Reviewed***	
		Dato/*Date*	**Sign.**	**Dato/*Date***	**Sign.**	**Dato/*Date***	**Sign.**
KL	**Helhetsvurdering/ *General Evaluation* ***						
KL	**Språk/*Style***						
KL	**Teknisk/Technical** **- Skjønn/*Intelligence*** **- Total/*Extensive*** **- Tverrfaglig/ *Interdisciplinary***						
KL	**Utforming/*Layout***						
CH	**Slutt/*Final***						
JGS	**Kopiering/*Copy quality***						

*** Gjennomlesning av hele rapporten og skjønnsmessig vurdering av innhold og presentasjonsform/**
On the basis of an overall evaluation of the report, its technical content and form of presentation

Dokumentet godkjent for utsendelse/ *Document approved for release*	**Dato/*Date***	**Sign.**